Covalent functionalization of graphene oxide with proteins

M.Sc. thesis

University of Jyväskylä

Department of Chemistry

3.6.2021

Elsa Korhonen

Abstract

The literature part of the master's thesis focuses on introducing potential functionalization methods for the covalent attachment of proteins on graphene oxide (GO) surfaces. The experimental part aimed at the covalent immobilization of horseradish peroxidase (HRP) on the laser-oxidized graphene-based microchip. Based on the preliminary studies with graphene oxide flakes, both crosslinker systems, glutaraldehyde (GA) and APTES-glutaraldehyde, resulted in a similar outcome of the HRP immobilization. The thermogravimetric analysis and FTIR spectroscopic results suggested the formation of covalent bonds between the components of the GO-crosslinker-HRP systems.

The GA-based crosslinking method was chosen for the protein immobilization studies with the graphene-based microchip. From the atomic force microscopy (AFM) images of the microchip after the treatment with GA and HRP solutions (in PBS buffer), line-shaped structures and elevated dots could be observed, assigned to be GA crosslinkers and HRP protein molecules, respectively. The Raman spectra of the oxidized areas showed shifting of the D, G, and 2D bands towards lower Raman shifts after HRP immobilization, which agree with the former results, indicating a successful immobilization of HRP. Also, the D band areas of the oxidized regions increased after HRP immobilization, suggesting an increased number of defects in the graphene lattice. Based on the AFM and Raman spectroscopy results from the experiments with the chip, the covalent attachment of HRP to the chip's surface *via* GA crosslinker could not be fully proved.

Tiivistelmä

Pro gradu -tutkielman kirjallisuusosassa perehdyttiin menetelmiin, jotka voisivat soveltua proteiinien kiinnittämiseen grafeenioksidin pintaan kovalenttisen sitoutumisen kautta. Kokeellisessa osassa oli tavoitteena kiinnittää linkkerimolekyylien avulla piparjuuriperoksidaasi (HRP) -entsyymimolekyylejä laserilla hapetetun grafeenin pintaan. Alustavissa kokeissa testattiin kahta menetelmää HRP:n kiinnittämiseksi grafeenioksidihiutaleisiin. Menetelmät erosivat käytettyjen linkkerimolekyylien suhteen. Ensimmäisessä menetelmässä käytettiin glutaraldehydiä ja toisessa APTES:sta ja glutaraldehydistä muodostuvaa linkkeriä. Termogravimetrinen analyysi ja FTIR-mittausten tulokset viittasivat kovalenttisten sidosten muodostumiseen grafeenioksidin ja linkkerien sekä linkkerien ja HRP:n välille. Glutaraldehydiin perustuva menetelmä valittiin varsinaiseen kokeeseen, jossa käytettiin laserilla käsiteltyä grafeenipohjaista mikrosirua. Mikrosirusta otetuista AFM-kuvista havaittiin kohonneita viivamaisia ja pistemäisiä rakenteita funktionalisoinnin jälkeen, joiden pääteltiin olevan glutaraldehydiketjuja ja HRP-proteiinimolekyylejä. Mikrosirun hapetetuista alueista mitatut Raman-spketrit viittasivat muutoksiin hapetetun grafeenin elektronirakenteessa: D-, G- ja 2D-vöiden Raman-siirtymät pienenenivät ja D-vyön pinta-ala kasvoi funktionalisoinnin jälkeen. Muutosten pääteltiin johtuvan grafeenioksidin ja linkkerien tai HRP:n välisistä vuorovaikutuksista. Tulosten perusteella ei kuitenkaan voitu varmistaa HRP:n kovalenttista kiinnittymistä mikrosirun grafeenioksidipintaan glutaraldehydin välityksellä.

Preface

The literature part of the master's thesis was started in June 2020 and was completed in May 2021. The experimental part was carried out at the Nanoscience Center at the University of Jyväskylä from August 2020 to December 2020. The topic was defined to concentrate on covalent protein immobilization methods, which could be used for the preparation of functional materials for biomedical applications. I would like to thank Professor Maija Nissinen for supervising my master's thesis and Doctoral Researcher Johanna Schirmer for supervising the experimental work. I would also like to thank Dr Manu Lahtinen for carrying out thermogravimetric analysis from the graphene oxide flake samples.

Table of Contents

Abbreviations

6AMPC	6-(azidomethyl)-2-pyridinecarbaldehyde
AFM	atomic force microscopy
APTES	3-aminopropyltriethoxysilane
APTMS	3-aminopropyltrimethoxysilane
BSA	bovine serum albumin
ChT	chymotrypsin
CRGO	chemically reduced graphene oxide
CuAAC	copper-catalyzed azide-alkyne cycloaddition
DSC	differential scanning calorimetry
EDC/EDAC	1-ethyl-3-(3-dimethyl aminopropyl) carbodiimide
ECM	extracellular matrix
EPL	expressed protein ligation
FTIR	Fourier transform infrared
GA	glutaraldehyde
GO	graphene oxide
HRP	horseradish peroxidase
LPO	lactoperoxidase
MB	methylene blue
mCPBA	meta-chloroperoxybenzoic acid
N_3	azide
NHS	N-hydroxysuccinimide
OxOx	oxalate oxidase
PBS	phosphate-buffered saline
PEDOT	poly(3,4-ethylene dioxythiophene)

PEG	polyethylene glycol
pI	isoelectric point
RGD	peptide of arginine, glycine and aspartic acid
TEM	transmission electron microscopy
TGA	thermogravimetric analysis

LITERATURE PART

1 Introduction

Graphene oxide (GO) is an attractive material for biomedical applications over other carbon-based materials, owing to its better biocompatibility and ability to interact with biological cells and tissues. GO's good biocompatibility is based on its small size (one atom thick layer), large surface area, hydrophilicity, mechanical properties resembling the mechanical behavior of biological tissues, and the ease of functionalization with molecules, such as biomolecules. Therefore, functionalized GO materials have numerous potential applications in biomedical fields, such as in drug delivery, biosensing, bioimaging, cancer therapy, tissue engineering, and regenerative medicine.[1,2]

Biomaterials used in neural tissue engineering and regenerative medicine must mimic the natural environment of neurons, the extracellular matrix (ECM). Neurons need specific physical and chemical cues for their normal growth and biological functions. GO's electrical conductivity and oxygen-containing groups for functionalization with biological molecules make it advantageous material for nerve regeneration and neural interfacing applications.[3,4] Conductivity of GO improves neural cell-cell interactions, enhancing growth and regeneration of nervous tissue. In addition, the structural flexibility of GO enhances its ability to interact with cells and biomolecules, which further improves its biocompatibility.[5]

Although GO is a biocompatible material, it also has challenges in biomedical applications, such as cytotoxicity, biodistribution (non-biodegradability), and inflammatory responses. These problems can be solved by modifying GO to resemble the natural microenvironment of neurons by functionalizing it with biomolecules, such as ECM proteins. By functionalizing GO with ECM proteins, a three-dimensional substrate for the attachment and growth of neurons can be achieved. Also, by attaching cell adhesive molecules on the GO surfaces, biocompatibility towards neural cells can be enhanced.[3,5] Studies related to covalent GO functionalization with ECM proteins are scarce but utilization of other proteins, such as enzymes, have been widely published.

This master's thesis focuses on introducing covalent functionalization protocols of GO, which could be applicable for attaching proteins (compatible with nervous tissue) on the laser-oxidized graphene-based microchip. The literature part starts by introducing chemical properties and preparation methods of GO, and the most common methods used for the characterization of functionalized GO materials. Then, weak and covalent GO-protein interactions are presented with highlighting proteins' chemical moieties participating in those interactions. Chapter 4 focuses on covalent protein immobilization methods on GO and their preceding chemical modification methods. The literature part ends with examples of ECM protein immobilization on GO. The experimental part aimed at the covalent immobilization of horseradish peroxidase (HRP) on the laser-oxidized graphene-based microchip using glutaraldehyde as a crosslinker. Preliminary experiments with GO flakes using two different crosslinker systems are also reported.

2 Graphene oxide

GO is a graphene derivative with a honeycomb-like plane of sp^2 hybridized carbons. Graphene consists of an aromatic delocalized π-system network, making it a hydrophobic and inert material. Pristine graphene sheets have poor dispersibility in organic solvents, and they aggregate easily in aqueous solutions. GO is an oxidized form of graphene, with many advantages compared with pristine graphene. Because of oxygen-containing functional groups, GO has versatile opportunities for covalent functionalization, and it is well dispersible in water and polar organic solvents. Homogenous dispersal of graphene derivatives in aqueous solutions is crucial in the preparation and some applications of functional nanomaterials.[6,7]

2.1 Chemical structure

So far, any uncontroversial model to define the exact structure of GO has not been successfully developed. The most significant reasons for it are the nonstoichiometric atomic composition of GO and the lack of proper characterization methods.[6] Also, the number and chemical nature of functional groups are highly dependent on the preparation method and starting material used.[8,9] It is commonly accepted that GO monolayers contain mainly OH and epoxy groups on their basal plane and COOH groups on the edges,[6] but the real structure is more complicated. Also, attached OH groups can disrupt an otherwise flat surface morphology of GO sheets.[10]

Some proposed structural models for graphite oxide and GO are presented in this chapter. Chemically graphite oxide and GO are quite similar, but their structures differ. Graphite oxide is a stacked, multilayered structure of GO sheets, whereas GO exist as monolayers or few-layered stacks. GO can be produced from graphite oxide through exfoliation by sonication or intensive stirring. Especially sonication can cause damage to GO sheets leading to significant differences in their sizes.[6]

The most cited and well-known model describing the graphite oxide structure is the Lerf-Klinowski model (1998).[10,11] The Lerf-Klinowski model classifies the structure of graphite oxide into two different regions: non-oxidized aromatic regions of sp^2 hybridized carbons and highly oxidized regions where sp^3 hybridized carbons dominate. The relative sizes of these regions are determined by the oxidation degree of graphite oxide and the random distribution of the regions.[11] The highly oxidized regions of the graphite oxide's basal plane contain OH and epoxy groups, whereas the edges of GO layers have OH and COOH groups (Figure 1). Lerf and Klinowski presented two structural models of graphite oxide, with and without COOH groups.[10,11] This model has been criticized because Lerf and Klinowski could not indicate the presence of COOH groups by their nuclear magnetic resonance (NMR) spectroscopic studies, probably owing to a low number of COOH groups.[11,12]

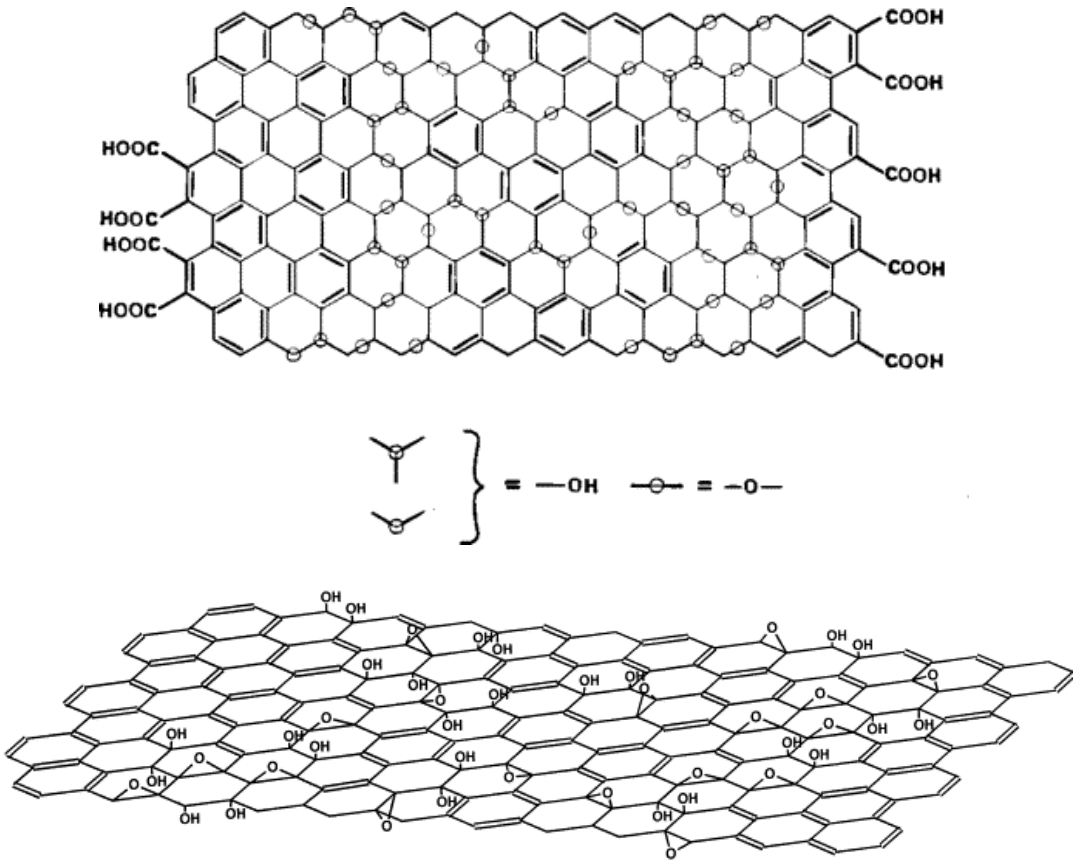

Figure 1. Two suggested structures of graphite oxide based on the Lerf-Klinowski model, with and without COOH groups. Reprinted with permission from[6], Copyright 1998, American Chemical Society (top). Reprinted from[5], Copyright 1998, with permission from Elsevier (bottom).

The Lerf-Klinowski model is based on NMR spectroscopic studies,[11] whereas the earliest structural models of graphite oxide were based on elemental analysis, chemical reactions, and X-ray diffraction (XRD) methods.[6] The first structural model of graphite oxide was presented in 1939 by Hofmann and coworkers.[13] Based on the model, graphite oxide consisted of repeating units of 1,2-epoxides on the sp^2 hybridized graphene plane. Six years later, in 1946, Ruess[14] proposed the model where graphite oxide consisted of the sp^3 hybridized carbon plane containing 1,3-epoxides and OH groups. In 1969, Scholz and Boehm[15] suggested the model in which graphite oxide contained hydroxyl and ketone groups but not epoxy groups.

Dekaný[16] proposed a structural model of graphite oxide in 2006 using widely different techniques (NMR, elemental analysis, XRD, FTIR, transmission electron microscopy (TEM), electron spin resonance, and X-ray photoelectron spectroscopy). In Dekaný's model, graphite oxide consisted of two distinct regions forming a corrugated carbon network: trans-linked cyclohexane chairs (1,3-epoxides and tertiary alcohols) and hexagon ribbons (cyclic ketones and quinones) (Figure 2).[16]

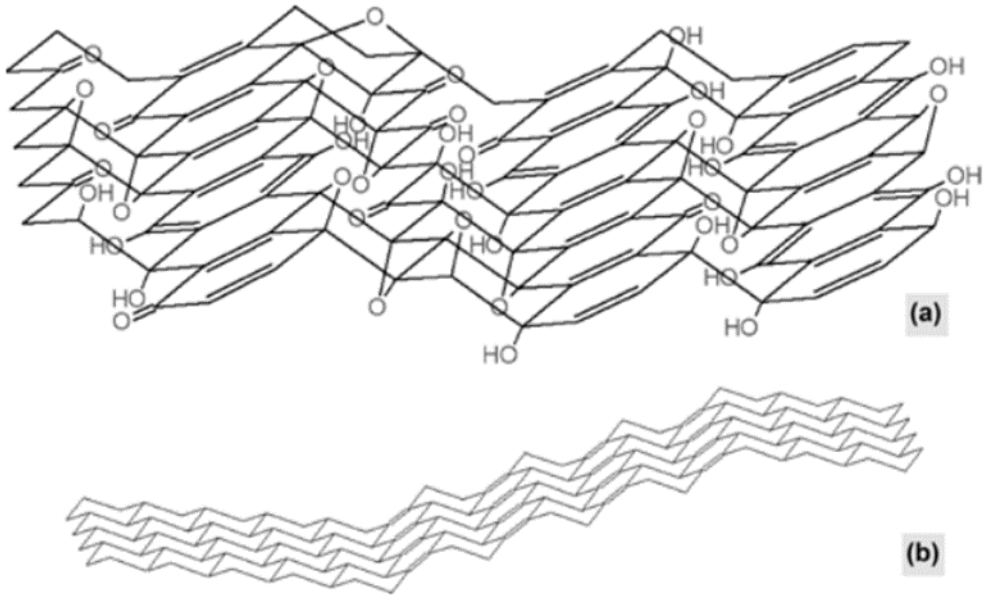

Figure 2. a) Dekaný's structural model of graphite oxide and b) its corrugated carbon skeleton. Reprinted with permission from[16], Copyright 2006, American Chemical Society.

In addition to highly oxidized and non-oxidized regions of GO layers (the Lerf-Klinowski model), there may also be defected sites in graphene lattice. Defects can form due to harsh reaction conditions or overoxidation because of evolving CO and CO_2 gases. Erickson *et al.*[17]

have imaged GO structure with TEM, which was oxidized from graphite by modified Hummers' method[18]. The study proved that GO contains three different structural regions: highly oxidized areas (82 %), graphitic regions (16 %), and hole defects (2 %).[17]

Although structures of graphite oxide and GO have been studied extensively, new structural models are still presented. In 2019, Filiz *et al.*[12] proposed a GO structure based on NMR and FTIR studies (Figure 3), which supports the Lerf-Klinowski model, and has some similarities with Dekaný's model. In the proposed structure, GO also contain lactone, ketone, and quinone groups in addition to hydroxyl, carboxylic acid, and epoxy groups. Also, some defects are included, which may form during graphite oxidation. Edges of the defects have mainly the same functionalities as the edges of GO sheets.[12]

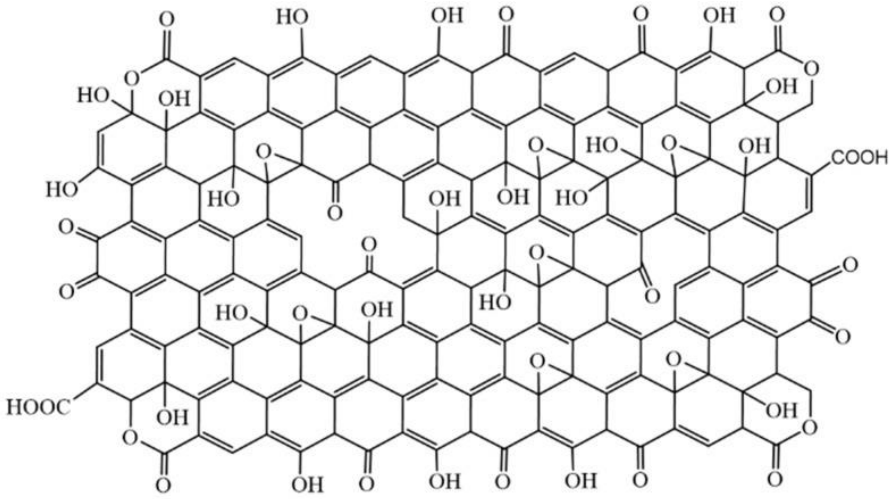

Figure 3. A proposed structure for GO monolayer by Filiz *et al.*[12] Reprinted from[12], Copyright 2019, published by MDPI, Nanomaterials; http://creativecommons.org/licenses/by/4.0/.

2.2 Preparation methods

Graphite oxide is mainly produced from natural graphite by chemical oxidation. GO monolayers can be exfoliated from graphite oxide using sonication in organic solvents or water. A commonly used method to produce graphite oxide from graphite is Hummers' method (1958)[18], in which graphite is oxidized by a mixture of sodium nitrate ($NaNO_3$), potassium

permanganate ($KMnO_4$), and concentrated sulfuric acid (H_2SO_4). A problem in this method is the formation of toxic gases, NO_2 and N_2O_4, and a low yield.[18] Therefore, several modifications or improvements of Hummers' method have been presented. Better yields or more practical procedures have been achieved by replacing some reagents or increasing their amount. For example, by excluding $NaNO_3$, increasing the amount of $KMnO_4$ and adding phosphoric acid (H_3PO_4) can be prevented the formation of toxic nitrogen gases.[19]

Another example is Yu *et al.*'s[20] improved Hummers' method with $NaNO_3$-free protocol (Figure 4). The method reduces the amounts of the reagents ($KMnO_4$ and H_2SO_4) needed in the synthesis by using K_2FeO_4 instead. In the first step (I), the intercalation compound of H_2SO_4 molecules and graphite forms, which starts to turn into graphite oxide by K_2FeO_4/ $KMnO_4$ pre-oxidation. In a deep oxidation step (II), more $KMnO_4$ is added, and the intercalation compound turns entirely into oxidized graphite. In the presence of water (step III), hydrolysis and exfoliation of graphite oxide take place, leading to separate GO monolayers. The main steps of this protocol are similar to the original Hummers' method except for the addition of $KMnO_4$ in two steps and the use of K_2FeO_4. Also, this method is faster and gives better yields.[20]

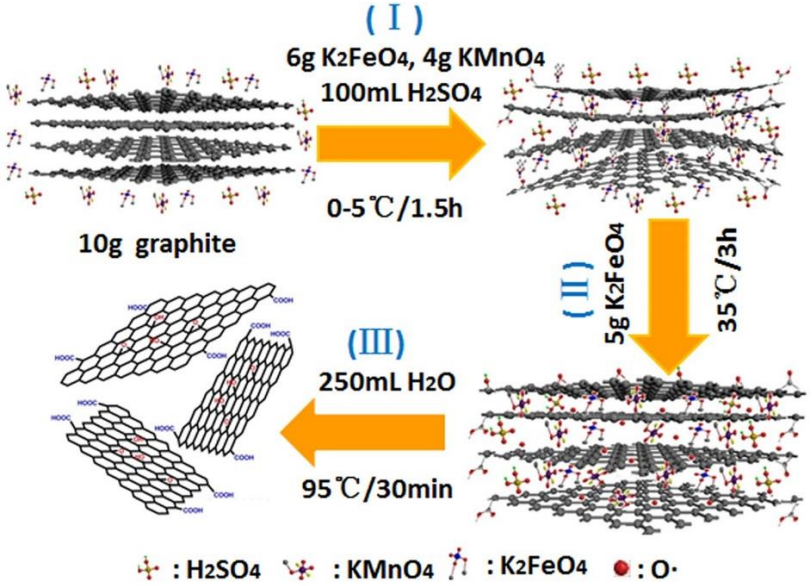

Figure 4. A scheme of the improved Hummers' method to prepare GO monolayers, illustrating exfoliation of monolayers from oxidized graphite. In the article, the amounts and places of oxidants (K_2FeO_4 and $KMnO_4$) are described other way round in the text than in the scheme. Reprinted from[20], Copyright 2016, published by Springer Nature; http://creativecommons.org/licenses/by/4.0/.

Pumera and coworkers[9] have studied the effects of reagents used in GO's preparation for its chemical composition. They observed that permanganate-based oxidants result in a higher number of oxygen groups and a higher proportion of carbonyl and carboxyl groups than chlorate-based oxidants (e.g., Staudenmaier's and Hofmann's methods). Also, they found out that the strength of nitric acid (concentrated vs. > 90 %) used in the oxidation of graphite by chlorate-based oxidant did not significantly affect the GO's oxidation degree.[9] Hence, selecting the oxidant for graphite oxidation can affect the relative amounts of oxygen groups of the prepared GO.

Instead of chemical oxidation, graphene can be oxidized by the laser-induced two-photon oxidation.[21,22] The method enables tuning of oxidation levels of monolayer graphene by controlling laser pulse energies and irradiation times. Also, shapes of oxidized areas can be tuned by a directed laser beam with low pulse energies (~ 10 μW). Oxidation starts from point-like areas, which eventually combine into larger oxidized areas. In addition, oxidation probability is five times higher near the already oxidized areas than in pristine graphene.[21,22] Chemical composition of laser oxidized graphene resembles chemically prepared GO, but relative numbers of hydroxyl and epoxy groups differ: 40 % of carbons are involved in C-OH bonds and 25 % in C-O-C bonds, whereas chemically oxidized graphene usually have more epoxy groups. Additionally, laser oxidized graphene has a more ordered structure than chemically prepared.[23]

2.3 Reactivity

Due to oxygen-containing functional groups, GO is more reactive towards covalent reactions than pristine graphene.[24] Also, GO's surface is negatively charged in water due to partial deprotonation of OH and COOH groups, enabling electrostatic interactions with proteins.[25,26] GO can be functionalized covalently *via* its COOH, OH, and epoxy groups. The edges of GO are usually the most reactive regions towards covalent reactions because there are more space and, therefore, versatile opportunities to different bond angles.[27]

COOH groups must be activated before functionalization, which can be done by carbodiimide formation (e.g., with EDAC) or treatment with thionyl chloride ($SOCl_2$). The activated COOH groups can react with amines and alcohols, forming amide and ester linkages through carbodiimide coupling or condensation reaction. GO functionalization *via* its OH groups can also be done through carbodiimide coupling with a carboxyl group-containing reagent. Additionally, OH groups can react with trialkoxysilanes and alkyltrichlorosilanes, forming silane linkages. GO functionalization *via* epoxy groups is mainly done through a ring-opening reaction using a nucleophilic reagent, usually an aromatic, aliphatic, or polymeric amine, or some carbanion.[24]

GO flakes interact with each other *via* non-covalent interactions, mainly through π-π stacking or H-bonding. OH and epoxy groups on the basal plane induce stacking of GO platelets through interlayer H-bonding (Figure 5a). Also, intralayer H-bonding can occur. When GO flakes are in a water environment, the interlayer spacing of GO flakes increases due to intercalated water molecules *via* H-bonding (Figure 5b and 5c). The number of H-bonds between GO's functional groups and water molecules increases as water content increases, enhancing the stacking of GO flakes. However, the high water content in the interlayer space of GO flakes eventually results in the degradation of GO interlayer bonds, reducing the stacking of GO flakes.[28]

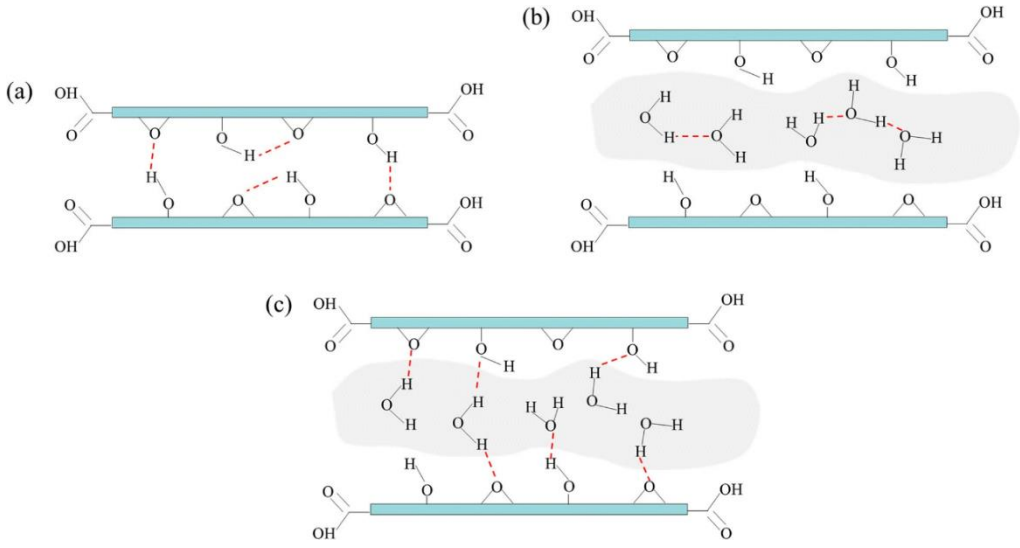

Figure 5. a) Inter- and intralayer H-bonding of functional groups of GO flakes. b) H-bonding between water molecules in GO's interlayer space c) and between GO and water molecules. The blue bar, red dash line, and gray shadow represent GO basal plane, H-bonds, and a cluster of water molecules, respectively. Reprinted with permission from[28], Copyright 2018, Springer Nature.

2.4 Characterization methods of functionalized GO materials

Many methods are needed to confirm the success of the covalent functionalization of GO and the presence of protein molecules on GO surfaces. Shen *et al.*'s[29] results of bovine serum albumin (BSA) functionalized GO nanosheets demonstrate the importance of the wide scope of methods to analyze the covalent protein immobilization. Protein molecules were covalently attached to GO *via* a diimide-activated amidation reaction, which is described in more detail in Chapter 4.1.[29]

Fourier transform infrared spectroscopy (FTIR) is a useful tool to study the success of GO covalent functionalization. The presence of possible crosslinkers or proteins attached to the GO material can be determined by FTIR spectroscopy based on their functional groups (e.g., Si-, COOH, and NH_2 groups) and formed bonds during the functionalization (e.g., amide, ester, ether). The characteristic IR spectrum of dried GO sheets contains peaks of O-H (~ 3450 cm^{-1}), C=O (~ 1650 cm^{-1}), C-O (carboxyl group, ~ 1400 cm^{-1}), C-O-C (~ 1250 cm^{-1}), and C-OH (~ 1100 cm^{-1}) vibrations (Figure 6).[29] After the protein immobilization (BSA), new peaks at 1690 cm^{-1} (amide I; C=O, C-N), 1570 cm^{-1} (amide II; N-H, C-N), and 1220 cm^{-1} (C-N of amide group) indicate the presence of the protein and success of the functionalization.[29]

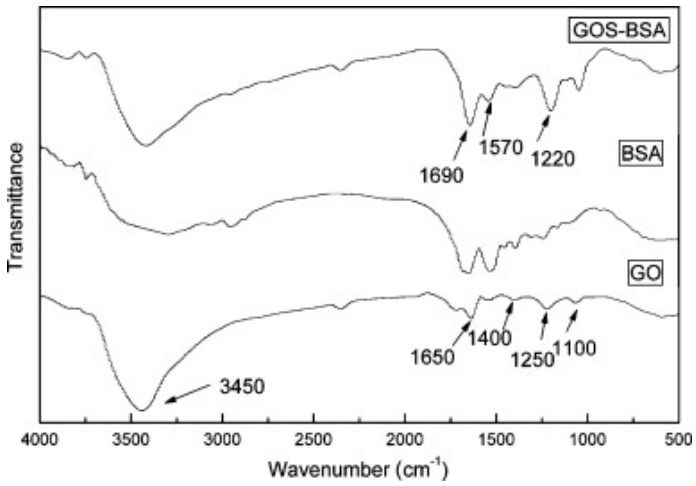

Figure 6. FTIR spectra of GO sheet (bottom), free BSA (middle), and immobilized BSA on GO (top). Reprinted with permission from[29], Copyright 2010, Elsevier.

However, IR spectra of functionalized GO materials can be challenging to interpret due to the overlapping peaks. Especially, IR vibrations of protein amide groups locate at the same region as the vibration of the imine bond (C=N, commonly formed bond between aldehydes and amines). Therefore, the separately measured reference spectra of a protein and possible crosslinkers used may be helpful.

Thermal events of materials can be studied by thermogravimetric analysis (TGA) in controlled conditions (temperature, heating/cooling rate, gas atmosphere, and pressure). In GO functionalization, TGA is used to determine the structural changes of GO material after the functionalization based on the materials' thermal decomposition. A TG curve for GO is shown in Figure 7. Only one main thermal event can be observed: removal of labile oxygen-containing functional groups (mainly OH in the basal plane) around 200 ºC - 400 ºC. Also, in the range of 500 ºC - 700 ºC, more stable groups are removed. The thermal stability of GO is significantly lower than graphite's, but it can improve after functionalization if labile oxygen groups are consumed during the functionalization. However, the thermal stability of BSA functionalized GO (GOS-BSA) is lower than GO, which is probably due to the incorporation of the protein.[29]

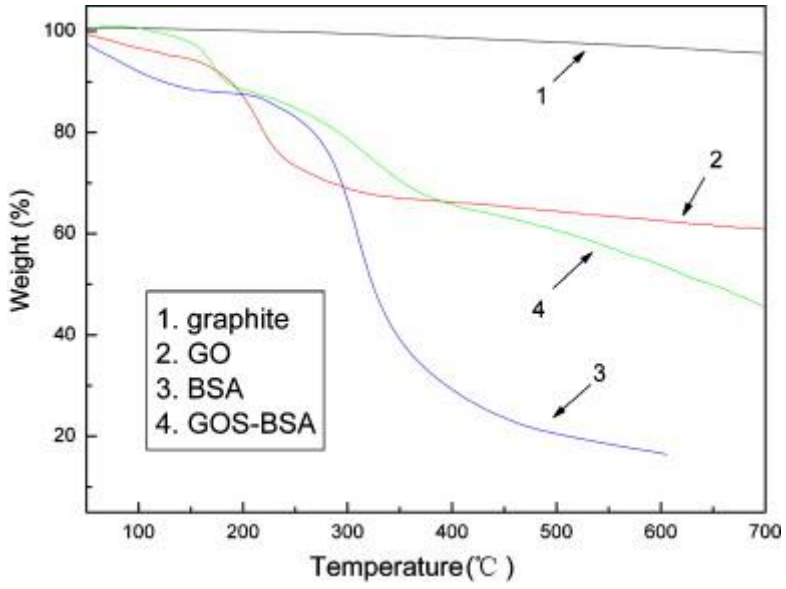

Figure 7. TG curves of graphite (black), GO (red), free BSA (blue), and BSA functionalized GO (green). Reprinted with permission from[29], Copyright 2010, Elsevier.

Raman spectroscopy is commonly used to study structural defects in the graphitic lattice or oxidation degree of GO. The most important bands in the Raman spectrum of graphene and GO

are D (1350 cm^{-1}), G (1580 cm^{-1}), and 2D (2690 cm^{-1}) bands. D band gives information about defects (sp^3 hybridized carbons) in the graphene lattice. In pristine graphene, the D band is usually weak because its height is directly related to the number of the sp^3 hybridized carbons. The G band is the most intense peak in the Raman spectrum of pristine graphene, and it is originating from the in-plane vibration of the sp^2 hybridized carbons in the lattice. Based on the shapes, positions, and a ratio (I_{2D}/I_G) of the 2D and G bands, the number of graphene layers be concluded: For single-layer graphene, the peak shapes are sharp and symmetrical, and as the number of layers increases, the broader and at higher wavenumber the peaks are. However, the positions of the 2D and D bands are dependent on the laser excitation energy.[30,31]

Raman spectroscopy can also be used to evaluate the level of functionalization of GO when functionalization results in the transformation of carbons' hybridization (sp^2 to sp^3) and changes in the GO's oxidation degree. When the functionalization involves other than oxygen groups of GO (e.g., C-C double bonds of graphitic lattice), the result can be observed by Raman spectroscopy. The degree of disorder in graphene lattice can be concluded by calculating the I_D/I_G ratio. In the low defect density, the ratio of I_D/I_G increases as the disorder in graphene lattice increases. However, at higher defect density, the ratio I_D/I_G decreases, although the disorder further increases.[30,31] Also, an unchanged Raman spectrum after functionalization of GO could indicate the success of the functionalization, if the functionalization does not affect the properties of graphene lattice.

Figure 8 shows the characteristic Raman spectrum for GO. After the covalent immobilization of BSA on GO through diimide-activated amidation, D and G bands shift about 50 cm^{-1} towards lower Raman shift values. The band shifts were concluded to result from the transformation of the structure from amorphous GO sheets to partially nanocrystalline BSA-GO material. Also, during the functionalization, the number of sp^2 hybridized carbons slightly increased, which was confirmed by the decrease of I_D/I_G ratio after the functionalization (Figure 8).[29]

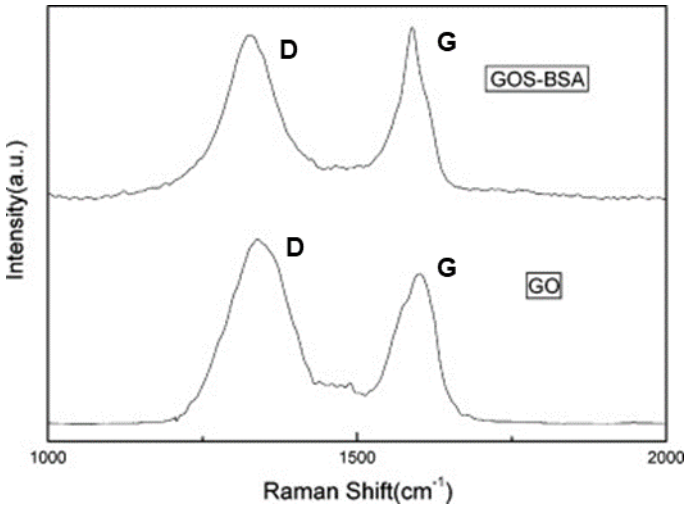

Figure 8. Raman spectra of pristine GO sheet (below), and immobilized BSA on GO (above). Adapted with permission from[29], Copyright 2010, Elsevier.

Atomic force microscopy (AFM) is an effective tool to analyze surface morphologies of materials. AFM gives information about the heights of particles related to the substrate's surface. Because GO has a flat surface morphology, except for the stacking of GO flakes, it is possible to study protein immobilization on GO surfaces.[32] Average thickness of pristine GO nanosheet is around 1.1 nm (Figure 9a). After the addition of BSA, BSA molecules can be observed on top of GO nanosheets (Figure 9b).[29]

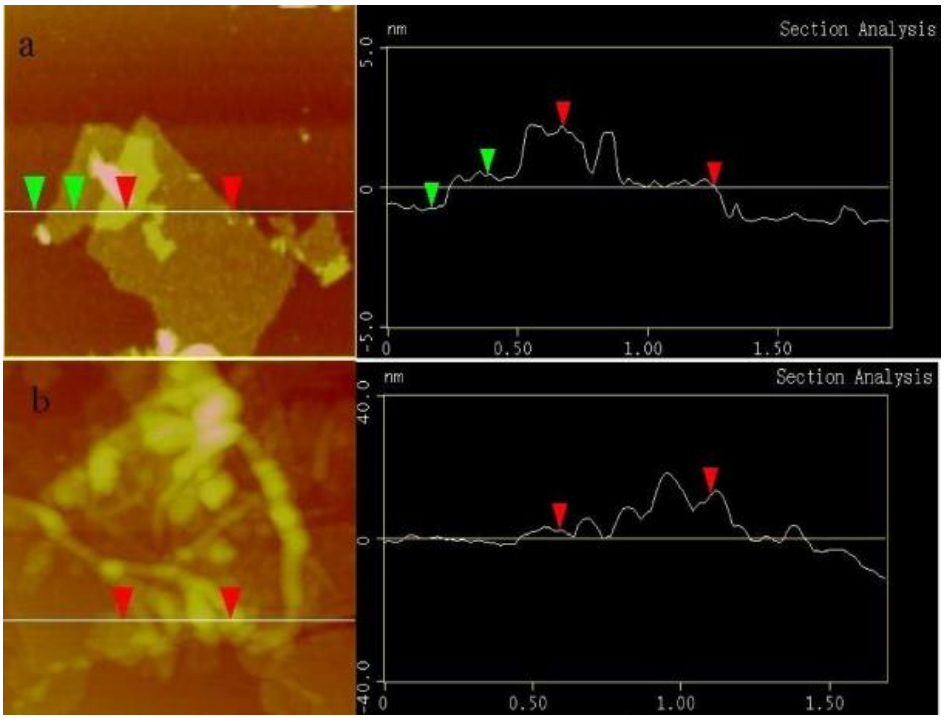

Figure 9. AFM images with high profiles. a) Pristine GO nanosheets and b) BSA-functionalized GO nanosheets. Reprinted with permission from[29], Copyright 2010, Elsevier.

3 GO-protein interactions

3.1 Structure of proteins

The proteins of living organisms consist of 20 amino acids, which have chemically different side chains. Amino acids can be classified into five classes based on the chemical nature of their side chains: non-polar aliphatic, polar, aromatic, positively charged, and negatively charged amino acids. Amino acids are linked together *via* peptide bonds, forming peptide chains of different lengths. All polypeptides have an amino terminus (*N*-terminus), an amino acid residue with a free α-amino group. Similarly, polypeptides have a carboxyl terminus (*C*-terminus) in their other end containing a free carboxyl group. When the molecular weight of a polypeptide chain is above 10 kDa, it is called protein.[33a]

All proteins have a specific three-dimensional structure or structures, which are essential for their function. However, structures of proteins are not static, but they can rearrange without losing their function. A protein structure is held together mainly by weak interactions, but there can also be some covalent disulfide bonds. In a water environment, hydrophobic interactions are the main force stabilizing the protein structure: Hydrophobic side chains of amino acids are directed towards the protein interior, avoiding contact with water molecules. In addition, stabilizing hydrogen bonding and electrostatic interactions can occur.[33b]

Most proteins are water-soluble because of hydrophilic amino acid residues (polar or charged) on their surfaces. However, proteins can still have some hydrophobic regions on their surfaces. The presence of charged amino acids determines the overall charge of proteins: lysine and arginine provide a net positive charge and aspartate and glutamate a net negative charge at neutral pH. In addition to amino acids, proteins can also have additional chemical moieties bound to a polypeptide chain, such as lipids, oligosaccharides, and phosphates.[33a,b]

Because of the exceptional structural and functional diversity of proteins, evaluating their interactions with GO materials is problematic. However, proteins' surface properties can be estimated based on their size, structural stability, and chemical composition. Small and rigid

proteins (e.g., lysozyme, lactoglobulin) are structurally stable, whereas larger proteins (e.g., albumin) tend to undergo conformational changes more easily. Also, larger proteins adsorb stronger to a surface because of the larger surface contact. A protein structure can be divided into smaller domains based on the chemical nature of structural regions: hydrophilic or hydrophobic, polar or non-polar, and charged or uncharged regions.[34]

3.2 Non-covalent interactions

GO can interact with proteins through covalent or weak interactions. Interactions involved in non-covalent protein immobilization are highly dependent on GO's surface morphology, functional groups and oxidation degree, and surface chemistry of proteins. Weak interactions participating in protein immobilization can be hydrogen bonding, electrostatic, hydrophobic, van der Waals, and π-π interactions. Protein immobilization can retain multiple weak interactions, or one interaction can be a driving force. Especially in hydrophobic, van der Waals, and π-π interactions, surface area, electron density, and protein geometry have a key role in the formation of the interactions.[3,35]

Electrostatic interactions can form between GO's negatively charged oxygen functionalities (carboxylates and hydroxylates) and positively charged protein surfaces. The charges can also be *vice versa* if GO is functionalized with positively charged molecules. Because of various oxygen-containing functional groups of GO, it can act as a hydrogen bond donor or acceptor and form H-bonds with functional groups on proteins' surfaces. On the other hand, hydrophobic graphitic regions of GO enable hydrophobic and π-π interactions with proteins. For hydrophobic interactions, the proteins must have hydrophobic amino acids on their surfaces. In addition, π-π-stacking requires that a protein contains some π-electron systems on its surface, such as an aromatic side chain of tryptophan residue.[25,35]

Amino acids, which have positively charged or aromatic side chains (Figure 10) have been observed to adsorb onto GO *via* electrostatic interaction and π-π stacking interactions, respectively.[36] Order of adsorption strength was Arg > His > Lys > Trp > Tyr > Phe. Other 14

amino acids had minor adsorption capacity. Unlike the other six adsorbed amino acids, histidine was observed to adsorb on GO *via* both electrostatic and π-π stacking interactions. The experiments were confirmed with peptides of different amino acid sequences, showing the importance of the above-mentioned amino acids for the adsorption. Positively charged peptides containing some Lys and Arg residues attached to GO *via* electrostatic interactions, whereas negatively charged peptides containing some aromatic His, Trp, Phe, and Tyr residues adsorbed onto GO through π-π interactions. Additionally, negatively charged peptides containing positive Arg residues showed some adsorption on GO, but the similar peptide without Arg residues did not.[36] The results suggest that these amino acids (Figure 10) are the central amino acids participating in electrostatic and π-π stacking interactions in protein immobilization on GO.

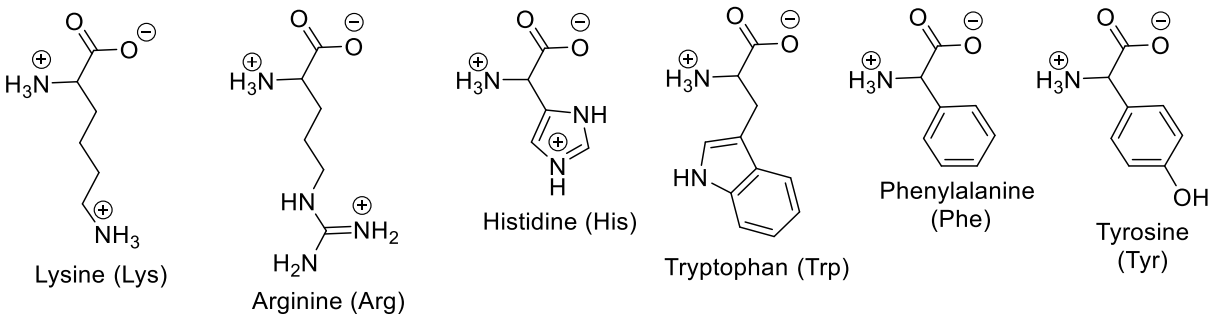

Figure 10. Amino acids with positively charged or aromatic side chains at neutral pH.

Interactions between proteins and GO can be complex because of many variables. The surface charge of proteins is highly dependent on the pH and ion concentration of a buffer.[25] Each protein has a specific isoelectric point (pI), which is the pH in which a protein does not have any net charge. Below protein's pI, it has a positively charged surface, and above its pI, a negatively charged surface. The further the pH of a solution is from the protein's pI, the more charges exist on the protein surface.[33a] Also, the density and chemical nature of oxygen-containing groups and the size of graphitic regions of GO can vary because of different preparation methods and storing conditions.[25] Therefore, there is much variation in interactions involved in protein immobilization on GO. GO-protein interactions are summarized in Table 1.

Table 1. Summary of possible weak interactions between GO and an immobilized protein

Interaction	The reactive group of GO	The reactive group of protein
Electrostatic	Carboxylate and hydroxylate (COO^- and O^-)	Positively charged amino acids (Lys, Arg, His)
Hydrogen bonding	OH, COOH and epoxy	Most of the amino acids
Hydrophobic	Graphitic regions (sp^2 hybridized carbon network)	Hydrophobic (non-polar) and aromatic amino acids (Trp, Tyr, Phe, His)
π-π stacking	Graphitic regions	Aromatic amino acids (Trp, Tyr, Phe, His)

3.2.1 Examples of protein immobilization

Zhang *et al.*[37] have suggested that electrostatic interactions dominate between immobilized protein (horseradish peroxidase, HRP) and GO. Protein immobilization was done by incubating HRP and GO in phosphate buffer for 30 min at 4 ºC and spontaneous attachment of the protein was confirmed by AFM. The nature of the interactions between HRP and GO was studied by repeating the experiments with phosphate buffers of different pH levels. It was observed that at acidic pH (< 7.2), HRP loading on GO was greater than at basic pH (> 7.2), which was concluded to result from attractive electrostatic interactions between positively charged HRP and negatively charged GO surface at acidic pH. It was assumed that significant electrostatic repulsion would occur above pH 7.2 because GO sheets have a total negative charge at pH ranges of 4 - 11, and HRP has a total negative charge above pH of 7.2. However, HRP loading was only 30 % greater at pH 4.8 than 8.8, indicating the presence of other interactions in the system, which were concluded to be hydrogen bonds. In addition, the biological activity of HRP reduced after immobilization owing to possible conformational changes caused by the immobilization.[37]

Zhang *et al.*[37] also studied protein immobilization with lysozyme at pH 7, in which it has a positively charged surface. Lysozyme has a pI of 10.3, whereas HRP has 7.2, denoting that lysozyme has more positive charges on its surface around neutral pH than HRP. Protein loading of lysozyme on GO was seven times greater than the HRP loading at pH 7.0, indicating that lysozyme has more favorable surface chemistry for interaction with GO. Also, lysozyme

retained its biological activity as opposed to HRP. Zhang and coworkers[37] concluded that the surface charges of proteins and GO determine the interactions involved in the protein immobilization.[37]

Usually, adsorbed proteins have a static orientation to maximize favorable interactions with the surface. However, adsorbed proteins can change their orientation if the conditions are dramatically changed. For example, at a low number of β-lactoglobulin proteins on a negatively charged surface, electrostatic interactions form between the protein and the surface. When the protein concentration increases, attractive protein-protein interactions appear, which changes the proteins' orientation relative to the surface (Figure 11). This results in the degradation of attractive interactions between the proteins and the surface.[34] Therefore, in non-covalent protein immobilization, it is important to consider that the used protein concentration is favorable for protein-surface interactions.

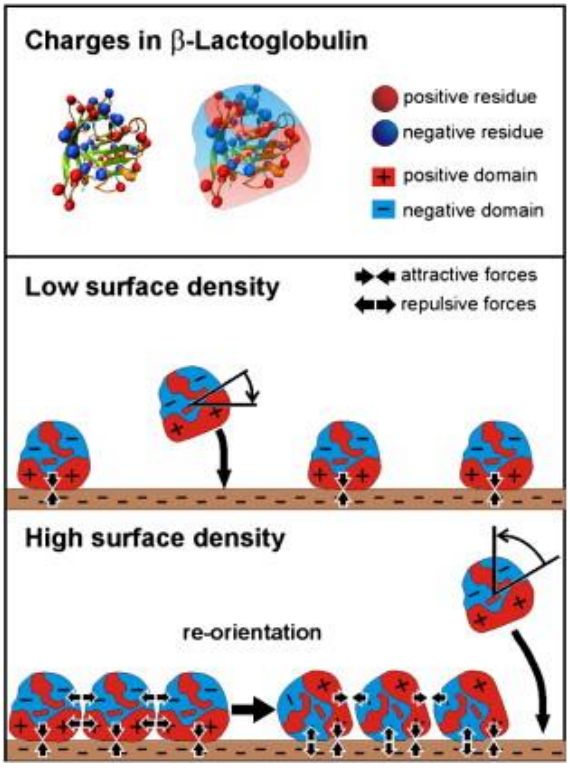

Figure 11. Schematic representation of orientational changes of adsorbed proteins induced by electrostatic interactions. Top: Distribution of positively and negatively charged amino acids of β-lactoglobulin protein into charged domains. Middle: Protein orientation includes only protein-surface interactions at low surface density. Bottom: The number of protein-protein interactions increases at high protein surface density. Reprinted with permission from[34], Copyright 2011, Elsevier.

Strong adsorption of BSA on GO has been proved to occur mainly *via* hydrophobic interactions.[38] BSA (pI = 4.5) was incubated with GO in the buffer at pH 7.4. Successful BSA immobilization was confirmed by AFM and fluorescence lifetime imaging microscopy. Interactions between immobilized protein and GO could not be electrostatic because BSA is negatively charged at pH 7.4. Therefore, the interactions were concluded to be hydrophobic, which was further confirmed by fluorescence quenching experiments. Tryptophan and tyrosine are fluorescent molecules, so hydrophobic interactions with GO can quench BSA's fluorescence. When the concentration of GO was increased in BSA-buffer solution, the intensity of BSA fluorescence decreased.[38]

Increasing the reduction extent of GO has been suggested to reinforce the hydrophobic interactions involved in protein immobilization.[39] Chemically reduced graphene oxide (CRGO) has fewer oxygen-containing functional groups than GO and resembles more pristine graphene. Therefore, the importance of electrostatic interactions and H-bonding decreases because of a lower number of hydrophilic groups. In the study, the reduction extent of GO was controlled by the reaction time. The more GO was reduced, the higher the protein loading was. The pH of the buffer did not affect protein loading on CRGO, indicating the absence of electrostatic interactions.[39]

Proteins used in the study (HRP and oxalate oxidase (OxOx)) are water-soluble, denoting that they have a hydrophilic surface.[39] Contact angle measurements, on the other hand, confirmed increasing hydrophobicity of GO with increasing reduction extent. These observations suggest that conformational changes of proteins may occur during the immobilization because the protein loading was higher on more hydrophobic CRGO than GO. In addition, the activity of HRP reduced as the reduction extent of CRGO increased, which further confirms conformational changes. However, decreasing activity was not observed for hydrophobic surface-bearing OxOx.[39] It is commonly accepted that water-soluble proteins can undergo conformational changes to have the more favorable orientation of hydrophobic residues for hydrophobic interactions with GO.[25]

Dichtel and coworkers[40] have developed a method to immobilize a protein on GO by non-covalent interactions without destroying its structure by hydrophobic interactions. Unmodified GO is known to be one of the strongest inhibitors of the chymotrypsin (ChT) enzyme, which is

why ChT was used in the experiments. The method is based on the use of tripodal molecules, which have three aromatic pyrene moieties to interact non-covalently with GO's aromatic regions. Thus, the denaturation of ChT can be prevented. Used tripod **1** has an active group that can react covalently with primary amines of proteins. ChT's reaction with tripod **1**-functionalized GO retained its enzymatic activity due to the absence of conformational changes. ChT's interactions with unmodified GO led to the loss of its structure and activity (Figure 12).[40]

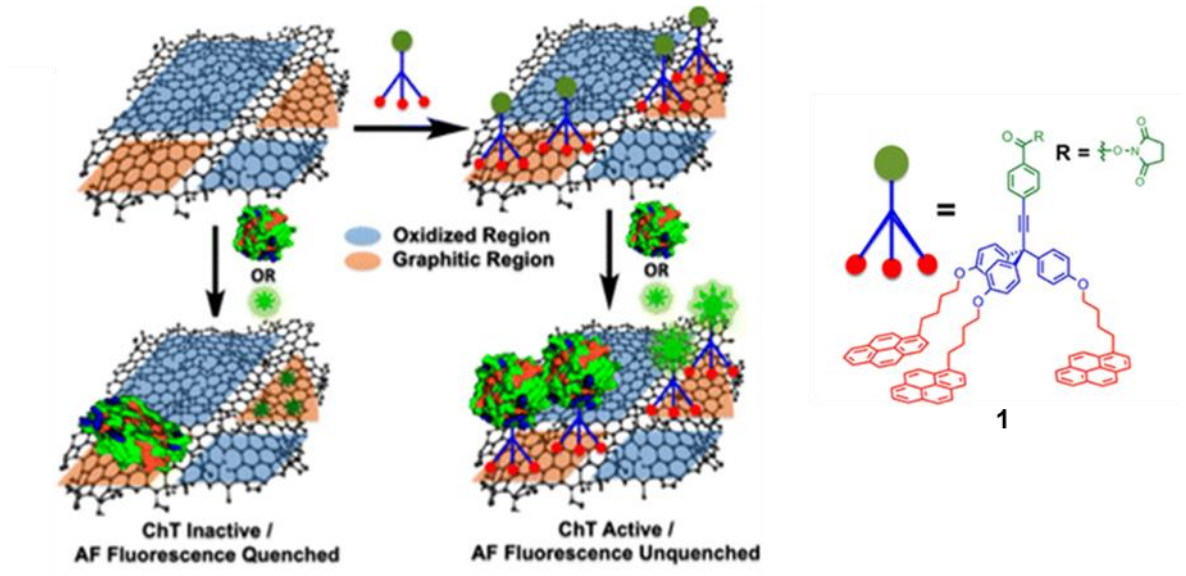

Figure 12. Schematic presentation of the interaction of the protein with GO (left) and with the tripod **1** functionalized GO (right). Adapted from[40], Copyright 2015, American Chemical Society.

3.3 Covalent interactions

It is still unknown which amino acids of proteins participate in covalent reactions with solid substrates. In covalent GO-protein interactions, it is commonly assumed that amino and carboxylic acid groups on protein surfaces are the key groups involved in the immobilization on GO.[25] Figure 13 presents the most common amino acid residues used for bioconjugation of proteins with other biomolecules or chemical tags. The same residues can also be applicable for protein immobilization on GO, with or without preceding chemical modification of GO. In addition, *N*-terminal amino groups and *C*-terminal carboxylic acid groups can participate in covalent bonding, for example by forming amide linkages.[41,42]

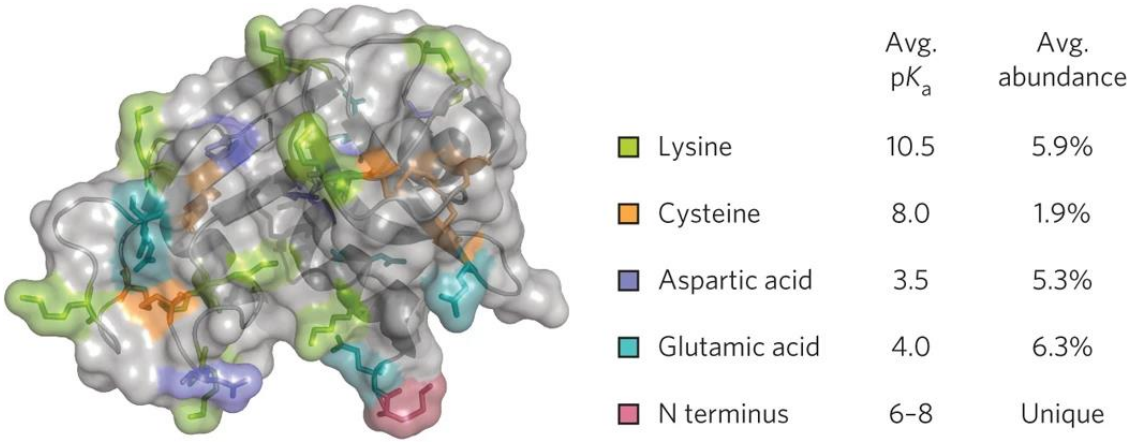

Figure 13. Schematic presentation of the distribution of commonly used amino acid residues in bioconjugation, including their average abundances and the pK_a values (RNAse A enzyme). Reprinted by permission from[41], Copyright 2017, Springer Nature.

Lysine residues are the most involved in covalent reactions due to their reactive ε-amino groups and relatively high abundance on protein surfaces. Also, α-amino groups of *N*-terminal amino acid residues are usually on protein surfaces and hence involved in covalent reactions, but their number in proteins is much lower than lysine residues. More selective covalent binding can only be achieved by reaction only *via* protein's *N*-terminus, especially when a protein consists of a single polypeptide chain (one reactive α-amino group).[41]

4 Covalent functionalization of GO

Covalent and non-covalent protein immobilization can lead to the disruption of a protein structure, which is mostly held together by non-covalent interactions, and further to protein denaturation and loss of its biological function through conformational changes. Covalent interactions usually enable more ordered and stable protein immobilization than weak interactions.[43] Additionally, covalent bonding enhances stability against heat, pH, solvents, and storage.[3] Although non-covalent interactions usually are weaker than covalent interactions, they can rival some covalent bonds when they occur over a large surface.[35]

Protein immobilization on a solid support *via* weak interactions results in random protein orientation. Although covalent protein immobilization can result in specific protein orientation on a support, it requires that both a protein and a support have specific groups which can react together selectively. In the case of a protein, it means that a specific chemical group is added to a certain position of a protein so that the protein conformation and function are retained. Some of the covalent protein immobilization protocols are based on the use of natural, unmodified proteins, which can more often result in the loss of protein conformation after protein-GO interactions than the use of modified proteins.[44] This chapter presents both random (crosslinking) and site-specific approaches (click reactions, Staudinger ligation) for covalent protein immobilization on GO.

4.1 Diimide-activated amidation

Diimide-activated amidation (Figure 14) is a commonly used and relatively straightforward method for the covalent attachment of proteins to materials. It has also been used for covalent protein immobilization on graphitic materials such as carbon nanotubes and GO.[45] The amidation reaction occurs between activated carboxyl groups of GO and amino groups of proteins.[29] Proteins with many lysine or arginine residues on their surfaces (e.g. bovine serum albumin) are probably favorable for the amidation due to the greater number of reactive amino

groups. The main disadvantage of the method is that GO may contain a low number of COOH groups, so the functionalization will remain low.[46]

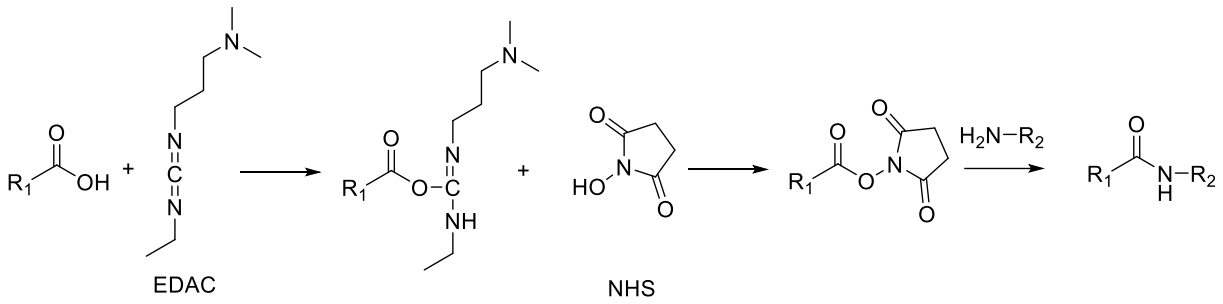

Figure 14. A general reaction path of diimide-activated amidation.

Protein functionalization of GO *via* diimide-activated amidation has three main steps (Figure 15). In the first step, COOH groups of GO are activated with N-ethyl-N'-(3-dimethyl aminopropyl) carbodiimide (EDAC) hydrochloride forming reactive O-acylisourea intermediate. Then, N-hydroxysuccinimide (NHS) is added forming succinimidyl intermediate (step 2), which reacts with the amino groups of protein, forming an amide bond between chemically modified GO and a protein (step 3).[29] NHS is needed in the reaction because O-acylisourea intermediate is very reactive in an aqueous environment, and its lifetime may not be long enough for the reaction with a protein. Without NHS, intermolecular conjugation of proteins rich in amino and COOH groups on their surfaces can occur.[45]

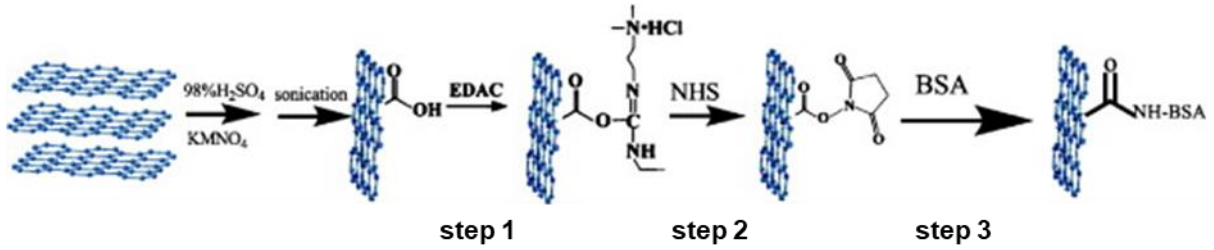

Figure 15. Protein immobilization on GO *via* diimide-activated amidation reaction. Adapted with permission from[29], Copyright 2010, Elsevier.

4.2 Carboxylation and amination

GO usually contains fewer COOH groups than other functionalities, and they usually locate at the edges of GO sheets. However, more COOH groups on the basal plane of GO can be synthesized by carboxylation of epoxy and OH groups, which enhances GO's water solubility. A widely used method is to treat GO with chloroacetic acid **2** under strongly basic conditions such as sodium hydroxide-water solution (Figure 16). Chloroacetic acid **2** reacts with epoxy groups through a ring-opening reaction forming OH and O-COOH groups. OH groups can further react to O-COOH.[47]

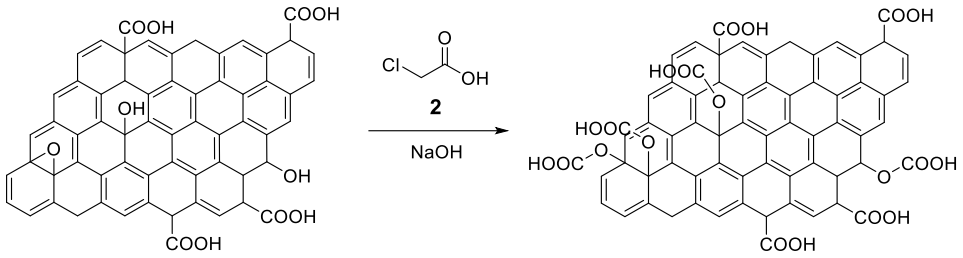

Figure 16. General carboxylation protocol of GO with chloroacetic **2** acid and sodium hydroxide.[47]

Faghihi e*t al.*[47] have studied the efficiency of the GO carboxylation method. GO carboxylation was performed in four different chloroacetic acid concentrations (0.5, 1, 2, and 3 M) using a 4 M NaOH water solution. Quantitative amounts of COOH groups of GO and carboxylated GO samples were estimated by methylene blue (MB) assay, as an MB molecule can interact covalently with a COOH group. Hence, the change in MB concentration before and after the reaction can estimate the number of COOH groups in GO. Based on the experiments, the number of COOH groups increased significantly after carboxylation with 1 M or 2 M chloroacetic acid.[47]

A large amount of COOH on the GO surface may, however, be unfavorable for covalent protein immobilization: The GO surface can be highly negatively charged, which attracts positively charged molecules *via* electrostatic interactions. Also, the folding of GO sheets can be more probable when the number of COOH is substantial.[47]

Carboxylation of GO requires strongly basic conditions. However, strong bases, such as NaOH with chloroacetic acid, can cause partial reduction of GO resulting in a lower number of oxygen-containing functional groups. Bianco *et al.*[48] have observed partial reduction of GO during carboxylation by the same method mentioned above. C/O ratio was higher after carboxylation, and the number of COOH groups increased, but the number of C-O bonds decreased, indicating the removal of labile oxygen-containing groups.[48]

Bianco *et al.*[48] also studied how efficient GO carboxylation is in the GO double functionalization (Figure 17). At first, GO was functionalized with aminated PEG **3** through an epoxide ring-opening reaction. Then, epoxy and OH groups of the amine-functionalized GO were carboxylated, leading to a significantly lower number of amine groups than before carboxylation. After diimide-activated amidation of COOH groups with an aminated PEG polymer chain **3**, the number of amine groups increased but was still remarkably lower than after the first NH_2-PEG functionalization. However, a more efficient NH_2-PEG double functionalization of GO was achieved without carboxylation, although the number of GO COOH groups was lower.[48]

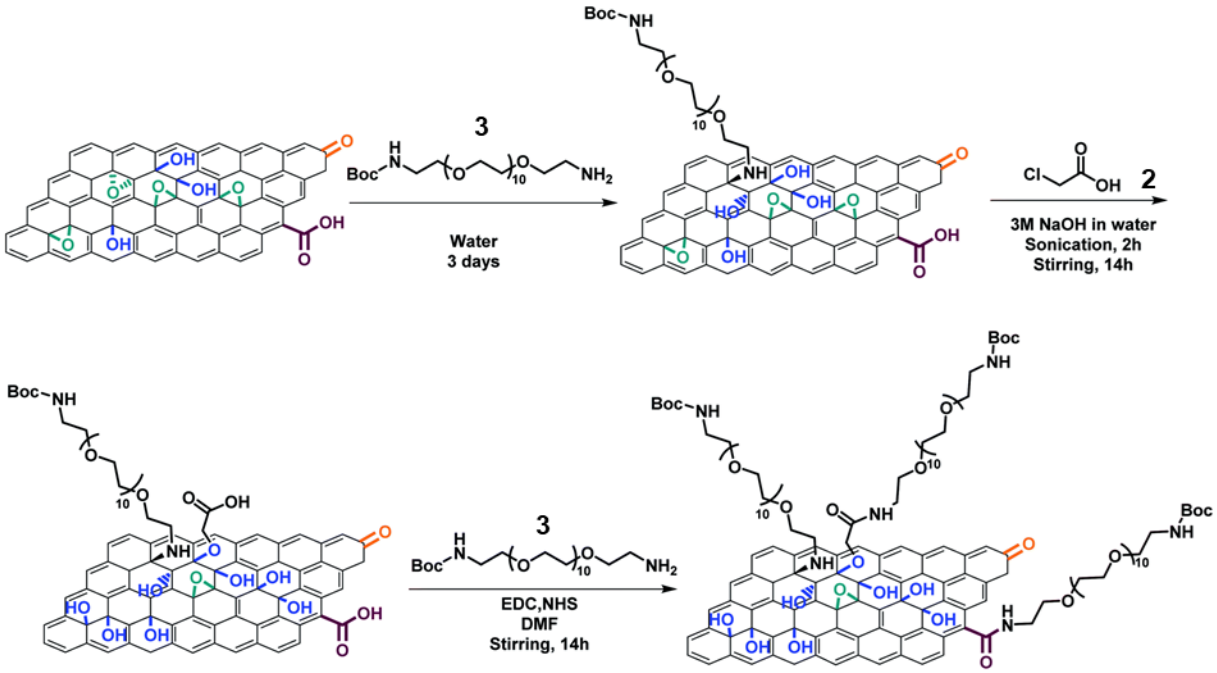

Figure 17. Double functionalization of GO *via* epoxide ring-opening (top) and diimide-activated amidation after carboxylation (bottom). Reprinted from[48], Copyright 2020, published by The Royal Society of Chemistry, https://creativecommons.org/licenses/by-nc/3.0/.

Instead of carboxylation, GO can be aminated for further functionalization or direct reaction with the COOH group of a protein. Epoxy groups of GO are reactive to nucleophiles and will react through ring-opening reactions. Salvio and coworkers[49] have developed a method to synthesize amino-functionalized GO flakes. An epoxide ring-opening reaction was conducted using sodium azide, which led to the formation of OH and azide groups. Then, azide groups were reduced to amines using the reducing agent lithium aluminum hydride ($LiAlH_4$). Although the method resulted in a high degree of functionalization, its total duration only for GO functionalization is almost one month, and the reaction can also form explosive intermediates.[49]

4.3 Crosslinking

4.3.1 Glutaraldehyde

Proteins can be attached to GO *via* chemical crosslinking, which means that a protein and GO are connected *via* a crosslinker molecule. In polymer chemistry, crosslinking means covalent linkages between the polymer chains. This idea can also be applied to the covalent protein immobilization on GO. By using crosslinkers or spacer molecules to attach a protein to GO, its quaternary structure and hence biological function can be retained. Crosslinkers increase the distance between GO and protein when direct absorption *via* non-covalent interactions on GO reduces.[25]

A widely used crosslinking agent for bioconjugation is glutaraldehyde **4** (GA; Figure 18). It has also been used for covalent protein immobilization on GO. Advantages of using GA are good solubility in water and organic solvents and high reactivity. However, in aqueous solutions, GA can exist in various forms, such as monomer, dimer, or polymer chains, depending on pH and other chemical species in the solution (Figure 18).[50] Approximately 13 possible structural forms of GA in aqueous solution complicate the prediction of its reaction outcomes. Also, polymerization causes a problem, as it diminishes the organization of the functionalization. However, polymerization can be avoided by using small amounts of GA relative to the quantity

of GO.[51,52] GA polymer chains can be converted back to monomers at neutral or basic pH by heating or sonication.[50]

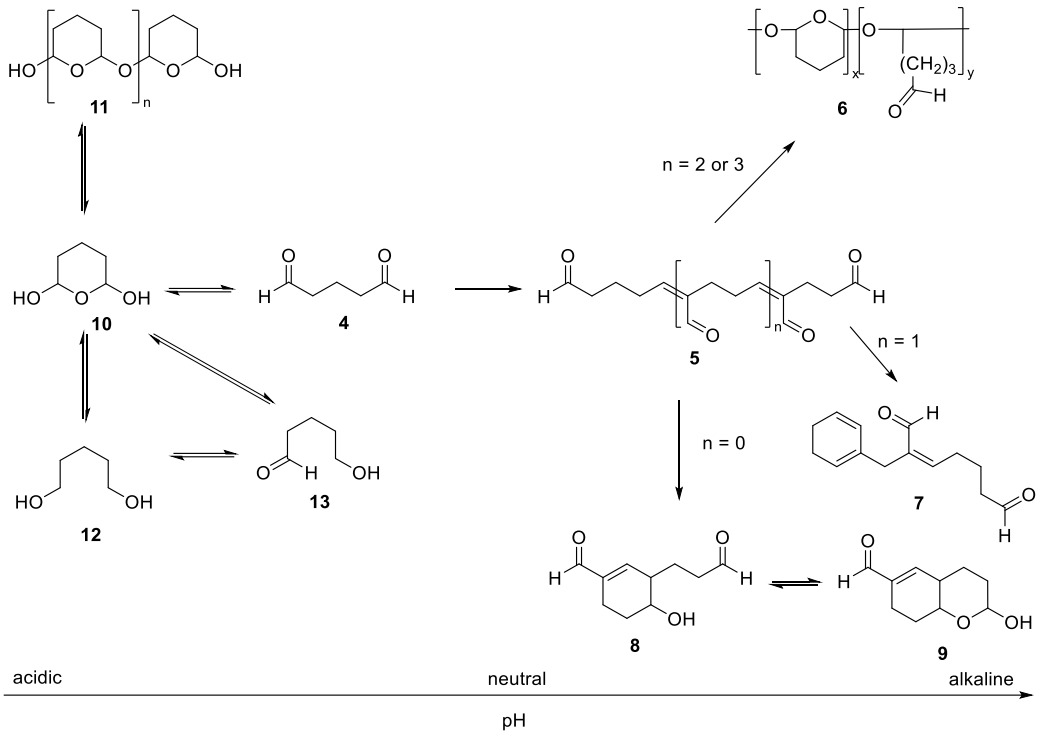

Figure 18. Some possible structural forms of GA in the aquatic environment at different pH.[50]

There is still no agreement on the primary structure of GA in each pH, but many suggestions have been presented. In some studies, commercially available GA solutions have been observed to be mainly mixtures of GA polymers, such as forms **5-7** at neutral or alkaline pH (Figure 18). Also, forms **8** and **9** have been suggested to exist in alkaline solutions. Only a tiny amount of form **5** was found at acidic pH, and GA was predicted to be mainly in form **4** and its hydrated forms **10**, **12,** and **13** (equilibrium between the forms). On the other hand, it has been proposed that acidic aqueous solutions of GA could contain structures of **4**, **10,** and **11**.[50] Because of many suggested GA structures in an aqueous solution, GA is presented as its monomer **4** in the GO functionalization reactions for clarity.

Aldehydes react with amines forming imines and with alcohols forming hemiacetals and acetals, depending on the stoichiometric amount of alcohol.[53] Hence, in GO functionalization, GA will react with hydroxyl groups of GO forming hemiacetal or acetal bridges (assuming that GA is in form **4**).[51,52] The order of addition of GO or GA may determine how aldehyde groups of GA react with hydroxyl groups of GO. Tan *et al.*[51] have shown that when GA is slowly (dropwise)

added to the GO-water dispersion, GA forms crosslinks between GO sheets *via* both terminal aldehydes (Figure 19a). However, if the GO dispersion is added slowly to the GA solution, GA molecules react only *via* one terminal aldehyde group forming GA grafted graphene oxide nanosheets (Figure 19b). This is most likely due to the smaller number of available hydroxyl groups.[51]

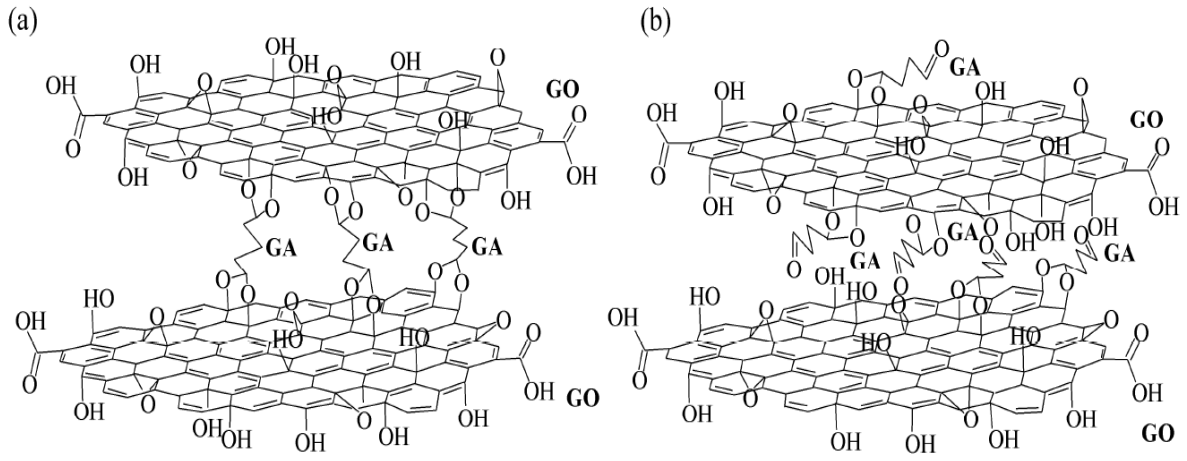

Figure 19. a) GA crosslinked and b) GA grafted GO nanosheets. Reprinted by permission from[51], Copyright 2013, Springer Nature.

After the covalent functionalization of GO, structural changes can be semiquantitatively analyzed with the unvarying C=C peak near 1630 cm^{-1}. The FTIR spectra of GA crosslinked GO (GA-GO_2) and GA grafted GO (GA-GO) show differences: The higher intensity of C=O stretching at ~1724 cm^{-1} (aldehyde) compared with C=C peak indicate the unreacted aldehyde groups in GA-GO compared with GA-GO_2 (Figure 20). The corresponding relative intensities between GA-GO_2 and non-functionalized GO were close to each other (0.61 and 0.59), indicating no remarkable change in the number of aldehyde functionalities after GA functionalization.[51]

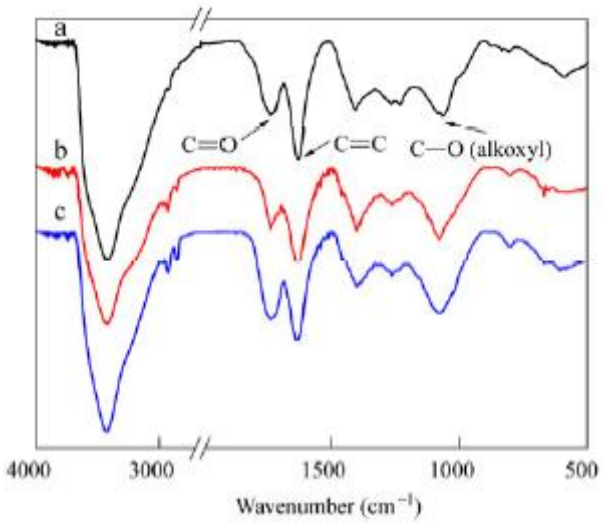

Figure 20. FTIR spectra of freeze-dehydrated a) GO, b) GA-GO (crosslinked), and c) GA-GO (grafted). Reprinted by permission from[51], Copyright 2013, Springer Nature.

Successful covalent binding of GA to GO can be observed from several FTIR peaks (Figure 20). The peaks at 2800-3000 cm^{-1} correspond probably to the C-H stretching of GA. Also, the relative intensities of C=C (~1625 cm^{-1}) and C-O (alkoxy, ~ 1100 cm^{-1}) peaks increase after GA binding, which indicates the increase in the number of alkoxy groups and suggests the presence of covalent bonds between GA and GO.[51] It has also been observed that the relative intensities of OH-group peaks at 3300-3500 cm^{-1} reduced remarkably after GA or glyoxal binding to GO. This indicates that these dialdehydes react with OH groups of GO.[54]

As some aldehyde groups of GA remain unreacted after the reaction with GO, they can further react with NH_2 groups of proteins, such as a free amino group in the *N*-terminus of the polypeptide chain forming imine bonds (Schiff bases, enhanced in alkaline pH).[55] It has been experimentally proved that GA is most reactive towards unprotonated ε-amino groups of lysine amino acids.[56] Although most lysine residues are protonated at acidic and neutral pH, a low number of unprotonated lysine residues are sufficient to transfer acid-base equilibrium towards deprotonation. As polar moieties, lysine residues usually locate on protein surfaces. Lysine side chains are generally not in enzymes' active sites, which means that the enzyme's conformation and biological activity retain after modification to a lysine residue.[50] Histidine and tyrosine residues can also react with GA, but they are less reactive than free amino groups.[56]

Figure 21 presents the proposed reactions of monomeric and polymeric forms of GA with an amino group of protein. The most common way to describe the reaction is Schiff base formation, in which imine bond forms between amino and aldehyde groups (Figure 21a). The formed Schiff base is very unstable, especially in acidic pH, and will easily return to free starting materials. However, Schiff base formation is enhanced in alkaline pH, and imine bond can be converted to a more stable imine linkage by using a reducing agent.[57a] In addition to a Schiff base formation, many other reactions may happen due to various structures of GA. Figure 21b presents possible reaction pathways of polymeric GA and protein molecules. In reaction 1, a protein reacts with GA's aldehyde group, forming a Schiff base, stabilized by conjugation in the GA polymer chain. Another possibility is reaction 2, where a protein reacts with an ethylenic double bond. However, this reaction requires an excess of amino groups.[50]

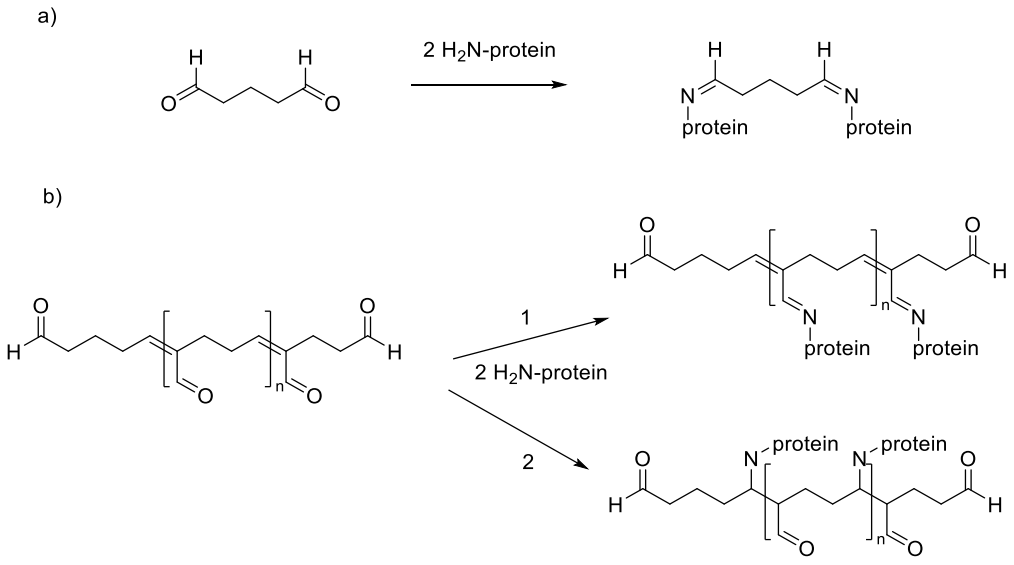

Figure 21. Proposed reactions between GA and a protein. a) Schiff base formation.[57a] b) Schiff base formation stabilized by conjugation (reaction 1), and conjugated addition of a protein to the ethylenic double bond of GA polymer (reaction 2).[50]

Lactoperoxidase enzyme (LPO) has been covalently immobilized on GO flakes *via* GA crosslinker (pH 6.8),[55] which can also crosslink GO sheets together (Figure 22). The thermal stability of crosslinked LPO was better than free LPO's stability, and crosslinked LPO had maximum enzymatic activity at a higher temperature and more alkaline pH than free LPO. Formed bonds between LPO's lysine residues and GA resulted in a net anionic charge to the system, which might cause the pH change of LPO. The increase in optimum pH, on the other hand, can result from the reduced free movement of crosslinked LPO.[55]

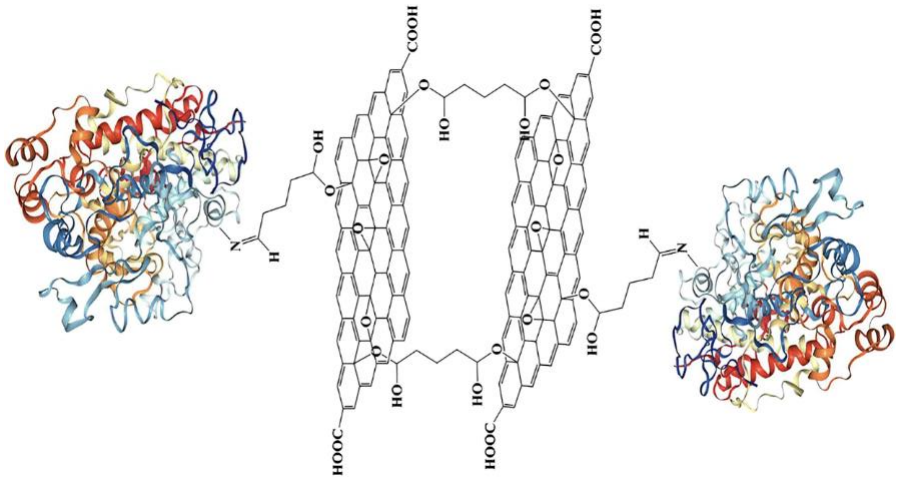

Figure 22. Crosslinking between GO-GA and GA-enzyme (lactoperoxidase). Reprinted by permission from[55], Copyright 2018, Springer Nature.

4.3.2 Silane crosslinkers

The surface of GO can be functionalized with organosilanes and further other crosslinkers. In the presence of water, silanes hydrolyze easily into reactive silanols, and they can form Si-O-Si bonds on the surface of GO through silanol condensation (Figure 23a).[57b] However, the formation of silane coating requires that silanols are close to each other. For example, surface silanization of GO have been done with (3-aminopropyl) triethoxysilane (APTES) under mild reaction conditions.[58] APTES can react either *via* its amino group forming amine linkage with GO's epoxy group or *via* its ethoxysilane group forming Si-O-C bonds with OH groups of GO (Figure 23b). Serodre *et al.*[58] have proposed that both reactions occur simultaneously, resulting in amino and silanol groups on the surface of functionalized GO. The number of epoxy and OH groups decreased at the same time as amine and Si-O-C bonds formed, which was confirmed with XPS, FTIR, and TGA-FTIR measurements.[58]

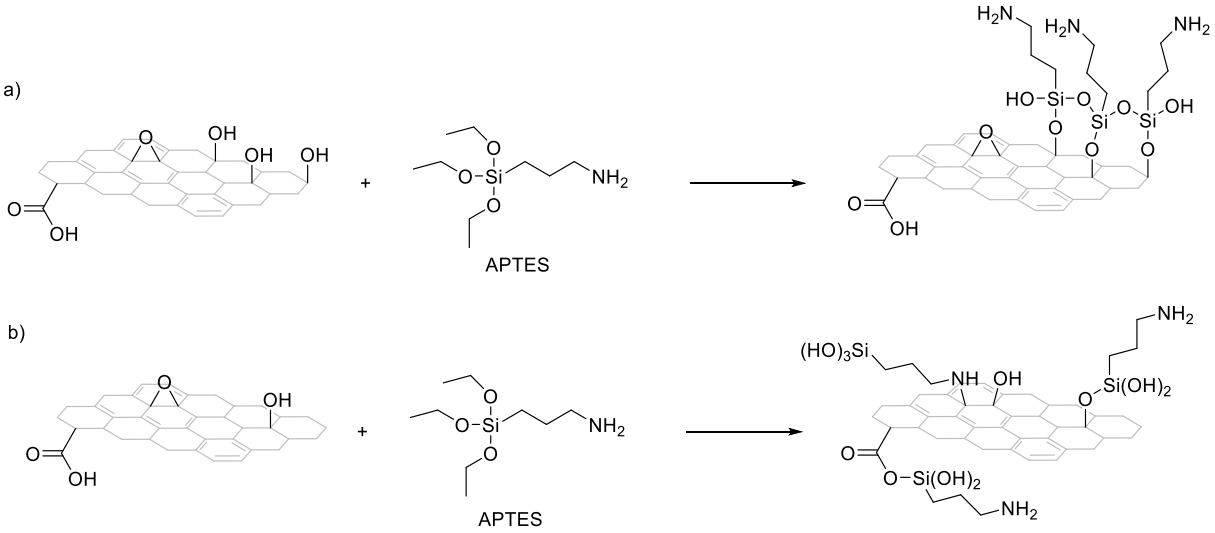

Figure 23. a) Reaction of GO with APTES and formation of silane coating through silanol condensation in water. [57b] b) Three possible types of reactions between APTES and GO in the presence of water.[58]

Laccase enzyme has been immobilized on GO *via* a double crosslinker system, 3-aminopropyl trimethoxy silane (APTMS) and GA.[59] APTMS reacts with GO similarly to APTES. However, reaction with GO's OH groups is more favorable because it leaves free amino groups for GA crosslinking.[58] After amine functionalization, GA is added to insert aldehyde groups to GO, which can further react with amino groups of protein, such as laccase enzyme (Figure 24).[59]

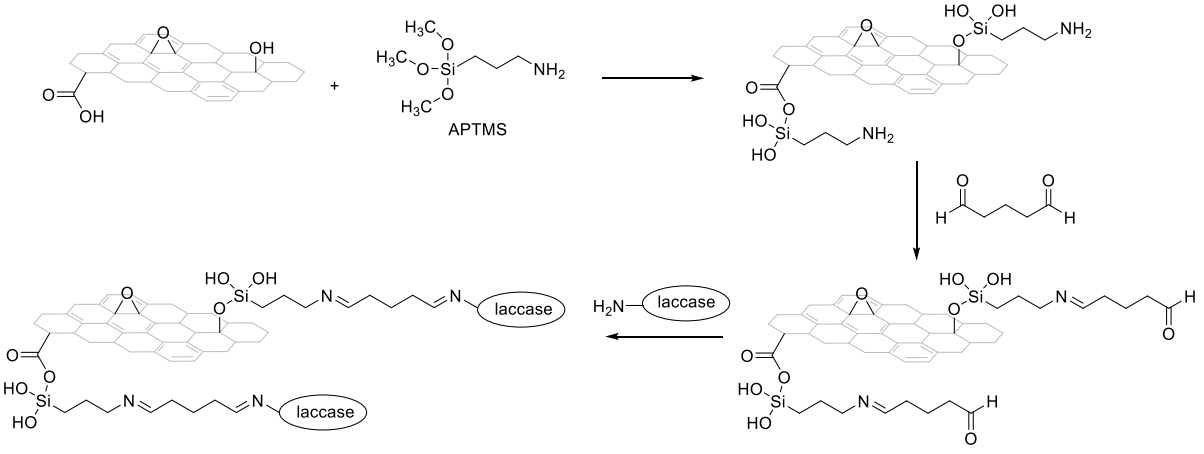

Figure 24. Schematic representation of laccase immobilization on GO using APTMS and GA crosslinkers.[59]

4.4 Click reactions

Sharpless *et al.*[60] introduced the term "click chemistry" in 2001 to describe fast, "spring-loaded", and highly selective organic reactions. In a typical click reaction, covalent bond forms between carbon and a heteroatom. The reaction has a high thermodynamic driving force (> 20 kcal/mol), enabling fast completion of the reaction. Also, click chemistry reactions have a high yield of final products, easy purification, high stereospecificity, and simple reaction conditions.[60] In biomedical applications, four click reaction types are commonly used; cycloaddition, nucleophilic ring-opening, non-aldol carbonylation, and carbon-carbon multiple bond addition reactions.[61] However, cycloaddition reactions are mainly utilized in functionalization of GO.

4.4.1 Copper-catalyzed azide-alkyne cycloaddition (CuAAC)

The most typical click reaction utilized in GO functionalization is copper-catalyzed cycloaddition of azides and alkynes (CuAAC), which forms stable triazole linkage in acidic or basic organic solvents. Copper (I) catalyst is needed in the reaction temperatures favorable for GO and proteins. Functional groups participating in azide-alkyne cycloaddition are unreactive toward biological molecules, such as proteins. Hence, the reaction is highly specific. Azide-alkyne reactions have been used for protein conjugation, so it would also be applicable for covalent protein immobilization on GO.[57c]

Alkynyl terminated poly(ethylene)glycol (PEG) and amino acids have been connected to azide-functionalized GO sheets utilizing the cycloaddition approach (Figure 25). First, COOH groups of GO were activated with EDC and NHS as in diimide-activated amidation. After that, 3-azidopropan-1-amine **14** reacted with the modified GO by EDC condensation, resulting in azide-functionalized GO. Then, alkynyl terminated amino acid or PEG chain was added, and selective cycloaddition of alkyne and azide took place (Figure 25).[62] This approach can be applicable also for larger macromolecules such as proteins and enzymes because they can be modified to have an alkyne group.[44]

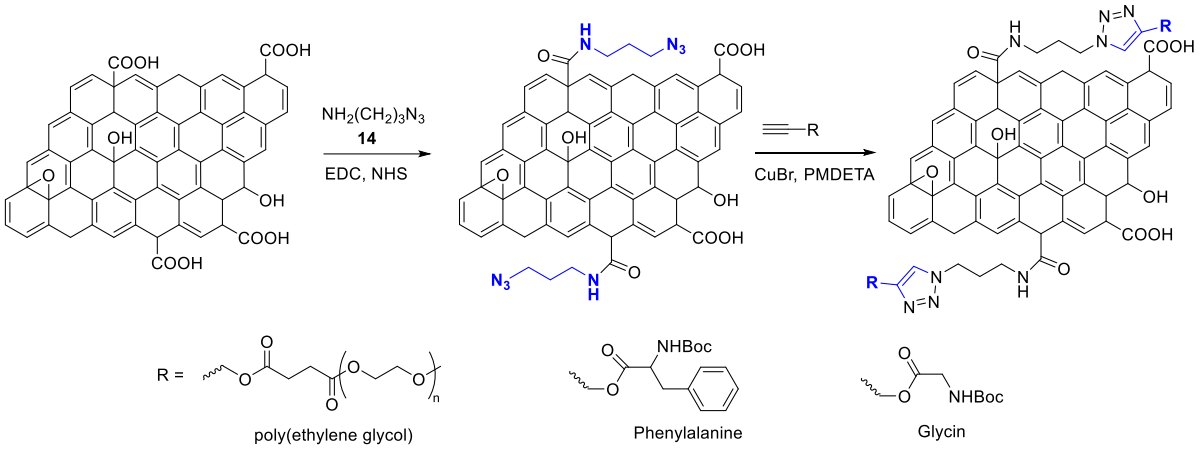

Figure 25. Covalent functionalization of GO with azide and addition of amino acids and polymers through CuAAC reaction. Adapted from the article[62].

Successful covalent attachment of azide groups on GO was confirmed from the FTIR spectrum, where the characteristic peak of azide groups at 2098 cm^{-1} can be observed. After the click reaction, the azide peak disappeared, and the peak at 1100 cm^{-1} indicated the stretching of C-O groups of PEG.[62]

The cycloaddition can also occur the other way round, between alkynyl functionalized GO and azide functionalized peptide (Figure 26). In Shi and coworkers' study,[63] hydroxyl groups of GO were converted to alkynyl groups through silanization with alkynyl-containing silane coupling agent **15**. The CuAAC reaction of functionalized GO and the azide-functionalized peptide was then performed.[63] The peptides used in the experiments were RGD peptides, a class of peptides enhancing cell adhesion. The abbreviation RGD signifies that this sort of peptides always contain an amino acid sequence of arginine (R), glycine (G), and aspartic acid (D).[64]

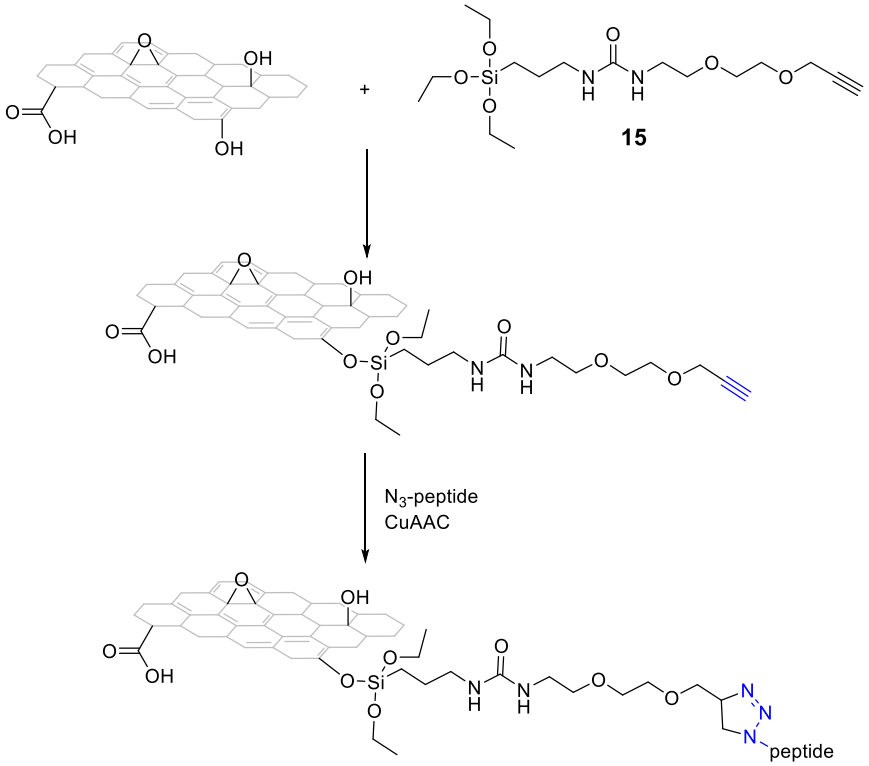

Figure 26. Reaction pathway of GO alkynyl-modification and azide-alkyne cycloaddition of the modified GO and azide-functionalized peptide.[63]

4.4.2 Double functionalization

Al-Jamal *et al.*[65] have modified GO to have both reactive sites, -N_3 and alkyne groups, for CuAAC double click reactions with propargyl-modified angiopep-2 **18** and di-azide-modified PEG **19** (Figure 27). N_3 groups were directly attached to GO through a 1,2-epoxide ring-opening reaction with NaN_3. Silyl-protected alkyne moieties **17** were attached to GO's COOH groups. After double functionalization of GO, an alkyne-modified peptide **18** was attached to GO *via* the first CuAAC click reaction. For the second click reaction with azide-PEG **19**, the silyl protecting group of GO propargyl group was removed. Both click reactions were achieved under the same reaction conditions. The advantage of this method is that COOH groups of GO are saved for later functionalization, such as adding alkyne functionality to GO. [65]

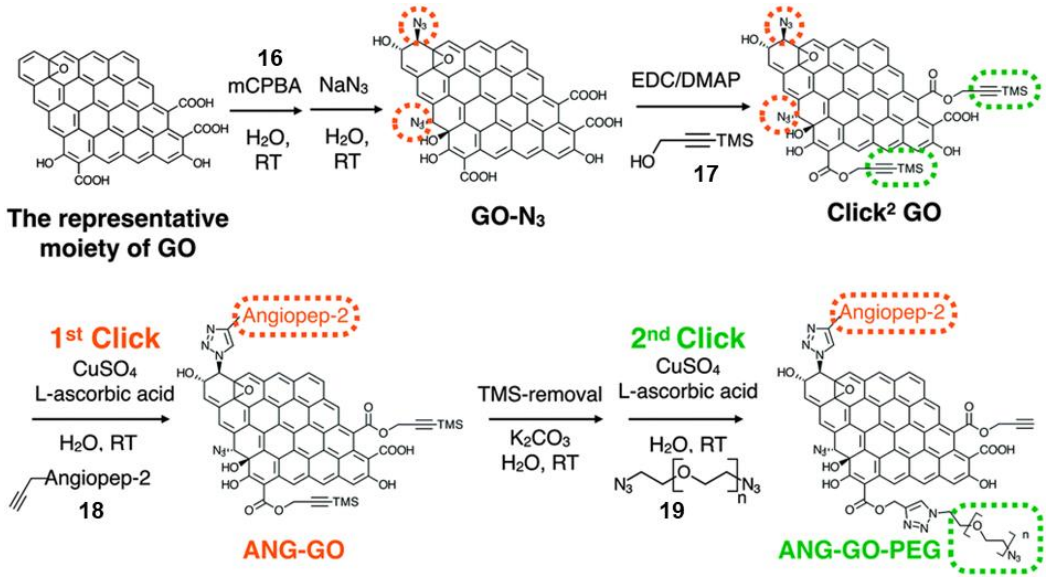

Figure 27. Double azide-alkyne functionalization of GO for sequential CuAAC click reactions with propargyl-angiopep-2 and azide-PEG. Reprinted from[65], Copyright 2015, Published by The Royal Society of Chemistry.

It is noteworthy that more epoxy groups are generated in the first step with *meta*-chloroperoxybenzoic acid **16** (mCPBA; Figure 27). With more epoxy groups, it is possible to enhance the number of azide groups resulting from the functionalization mentioned above. In the work of Al-Jamal *et al.*,[65] the azide content in functionalized GO was increased 14 % compared to GO without mCPBA treatment.[65]

Azide-functionalization of GO can also be done simultaneously *via* its OH and COOH groups (Figure 28).[66] When GO is treated with 2-chloroethyl isocyanate **20**, COOH groups form amide bonds, and OH groups form carbamate esters with the isocyanate. Then, chlorine atoms are substituted by azide groups using sodium azide. Azide-GO is water-soluble, but it tends to aggregate in the presence of copper ions.[66,67] This approach is useful when only azide functionalities of GO are needed but not as useful for CuAAC click reactions.

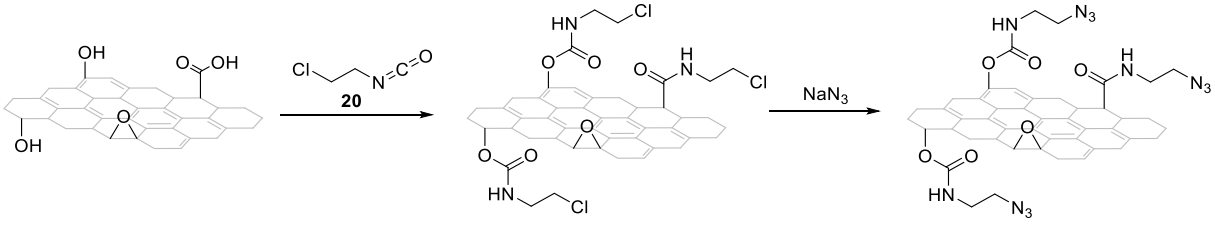

Figure 28. An alternative route for azide-functionalization of GO.[66,67]

Vacchi and coworkers[68] have studied the controlled double functionalization of GO *via* its hydroxyl and epoxy groups. Two different strategies conducted on different GO samples were analyzed (Figure 29). In the first approach (GO-OE → GO-OE-W), GO prepared by Hummers' method with the average thickness of 20 nm was used. In the second approach (GO-OE → GO-OE-EST), GO was prepared from carbon nanofibers by rolling and exfoliation into monolayers with thicknesses of 1 nm. This GO sample was more water dispersible and contained fewer aggregated GO sheets.[68]

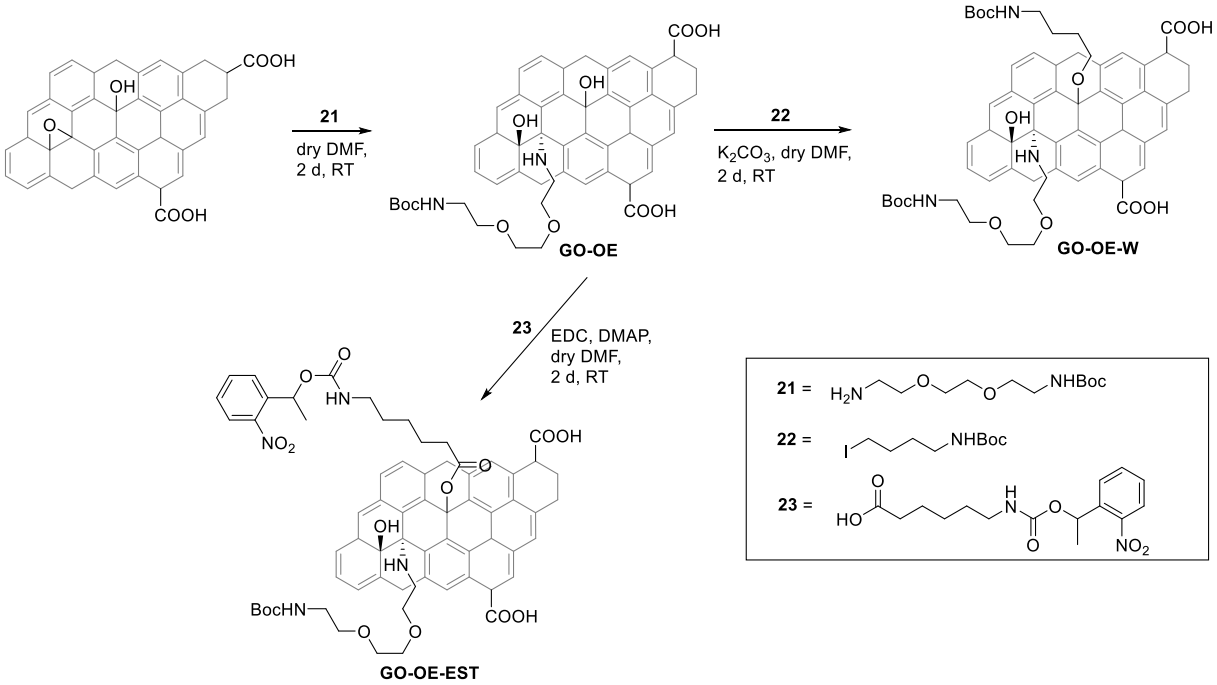

Figure 29. Two routes for GO double functionalization with protected amine derivatives. Adapted from[68].

In the first step of double functionalization, GO's epoxy groups react with monoprotected triethylene glycol diamine **21** through epoxide ring-opening reaction (Figure 29). Hydroxyl groups of the obtained GO-OE intermediate (step 1) further react with Boc-protected 4-iodo-butylamine **22** through Williamson ether synthesis. Protecting groups of both amines can be simultaneously removed with HCl in 1,4-dioxane. Although double functionalization was successful, the Williamson reaction did not yield as high amine loading as an equivalent monofunctionalization approach without an epoxide ring-opening reaction. Possible reasons for the lower functionalization degree of the second reaction can be instability of some GO's OH groups or steric hindrance caused by molecules inserted into GO's surface after the first reaction.[68]

In another approach, the opening of epoxy groups is followed by the esterification reaction of GO's hydroxyl groups (Figure 29). Intermediate GO-OE reacted with synthesized 1-(2-nitrophenyl) ethyl carbamate-protected amine **23** in the presence of coupling agents EDC and DMAP. Two protecting groups for primary amines were used, Boc- and 1-(2-nitrophenyl) ethyl carbamate, to enable selective amine derivatization. The final product GO-OE-EST was treated with HCl in 1,4-dioxane to remove the Boc-protecting group. Then, 1-(2-nitrophenyl) ethyl carbamate protection was removed by irradiating at 365 nm. As in the first approach, also here the second reaction yielded lower amine loading than the same reaction in GO's monofunctionalization.[68]

In conclusion, the introduced double functionalized GOs could be applicable for covalent protein immobilization, for example, *via* proteins' *C*-terminus through amidation reaction. The total functionalization degree of both double functionalization approaches is higher than each functionalization individually because both OH and epoxy groups can be utilized for protein immobilization. The second approach enables the preparation of multifunctional GO materials, whereas the first one enhances the total amount of immobilized protein.

Also, other reactive moieties can be inserted on GO *via* double functionalization, such as a benzoquinone molecule. Shi and coworkers[69] have developed a method in which Boc-protected cysteamine **24** and benzoquinone **25** are linked to GO leading to two different reactive sites for further modifications (Figure 30). First, protected cysteamine **24** is added to GO dispersion, forming new OH groups and thioether linkages through epoxide ring-opening reaction. Then, benzoquinone **25** reacts with GO's OH groups through nucleophilic substitution reaction resulting in grafted hydroquinone on GO. Benzoquinone **25** is reactive towards amines, azides, phosphines, and thiols (Michael addition), and it has been used to conjugate biomolecules, such as proteins. Here, phenylalanine derivative **26** was covalently attached to GO via hydroquinone through a nucleophilic addition reaction. 3-(pentafluorothio)-phenylalanine **26** was chosen for the reaction because it has COOH groups, which can further react with amines or alcohols. Also, fluorine moiety facilitated the characterization of the double functionalized GO derivatives.[69] An advantage of the presented method is the diversity of possible reactions, enabling the conjugation of various biomolecules, including proteins.

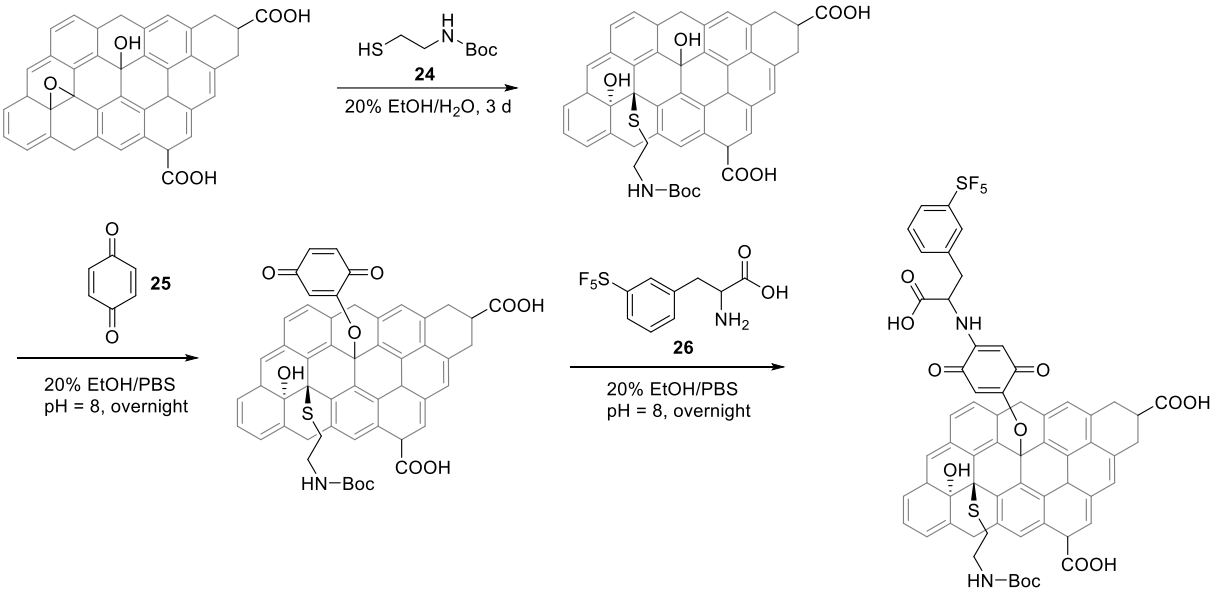

Figure 30. Reaction pathway for benzoquinone-based double functionalization of GO.[69]

4.4.3 Staudinger ligation reaction

In bioconjugation techniques, Staudinger ligation is an efficient, fast, and selective method to synthesize, modify and label proteins and peptides, and immobilize them on solid surfaces. Staudinger ligation is a click-type reaction with biocompatible reaction conditions, in which an amide bond forms in three steps between acylated phosphane and azide-containing moiety (Figure 31).[70]

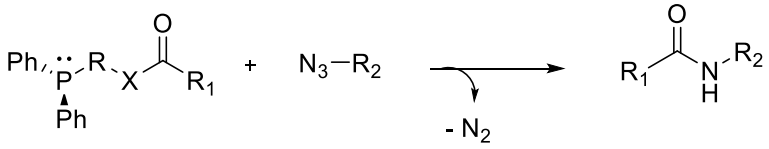

Figure 31. A general reaction of Staudinger ligation.[70]

Studies concerning protein immobilization on GO through Staudinger ligation were not found, but it has been done on other materials. The reactive phosphane derivatives can be introduced onto solid surfaces containing amine groups, which could also be applied to similar functionalization of GO. Soellner *et al.*[71] have immobilized a protein on phosphinothioester-derivatized glass surface *via* Staudinger ligation reaction (Figure 32). In the first step, the

amine-derivatized glass surface is modified with succinimidyl (NHS) ester terminated PEG **28**. Then, phosphinothioester moiety is introduced *via* phosphine-containing reagent **29**. Staudinger ligation was conducted using two differently labelled peptide chains of RNase S´ enzyme, which was followed by incubation with S-protein leading to the generation of active RNase S´ enzyme: Azido group either replacing an ε-amino group of lysine ((N_3) Lys1 S15) or in the PEG-terminus of the peptide chain (N_3-PEG-S15). The Staudinger ligation of the enzyme through lysine residue resulted in lower yield and enzymatic activity (51 % and 85 %, respectively) than the reaction through the PEG-terminus of the enzyme (65 % and 92 %, respectively).[71]

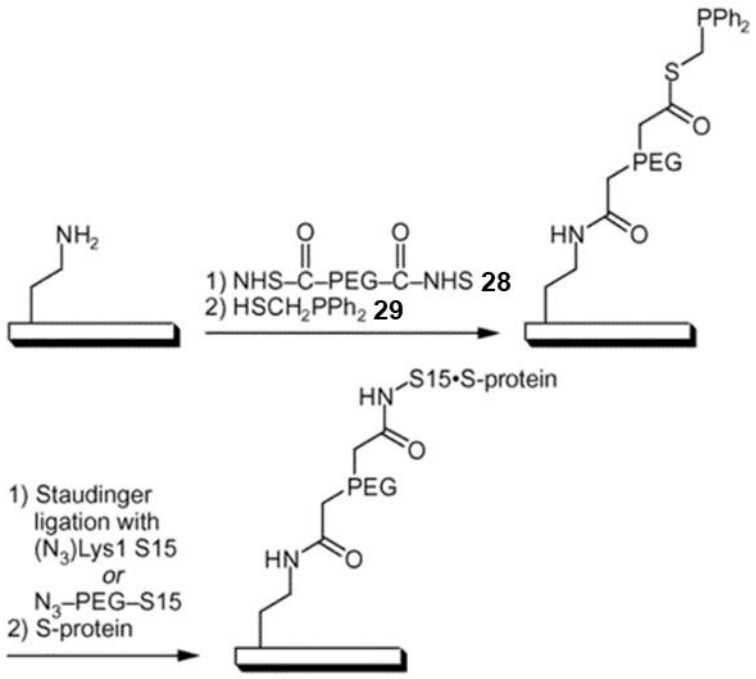

Figure 32. Phosphane group introduction to amine-containing surface and Staudinger ligation of an enzyme to a solid surface. Reprinted with permission from[71] Copyright 2003, American chemical society.

4.4.4 Azide and alkyne labeling of proteins

Proteins can be chemically or biochemically modified to have unnatural reactive groups for covalent reactions such as azide or alkyne groups. The presence of unnatural groups on protein surfaces enables selective covalent reactions through these groups, typically click reactions. For

example, azido-moiety can be added into lysine residues or *N*-terminus of proteins using diazo compound **30**, which replaces protein's primary amine group with its azide group (Figure 33).[72]

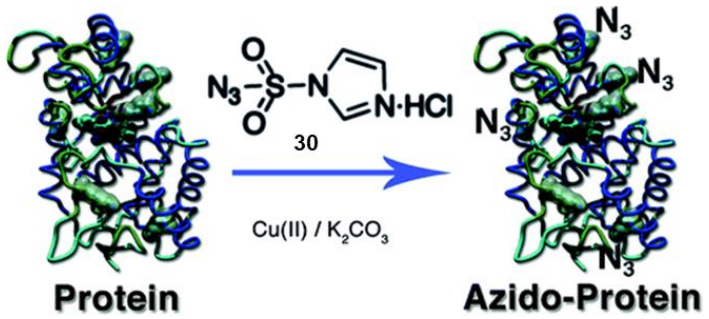

Figure 33. Azide labeling of protein with diazo compound **27**. Adapted with permission from[72]. Copyright 2009, American Chemical Society.

A more selective method to introduce azide group into protein is Inoue *et al.*'s[73] method, in which azide group is added specifically on protein's *N*-terminal amino group (Figure 34). The method is based on the use of bioconjugation reagents, derivatives of 6-(azidomethyl)-2-pyridinecarbaldehyde **31** (6AMPC). 6AMPC derivatives enable both selective azide-labeling of protein's *N*-terminus and the CuACC reaction with alkynes.[73]

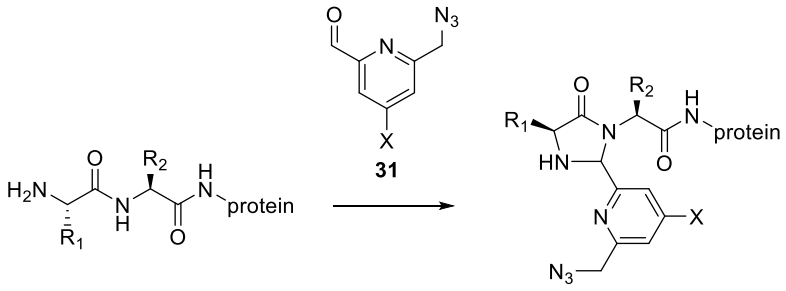

Figure 34. *N*-terminal azide-labeling of protein. Adapted from the article[73].

Chemical alkyne-labeling of peptides has been done earlier,[65] but in the case of proteins, alkyne-labeling often requires semisynthetic or biosynthetic (e.g., genetic engineering) approaches[44]. A common method to introduce chemical groups to proteins is expressed protein ligation (EPL), in which a chemically labeled polypeptide chain is added to the *N*- or *C*-terminus of a biologically produced protein. EPL method can also be used for the introduction of other functional groups.[74]

4.4.5 Thiol-ene click reaction

Seppälä *et al.*[75] have developed a one-step synthesis, in which carbon-carbon double bonds of GO react with thiols through thiol-ene click reaction (Figure 35). In the experiment, GO reacted with cysteamine hydrochloride **32** in the presence of a thermal catalyst, 2,2-azobis(2-methylpropionitrile) (AIBN). Because an amine group of the cysteamine **32** was protected by hydrochloride, deprotection was done with NaOH. The presented approach is an effective method for GO functionalization because thiol compounds are reactive towards C-C double bonds of the graphitic lattice. Also, it can be applied to other than amino-functionalization by changing the thiol reagent.[75]

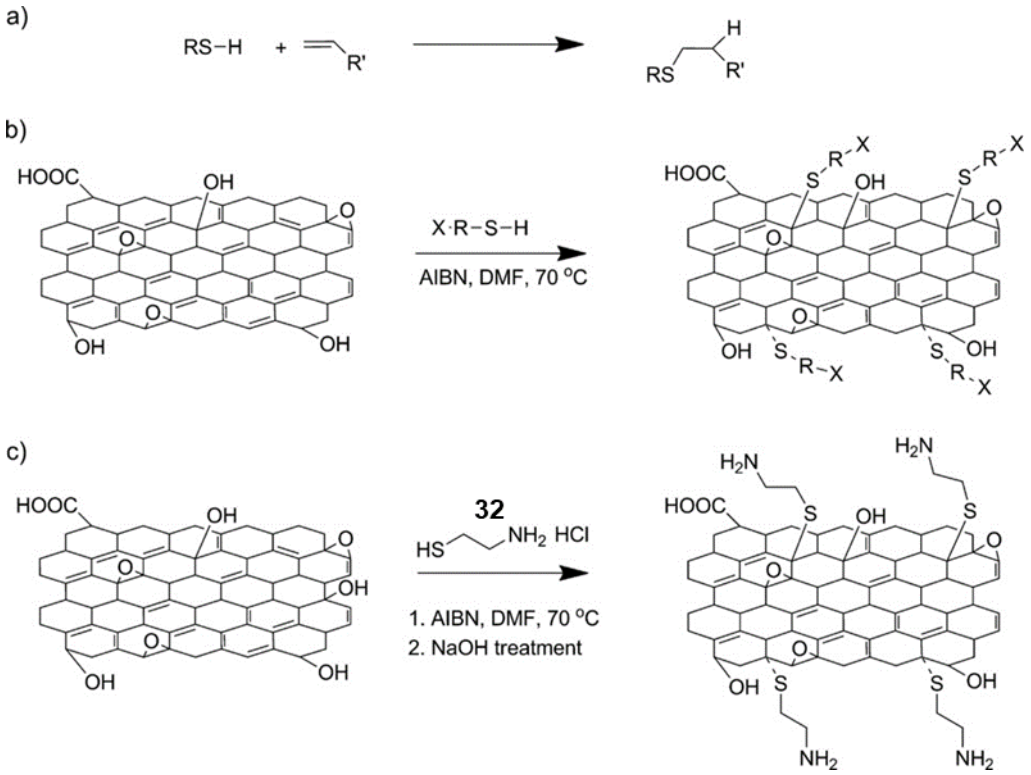

Figure 35. a) Schematic presentation of the thiol-ene click reaction. b) GO modification *via* thiol-ene reaction. c) Amino-functionalization of GO *via* thiol-ene reaction with cysteamine hydrochloride. Reprinted from[75], Copyright 2015, published by Wiley-VCH Verlag GmbH & Co.; https://creativecommons.org/licenses/by-nc/4.0/.

Literature about protein immobilization on GO using cysteamine crosslinker does not yet exist, but enzymes have been immobilized on graphene using cysteamine and GA double crosslinker system. At first, C=C bonds of graphene react with the thiol group of cysteamine, leaving the amino group free to react with GA. In the final step, an enzyme reacts with GA, which was

presented in more detail earlier (Chapter 4.3.1). All reaction steps were done at room temperature and pH 8.0.[76]

5 Immobilization of ECM proteins

5.1 Collagen

Many methods that have been used for collagen crosslinking could also apply to GO-collagen crosslinking. GA has been used to crosslink collagen chains to achieve mechanically stiff biomaterials. GA reacts most commonly with amine groups of lysine or hydroxylysine residues of collagen, but it can also react with histidine and arginine residues. However, these reactions are rare because the number of arginine and histidine residues in collagen is much lower than the number of lysine residues. Because other proteins have been covalently attached to GO using GA crosslinker, a similar approach could also be possible for collagen. However, the concentration of collagen must be considered. If the relative amount of collagen is significantly higher than reactive sites of GA-GO material, crosslinking of collagen could dominate.[77]

Diimide-activated amidation has been widely used for collagen crosslinking with other biomolecules or surfaces. This approach has been utilized to prepare GO-collagen aerogels,[78] but it could also be applicable for collagen immobilization on GO surfaces. In the first step, separate collagen and GO dispersions in acetic acid were prepared. Different concentrations of GO dispersions were then mixed in 2 wt-% of collagen solutions. After sonication, molding, and lyophilization, collagen and GO flakes were crosslinked together *via* amidation reaction by EDC and NHS (Figure 36). In the final step, the mixture was freeze-dried to obtain GO-collagen aerogels.[78]

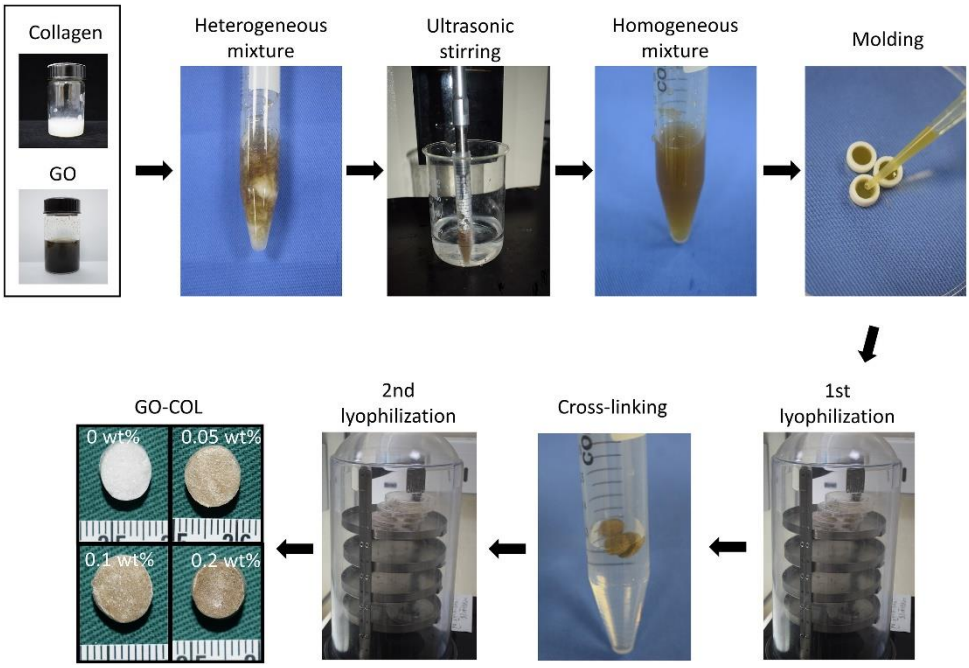

Figure 36. Preparation steps of GO-collagen aerogel synthesis. Reprinted with permission from[78] Copyright 2019, Elsevier.

FTIR measurements showed that the peaks originating from peptide bonds had greater intensity in the GO-collagen spectrum than in pure collagen aerogel. This indicates that GO (COOH) and collagen (NH_2) had reacted and formed an amide linkage. The presence of GO was confirmed by the Raman spectrum of the GO-collagen aerogel: D and G bands of GO could be observed.[78]

GO flakes have also been incorporated into commercially available collagen sponge by EDC-induced amidation (Figure 37).[79] EDC was added to GO-water dispersion to activate COOH groups which were further reacted with proteins' amino groups. Amide linkages formation between GO flakes and a collagen sponge were confirmed with FTIR and XPS measurements. NHS was not used, probably due to the use of a commercial collagen sponge in which intermolecular protein conjugation is not probable due to the static nature of the sponge. By staining GO-collagen material with dye was confirmed that GO flakes were evenly distributed into collagen sponge.[79]

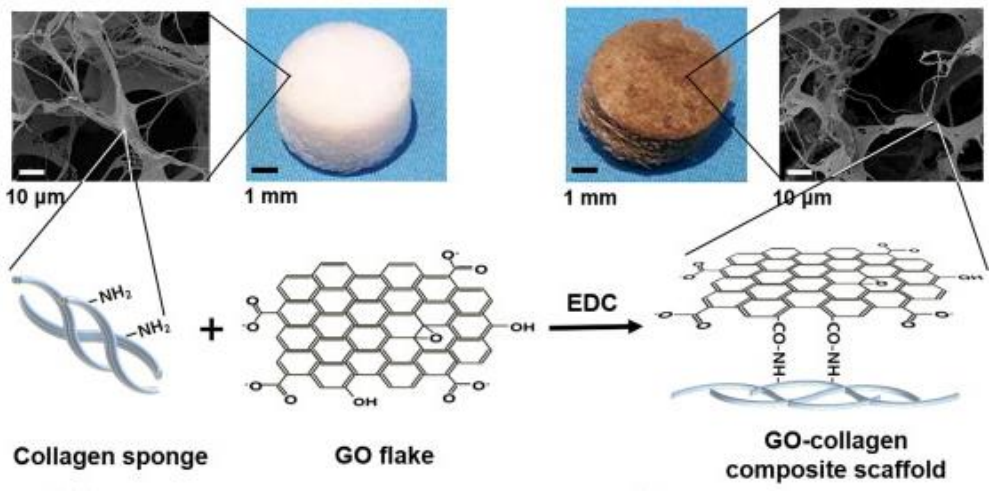

Figure 37. Preparation of GO-collagen scaffold *via* EDC-induced diimide-activated amidation. Reprinted from[79], Copyright 2015 with permission from Elsevier.

5.2 Laminin

Functional neurite outgrowth domain of laminin protein (p20 peptide) has been covalently attached on poly(3,4-ethylene dioxythiophene) (PEDOT) and GO composite film *via* EDC and NHS induced diimide-activated amidation.[80] PEDOT is a conducting polymer, making it suitable for, e.g., biosensing and tissue engineering, but it does not contain any reactive functional groups that could react with biomolecules. Therefore, the embedding of reactive GO rich with oxygen-containing functional groups makes PEDOT more applicable to these applications. Before adding p20 peptide, GO was embedded into the EDOT polymer network during electropolymerization: EDOT electropolymerized onto the electrode surface from the EDOT/GO water solution. Covalent crosslinking of laminin peptide to PEDOT/GO film was confirmed by FTIR and XPS studies indicating the formation of amide linkages (-NH_2 of laminin, COOH of GO).[80]

Neural biocompatibility of the PEDOT/GO films with (non-covalently and covalently functionalized ((p20 ADS and p20 COV, respectively)) and without laminin peptide were also studied (Figure 38).[80] The unmodified PEDOT/GO film was a favorable substrate for neural growth and neuron attachment. The density of neurons attached to all films was similar, but neurites were longer on the p20 COV film than unmodified and p20 ADS films.[80] Earlier, p20

peptide has been observed to enhance neurite outgrowth when incorporating into a conducting polymer network.[81] Therefore, it was concluded that p20 enhances neurite outgrowth only when covalently crosslinked on GO. It was suggested that weak interactions could disrupt p20 peptide conformation in p20 ADS PEDOT/GO film, leading to loss of biological activity.[80]

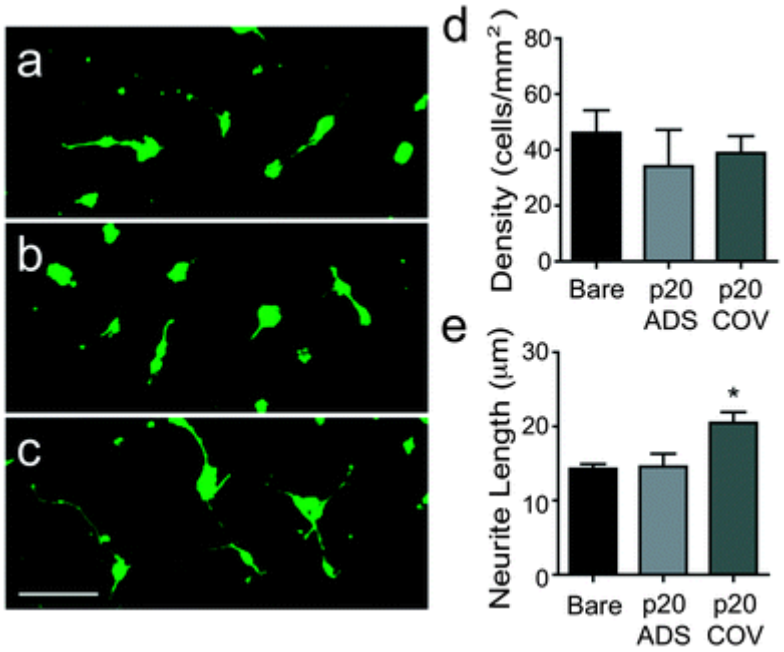

Figure 38. Fluorescent images of neurons cultured on a) unmodified (bare), b) physically adsorbed p20 peptide (p20 ADS), and c) covalently attached p20 peptide (p20 COV) PEDOT/GO films. Scale bar 50 μm. d) Neuron densities growing on the PEDOT/GO films and e) their average neurite lengths. Reproduced from[75] with permission from The Royal Society of Chemistry, conveyed through copyright clearance center.

6. Summary

The literature part focused on introducing the chemical properties of GO, possible interactions between proteins and GO, and covalent functionalization methods of GO making it more reactive towards covalent reactions with proteins. Also, some examples of protein immobilized GO systems containing ECM proteins, collagen and laminin, were presented.

GO is a hydrophilic material with excellent mechanical properties and diverse opportunities for chemical modification, making it a promising material for biomedical applications. Interactions involved in the attachment of proteins to GO can be covalent or non-covalent, or both types of interactions can be applied. In covalent protein immobilization, amide bond formation is typical between proteins and GO. Therefore, amino groups on the protein surfaces (-NH_2 of lysine or *N*-terminus) are important for the covalent bond formation. Covalent protein immobilization usually results in more specific and stable protein attachment on GO than protein immobilization through weak interactions. However, covalent protein immobilization can result in random or specific protein orientation relative to the GO surface, depending on the functionalization protocol used.

Although GO contains reactive oxygen-containing functionalities, covalent protein immobilization often requires a preceding chemical modification. COOH groups of GO can be activated to more reactive towards forming amide bonds with proteins. The number of COOH groups can also be increased, but there is no agreement if it will increase the final number of immobilized proteins. Epoxy groups of GO can be modified into amino groups, which can be beneficial for further functionalization. However, literature about protein attachment on amino-functionalized GO was not found.

Proteins have been attached covalently on GO using crosslinker molecules of different lengths. It has been suggested that the use of crosslinkers may retain proteins' biological function better than direct immobilization methods due to the increase of distance between a protein and GO. Glutaraldehyde is a commonly used crosslinker molecule, but it tends to polymerize easily, and it has 13 different structural forms in aqueous solutions. However, double crosslinker systems of organosilanes and glutaraldehyde are widely used.

Click reactions presented in this thesis could be potential methods for covalent attachment of proteins to GO, but so far, they have been used only for amino acids, peptides, or small proteins. Also, for the chemical functionalization of GO, cycloaddition reactions are mainly used. Double functionalized GO materials could potentially increase the total amount of immobilized protein or enhance the preparation of multifunctional GO materials, e.g., the use of two different proteins simultaneously.

EXPERIMENTAL PART

7. Motivation

GO can be functionalized with proteins directly[29] or by using crosslinkers such as glutaraldehyde (GA)[82], (3-aminopropyl)-triethoxysilane[83] (APTES) or polylysine and polyethylene glycol polymerchains[84]. Crosslinker molecules act as bridges between GO and proteins, potentially preventing the distortion of the quaternary structure of proteins. In this way, the proteins stay far away from the GO lattice, which could interact with proteins *via* weak interactions, such as hydrophobic and electrostatic interactions.[25]

In the experiments, horseradish peroxidase (HRP, EC 1.11.1.7) was used as a model protein for immobilization. HRP is a peroxidase enzyme, which is isolated from the roots of the horseradish plant. There are many isoenzymes of HRP in horseradish roots, but HRP C is the most abundant and studied form. HRP catalyzes the oxidation of different organic and inorganic compounds using hydrogen peroxide or other peroxides.[85] HRP has been studied extensively due to its potential for applications in medicine and biotechnology: HRP can be used, for example, as a biosensor, in cancer therapy and clinical diagnostics,[86,87] and it is used for enzyme labeling of antibodies to improve their detection. In addition, HRP can induce biodegradation of GO materials in the presence of hydrogen peroxide through enzymatic oxidation.[88,89]

Earlier, GA was commonly used for the conjugation of HRP to an antibody, as HRP has six lysine residues (Figure 10) and three of these locate on the surface of HRP.[90,91] Hence, HRP possibly reacts with GA *via* its amino groups on its surface or its *N*-terminus.[50] However, the use of GA for bioconjugation is hard to control because it tends to polymerize. Nowadays, there are more advanced crosslinkers for bioconjugation, but GA is still used.[57a,d]

The experimental part of the master's thesis focuses on the covalent immobilization of proteins on laser-oxidized graphene surfaces. Earlier, HRP has been attached to the laser-oxidized

graphene *via* weak interactions.[92] However, HRP immobilization on the chip through covalent interactions has not been done before. In this thesis, the experiments aimed to attach HRP covalently on the laser-oxidized graphene-based microchips using crosslinking chemistry. Preliminary experiments were done with GO flakes, using two different methods, which differed in the used crosslinker systems, glutaraldehyde[82] or APTES-GA[83]. From the GO flake experiments, information about the formed bonds between the components in the GO-crosslinker-HRP systems was achieved by FTIR and TGA measurements. A challenge in this work was to prove that the protein immobilization on the GO surface was covalent.

8. Materials and methods

All chemicals (Table 2) were used without any further purification. HRP (Sigma Aldrich, type IV, ≥ 250 units/mg, salt-free, lyophilized powder) was used as a model protein for the immobilization on GO materials.

Table 2. Chemicals used in the study

Chemical	Manufacturer	Purity
Graphene oxide	GRAPHENEA	4 mg/mL in H_2O (monolayer content > 95 %)
Glutaraldehyde	TCI	50 % in H_2O (w/w, ~ 5.6 M)
Ethanol	Altia Oyj	99.5 %
3-aminopropyltriethoxysilane	TCI	> 98.0 %
Sodium dihydrogen phosphate dihydrate	Merck	98 - 100.5 %
Di-sodium hydrogen phosphate dihydrate	Merck	99.5 %

A Mettler Toledo XP205 scale was used to weigh the chemical reagents and a Denver Instrument APX-200 scale was employed to measure the net weights of round-bottomed flasks and centrifuge tubes. A Hielscher UP50H ultrasonic processor was used to sonicate the mixtures of GO flakes and a solvent to fine suspensions. A Thermo Fisher Scientific Heraeus Megafuge 16 centrifuge was utilized between functionalization and washing steps to separate the synthesized GO materials from the reaction mixture.

8.2 Characterization of GO materials

FTIR: All IR spectra of the dried GO-flake samples were obtained with a Bruker Tensor 27 FTIR Spectrophotometer. The spectra were recorded on the spectral range 4000 - 400 cm^{-1} with a 4 cm^{-1} resolution and 128 scans for both samples and background.

AFM: A Bruker AFM-icon dimension microscope with a SCANASYST-AIR probe was used to assess the success of the immobilization on the chip. The AFM imaging was done with PeakForce Tapping mode and the PeakForce Setpoint was 2 nN. The AFM images were processed and analyzed with the NanoScope Analysis 1.9 software. The resolution of the AFM images was 10 nm.

Raman: A Thermo Scientific DXR Raman microscope with Olympus TH4-200 light power supply and DXR 532 nm filter was used to measure Raman spectra of the pure and functionalized GO flakes. The Raman measurements were performed with laser power of 10 mW (GO, GO-APTES-GA-HRP) or 0.5 mW (GO-GA-HRP), exposure time of 3 s and 10 exposures, using fluorescence correction. For further analysis, single Raman spectra were normalized to the G-band. Position and area values for specific bands were obtained by Lorentz multi-peak fitting of single spectra using Origin 2017 software.

Raman measurements of the chip were done using a home-built Raman setup with a backscattering geometry and a CW single-frequency laser (λ = 532 nm, Alphalas, Monolas-532-100-SM). The beam was focused on a sample and subsequently collected with a 100x microscope objective (Nikon L Plan SLWD 100x with 0.70 N.A.). The scattered light was dispersed in a 0.5 m imaging spectrograph (Acton, SpectraPro 2500i) using 600 g · mm^{-1} grating (resolution ~3 - 4 cm^{-1}). The signal was detected with an EMCCD camera (Andor Newton EM DU971N-BV) using 100 µm slit width. A beam splitter was placed between the objective and the spectrometer to observe the exact measurement point visually. The Rayleigh scattering was attenuated with an edge filter (Semrock). The approximate sample positioning was done manually with XYZ-stage (Newport, ULTRAling 462-XYZ-M) and fine-tuned with XYZ-piezo scanner (Attocube, ANPxyz101) with the smallest step of 50 nm in each direction. A laser power of ~ 0.25 mW was utilized.[21]

The spectra were integrated from Raman shift 1323 cm^{-1} to 1371 cm^{-1}, 1583 cm^{-1} to 1622 cm^{-1} and 2653 cm^{-1} to 2720 cm^{-1} in RamanMapViewer 2.0.0.1 to obtain Raman maps of D, G and 2D bands, respectively. For further analysis, single Raman spectra were normalized to the silica signal. Position and area values for specific bands were obtained by Lorentz multi-peak fitting of single spectra using Origin 2017 software. A_D/A_G ratios were calculated by dividing areas of the respective D and G bands.

TGA: TG/DSC measurements were carried out by Dr Manu Lahtinen. Thermal properties of the flake samples were examined with Perkin Elmer STA 6000 thermogravimetric TG/DSC analyzer. The measurements were made in an open platinum pan, under air atmosphere (flow rate of 40 mL/min), with a heating rate of 10 °C/min, in the temperature range of 22 ºC - 800 ºC. Temperature calibration of the analyzer was made using melting points of the indium (156.6 °C) and aluminum (660.1 °C) standards. A weight balance was calibrated by measuring the standard weight of 50.00 mg at room temperature. The sample weights used in the measurements were about 1 - 4 mg.

8.3 Preparation of PBS

Stock solutions were prepared by dissolving 35.61 g (0.20 mol) of $Na_2HPO_4 \cdot 2\ H_2O$ in 1 000 mL of deionized water and 31.20 g (0.20 mol) of $NaH_2PO4 \cdot 2\ H_2O$ in 1 000 mL of deionized water. To achieve 500 mL of 0.2 M PBS solution (pH = 7.3), 385 mL of the $Na_2HPO_4 \cdot 2\ H_2O$ and 115 mL of $NaH_2PO4 \cdot 2\ H_2O$ solution were mixed. The pH was verified with a Mettler Toledo InLab Micro pH electrode.

8.4 Preparation of HRP solution

1 mg/mL HRP solution (≥ 250 U/mL) was prepared by dissolving 0.99 mg of HRP in 1 mL of PBS (0.2 M, pH = 7.3). The solution was stored at 4 ºC.

8.5. Immobilization on GO flakes

Each immobilization experiment on GO flakes was done twice. As a starting material, vacuum-dried GO powder was used, prepared from 4 mg/mL GO water dispersion.

8.5.1 *via* glutaraldehyde

For the first experiment, 20 mL of 1 mg/mL GO solution in PBS (0.2 M, pH = 7.3) was prepared. 20 mL of PBS were added to 20.01 mg of vacuum-dried GO and the mixture was sonicated for 3 h in an ultrasonic bath (amplitude = 50 %, cycle 1).

On the next day, the GO suspension was sonicated again to achieve a fine suspension. Then, 0.38 mL of 50 % w/w GA water solution (~ 5.6 M, 2.139 mmol) was added to attain 1 % v/v solution of GA in the GO suspension. The mixture was stirred for 4 h under N_2 atmosphere at RT. The suspension was centrifuged for 10 min (13 245 × g) to separate the flakes from the supernatant. The flakes were washed by rinsing with 4 × 7 mL of PBS and resuspended to 10 mL of PBS in an ultrasonic bath. Approximately half of the intermediate product was lost during the washing: the flakes were so mucous-like (slimy) that transfer from centrifuge tube to a Büchner funnel was problematic. Some went through filter paper or stuck into it. Thereafter, washings were performed *via* centrifugation.

40 µL of 1 mg/mL HRP (≥ 250 U/mL) solution in PBS was added to the suspension of the GO-GA intermediate product. The mixture was stirred gently for 1 h at RT with a magnetic stirrer. Afterwards, the suspension was centrifuged for 5 min (2 737 × g). The supernatant was removed, and 7 mL of PBS were added on the top of the flakes which were subsequently let to set down. Finally, the liquid phase was pipetted away, and the final product (GO-GA-HRP) was stored in PBS.

For the characterization of the GO-GA-HRP product, PBS was removed from the product by washing with 3 × 300 µL of water. Between each washing, the suspension was centrifuged for 5 min (2 737 × g). After the last centrifugation, the supernatant was removed, and the flakes were resuspended to 1 mL of water.

The experiment was repeated once, using the double amount of each reagent. After GA functionalization, the reaction mixture was centrifuged for 15 min (13 245 × g). The flakes were washed with 3 × 14 mL of PBS and centrifuged between each washing for 15 min (13 245 × g). After HRP immobilization, the reaction mixture was centrifuged for 15 min (18 500 × g) and then washed with 2 × 14 mL of PBS and 1 × 14 mL of water, with centrifugation for 15 min (18 500 × g) in between each washing. The yield of the GO-GA-HRP was 33.6 mg (starting material: 40 mg of GO flakes). Additionally, longer centrifugation times and higher speeds were used to separate the GO material derivatives from the supernatant during the second experiment.

8.5.2 *via* APTES and glutaraldehyde

8 % (v/v) GA solution in water was required for the HRP immobilization, hence 5 mL of 8 % (v/v) GA water solution was prepared from 5.6 M GA water solution:

$$\mathrm{V(GA)} = 5\ \mathrm{mL} \times 0.08 = 0.4\ \mathrm{mL}$$

$$\mathrm{m(GA)} = \delta\,(\mathrm{GA}) \times \mathrm{V(GA)} = 1.06\frac{\mathrm{g}}{\mathrm{mL}} \times 0.4\ \mathrm{mL} = 0.424\ \mathrm{g}$$

$$\mathrm{n\ (GA)} = \frac{\mathrm{m\ (GA)}}{\mathrm{M(GA)}} = \frac{0.424\ \mathrm{g}}{100.129\frac{\mathrm{g}}{\mathrm{mol}}} = 4.2349 \times 10^{-3}\mathrm{mol}$$

$$\mathrm{V(GA, 5.6\ M)} = \frac{\mathrm{n\ (GA)}}{\mathrm{C(GA)}} = \frac{4.2349 \times 10^{-3}\mathrm{mol}}{5.6\ \mathrm{M}} = 0.7562\ \mathrm{mL} \approx 0.76\ \mathrm{mL}$$

0.76 mL of 5.6 M (50 % w/w) GA water solution was diluted with 4.24 mL of water.

20 mL of ethanol was added to 20.1 mg of vacuum-dried GO. The mixture was stirred and suspended in an ultrasonic bath. 0.5 mL of APTES (2.137 mmol) was added while stirring with a magnetic stirrer. The flask was equipped with a reflux condenser, and the reaction mixture was heated in an oil bath for 2.5 h at 80 ºC. After heating, the mixture was let to cool down and centrifuged for 10 min (13 245 × g). Since the separation was not completed, the centrifugation was repeated. The flakes were washed 3 × 10 mL of ethanol and 2 × 10 mL of water and centrifuged for 15 min (13 245 × g) between each washing. The GO-APTES product was let to dry overnight under vacuum.

On the next day, the GO-APTES product was centrifuged twice for 15 min (13 245 × g, 18 500 × g) and resuspended to 2.5 mL of PBS (0.2 M, pH = 7.3). 0.5 mL of 8 % v/v GA solution in water (4.235 mmol) was added to the suspension. The mixture was stirred for 6 h at RT, covered with parafilm. After 6 h, the mixture was centrifuged for 15 min (18 500 × g). The flakes were washed with 2 × 1 mL of PBS and 2 × 1 mL of water. The GO-APTES-GA product was resuspended to 20 mL of PBS to achieve a 1 mg/mL solution.

100 µL of 1mg/mL HRP (≥ 250 U/mL) solution in PBS was added to the suspension of GO-APTES-GA in PBS. The mixture was left to stir overnight for 18 h in an ice bath. After that, the liquid phase was pipetted away and the GO-APTES-GA-HRP product was washed with 3 × 1 mL of water, with centrifugation (15 min, 18 500 × g) between each washing. After the last washing, the supernatant was removed, and the final product was left to dry at RT.

The experiment was repeated once, using the double amount of each reagent. To improve the fineness of GO flakes in ethanol, a sonicator probe was used during the second experiment. However, it was more problematic to separate the flakes from supernatant in the different functionalization stages than in the first experiment with the same method. After centrifugation, the supernatants still contained GO derivatives. Therefore, washing steps after GA and HRP additions were adopted without centrifugation: after waiting for a couple of minutes, the color of the supernatant changed from black to light gray, indicating that most of the GO flakes had settled down. The supernatant was then pipetted away, and the flakes (resembling more dispersion) were washed with PBS and water. The yield of the GO-APTES-GA-HRP product was 15.65 mg (starting material: 40 mg of GO flakes).

8.6 Immobilization of HRP on the graphene-based microchip *via* glutaraldehyde

For immobilization on the chip, 0.625 U/mL HRP solution in PBS was prepared. 5 µL of ≥ 250 U/mL HRP solution was diluted to 1995 µL of PBS (0.2 M, pH = 7.3).

The amount of 50 % (w/w) GA water solution was calculated so that the ratio of GA and HRP was the same as in the experiments with GO flakes. HRP catalytic activity (µmol/min) in the chip experiment:

$$2\ \text{mL} \times 0.625\ \text{U/mL} = 1.25\ \text{U}$$

and in the flake experiment:

$$0.080\ \text{mL} \times 250\ \text{U/mL} = 20\ \text{U} \rightarrow$$

$$\frac{20\ \text{u}}{0.76\ \text{ml}} = \frac{1.25\ \text{u}}{\text{x}} \rightarrow 47.5 \approx 50\ \text{µl of 50 \% (w/w) GA water solution.}$$

1950 µL of PBS (0.2 M, pH 7.3) and 50 µL of 50 % w/w GA water solution (5.29 µmol) were added to a 5 mL glass vial (d = 24 mm). The chip was immersed into the vial with tweezers, the graphene layer pointing upwards. N_2 gas was trapped inside the vial with a lid to obtain a nitrogen atmosphere. The chip was incubated for 4 h at RT protected from light.

After 4 h of incubation in GA-PBS, the chip was washed with 3 × 1 mL of PBS and dried with N_2 flow. Afterwards, the chip was immersed in 2 mL of the prepared 0.625 U/mL HRP solution and incubated for 1 h at RT. The chip was washed with 3 × 1 mL of PBS and 3 × 1 mL of water. In the final step, the chip was rinsed with N_2 flow and left to dry at RT overnight.

9. Results and discussion

9.1 Immobilization of HRP on GO flakes

Covalent protein immobilization *via* GA crosslinker on GO has been studied before with other enzymes[55,82,93] but not with HRP. GA is a commonly used crosslinker in protein immobilization because of its diverse solubility and high reactivity, especially towards amines. However, GA can have at least 13 different forms in an aqueous solution depending on physical and chemical conditions, such as pH, temperature, and concentration, and a high tendency to polymerize. This can lead to different lengths of GA chains between GO and a protein.[50] Therefore, the prediction of the immobilization outcome is not apparent.

The proposed reaction of GO, GA and a protein that would occur at neutral pH is shown in Figure 39.[55] A possible side reaction is the bridging of GO flakes *via* the two aldehyde groups of GA that could cause agglomeration. Also, if there are OH groups close to each other on a GO flake, acetals can form instead of hemiacetals.[51] More information about GA crosslinking is described in the literature part, Chapter 4.3.1 Glutaraldehyde.

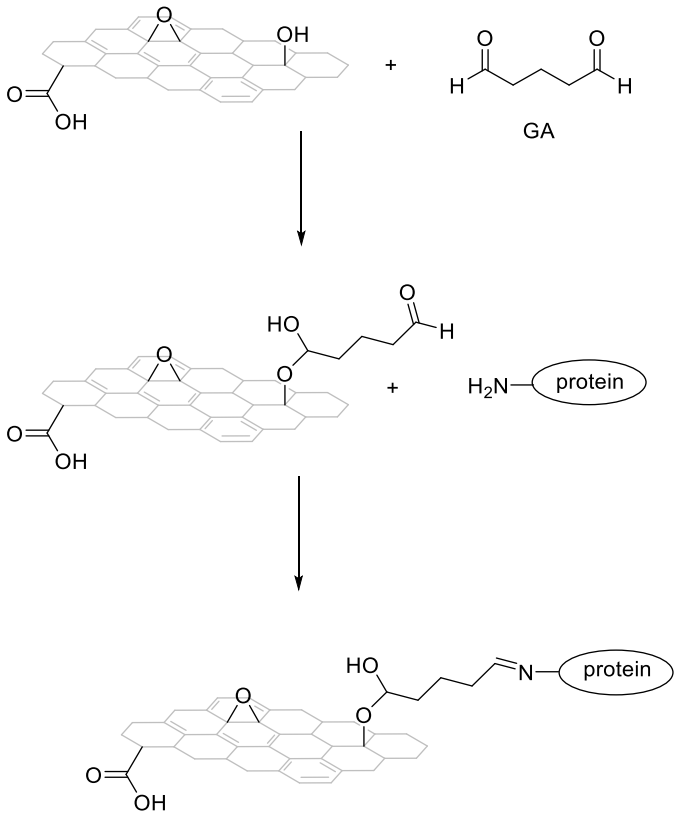

Figure 39. Proposed reaction pathway for GO functionalization with GA and a protein.[55]

The other functionalization protocol utilizes the double crosslinker system APTES-GA for covalent protein immobilization (Figure 40). The APTES-GA crosslinker system for the protein immobilization has been earlier used with other proteins[83] but not with HRP. The main difference of the two crosslinker system compared to GA is a longer distance between the graphene lattice and a protein. A possible reaction pathway was concluded based on two distinct studies[58,94] because a single mechanistic study did not exist. In terms of GA functionalization, it is more beneficial when APTES reacts with GO *via* its ethoxysilane groups leaving a free NH_2 group, which can further react with GA. However, APTES can also react with GO *via* its NH_2 group (Appendix 1).[58]

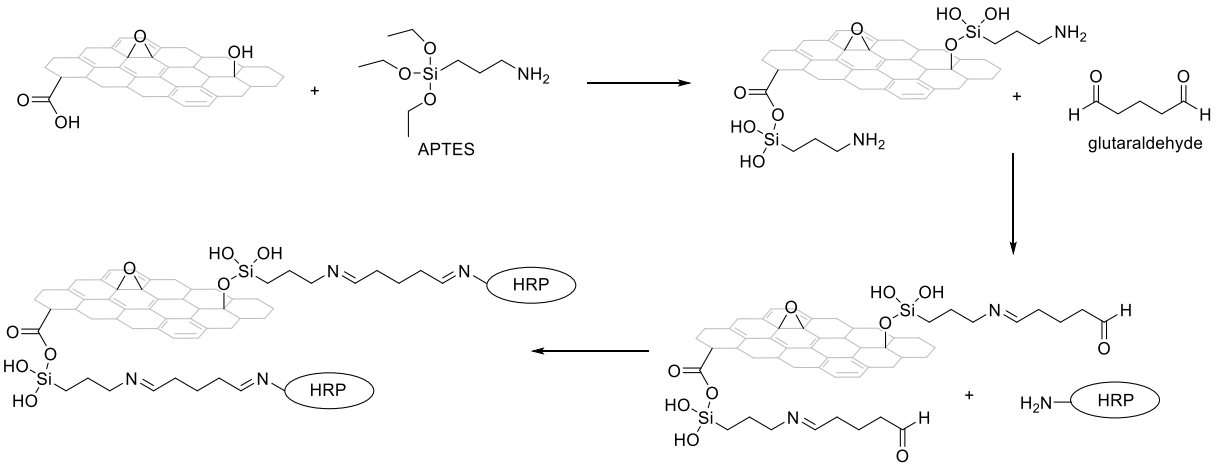

Figure 40. A proposed reaction pathway for GO functionalization with APTES, GA and HRP.[58,94]

The GO-GA-HRP and the GO-APTES-GA-HRP flakes were prepared following the protocols of the chosen articles.[82,83] In the articles, different proteins were used; protease, transferase and two types of peptides. In this project, an HRP enzyme was selected because of the previous studies on non-covalent immobilization of HRP on laser-oxidized graphene.[92] In the first experiment of each protocol, some changes were made. In both methods, it was not explicitly mentioned how the washing was done. Therefore, in the first experiment, the washing of the GO-GA material was tried by rinsing it with PBS and filtrating it using a Büchner funnel. The filtration was not successful because the GO material was trapped in the filter or went through it. Hence, afterwards, the washing steps were performed using centrifugation.

In both methods, GO flakes were suspended to a solvent (PBS or ethanol) by sonication to achieve fine black suspensions. Then, crosslinkers were added to GO suspensions. To avoid damaging the protein conformation, sonication was not used afterwards. After the addition of crosslinkers or HRP, some aggregates formed. Also, the GO-GA-HRP product tended to precipitate quickly after mixing. The GO-APTES-GA-HRP end products behaved differently: The product of the first batch precipitated, while the product of the second batch was suspended evenly in the buffer. The dried end products from both methods appeared different; GO-GA-HRP was a sticky black solid whereas GO-APTES-GA-HRP appeared as a fine black powder. Figures from intermediate products are shown in Appendix 2.

The yields were 33.6 mg for GO-GA-HRP and 15.65 mg for GO-APTES-GA-HRP, respectively (GO starting mass: 40 mg). Although the centrifugation speed was 15 000 rpm (the maximum possible with the used instrument), parts of the GO-materials remained in the supernatant after centrifugation (Appendix 2). This caused a decrease in the yields.

The average widths of the flakes were measured from the optical microscope images of GO flakes on mica discs using ImageJ software (Figure 41). The GO flakes have an average width of 5.26 µm, GO-GA-HRP flakes 10.39 µm and GO-APTES-GA-HRP flakes around 25.48 µm. The reason for the width variation of the flakes could be differences during the sample preparation. The GO-APTES-GA-HRP sample was first dried in vacuum and subsequently resuspended to water whereas GO and GO-GA-HRP samples were taken before the drying process. Anyway, the average width of GO-GA-HRP flakes is almost double compared to the width of the GO flakes. This indicates an increasing tendency of GO-GA-HRP flakes to agglomerate in the presence of GA or HRP. Similar agglomeration could also occur among the GO-APTES-GA-HRP flakes.

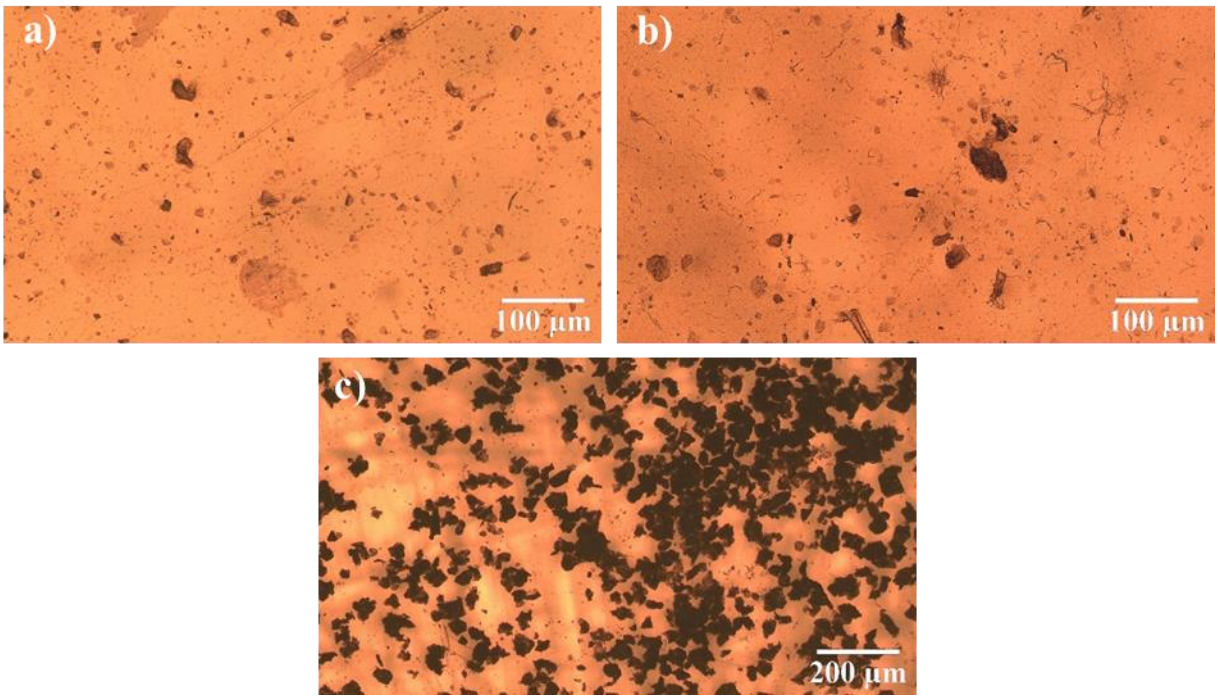

Figure 41. Optical microscope images of a) GO, b) GO-GA-HRP and c) GO-APTES-GA-HRP flakes.

The agglomeration of the flakes could be prevented by sonication in each functionalization step or by using a lower GO concentration in the suspension. In addition, the agglomeration caused

problems during AFM imaging of the dried GO flakes on a mica disc. The AFM images had a bad quality, which could be due to the uneven topography of the GO flakes or their agglomerates (Appendix 3). Also, liquid phase AFM was tried but the GO flakes moved simultaneously with the tip. A lower concentration of GO and lesser agglomeration could enhance the quality of AFM images of GO flakes.

9.1.1 FTIR

FTIR spectra were recorded at different stages of the functionalization. From the IR spectrum of GO flakes, characteristic peaks for GO can be observed (Figure 42). Corresponding vibrational modes and wavenumbers of the absorption bands are listed in Table 3. The hydroxyl groups of GO induce three bands (3313 cm^{-1}, 1375 cm^{-1} and 1040 cm^{-1}) that correspond to O-H stretching, O-H deformation and C-O stretching, respectively. The peak at 1720 cm^{-1} (C=O stretching) and the broad absorption band between 3300-2600 cm^{-1} (O-H stretching) are from the COOH groups. The aromatic π-system of GO causes the bands at 1610 cm^{-1} (C-C stretching) and 871 cm^{-1} (C-H deformation). GO also contains some epoxy groups, whose C-O-C stretching causes the band at 1168 cm^{-1}.[58,95,96]

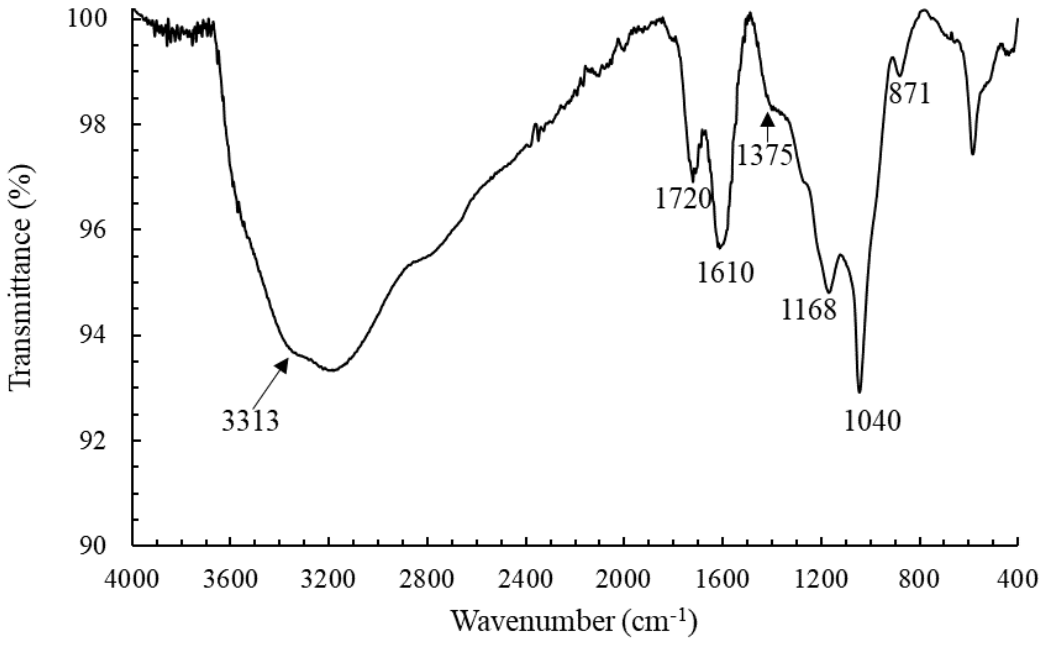

Figure 42. FTIR spectrum of the dried GO flakes.

Table 3. Absorption bands for vacuum-dried GO

Wavenumber (cm^{-1})	Functional group	Vibrational mode
3313	OH	O-H stretching
3300-2600	COOH	O-H stretching
3100-3000	aromatic system	C-H stretching
1720	COOH	C=O stretching
1610	aromatic system	C=C stretching
1375	OH	O-H deformation
1168	epoxy	C-O stretching
1040	sec. alcohol	C-OH stretching
871	aromatic system	C-H deformation

The IR spectra of GO-GA differ significantly from the corresponding spectra in the literature[51,52] (Figure 43). There should be an absorption band at 2800-3000 cm^{-1} in the spectrum of GO-GA caused by C-H stretching of the GA alkane chain.[51] However, the absorption band of OH group around 3200 cm^{-1} in the spectrum of GO-GA is so intense that it could cover the peak of C-H stretching. In addition, C=O stretching band of the aldehydes usually occur around 1700 cm^{-1}, but in the spectrum of GO-GA the broad band at 1643 cm^{-1} could originate from it.

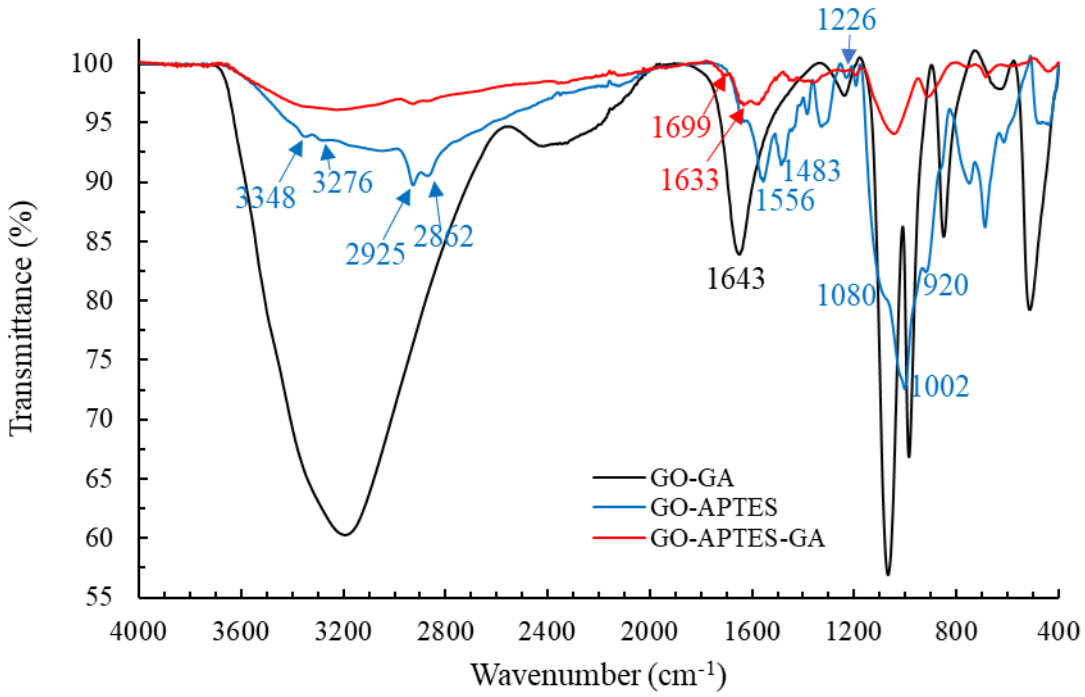

Figure 43. FTIR spectra of GO with crosslinkers.

APTES can react with the alcohol and carboxylic acid groups of GO, forming bonds between silicon and oxygen atoms that can cause the absorption band at 1080 cm^{-1} (Si-O-C, Figure 41).[97] The peak at 1002 cm^{-1} (Si-O-Si) indicates that APTES molecules have also reacted with each other (Appendix 1). Hydrolysis of APTES can occur easily in the presence of ethanol and water by cleavage of its ethoxy groups resulting in Si-OH stretching vibration at 920 cm^{-1}.[58,98] APTES has one amino group at the end of its alkyl chain that could cause the absorption bands at 3348 cm^{-1} and 3276 cm^{-1} (asymmetric and symmetric N-H stretching, respectively) and at 1556 cm^{-1} and 1483 cm^{-1} (deformation of H-bonding). The peaks at 2925 cm^{-1} and 2862 cm^{-1} could be related to asymmetric and symmetric C-H stretching of the alkyl chain of APTES, respectively.[99] Based on the IR spectrum of GO-APTES, it could be concluded that APTES is bound to GO covalently at least *via* its Si-atom. (Figure 43 and Table 4).

Table 4. Substantial absorption bands and related vibrations for vacuum-dried GO-APTES and GO-APTES-GA

Wavenumber (cm^{-1})	**Functional group**	**Vibrational mode**
GO-APTES		
3348	NH_2	N-H asymmetric stretching
3276	NH_2	N-H symmetric stretching
2925	CH_2	C-H asymmetric stretching
2862	CH_2	C-H symmetric stretching
1556 and 1483	NH_2	deformation (H-bonding)
1226	amine	C-N stretching
1080	Si-containing groups of APTES	Si-O-C
1002	Si-containing groups of APTES	Si-O-Si
920	Si-containing groups of APTES	Si-O stretching
GO-APTES-GA		
1699 or 1633	imine	C=N stretching

APTES could also react with the epoxy groups of GO *via* its amino group, which could be unfavorable regarding GA functionalization. The weak absorption band at 1226 cm^{-1} indicates C-N bonds between APTES and GO (Figure 43; Appendix 1).[58,100] After GA functionalization of GO-APTES, new peaks appear at 1699 cm^{-1} and 1633 cm^{-1}, which could originate from imine bonds[100] between APTES and GA.[94]

For proteins, characteristic absorption bands originate from peptide bonds between amino acids. Amide I absorption band in the range from 1600 cm^{-1} - 1700 cm^{-1} is the most intense peak for

proteins, and it is induced by C=O and C-N stretching vibrations of amide groups. The amide II absorption band appears in the region from 1510 cm^{-1} - 1580 cm^{-1}, which derives mainly from N-H bending in plane and C-N and C-C stretching vibrations.[101] After HRP immobilization on the GO-GA flakes, the IR spectrum changed significantly (Figure 44). A new absorption band occurred at 1633 cm^{-1}, which could be assigned to the amide I band of HRP or originate from an imine bond between GA and HRP (C=N stretching). However, an amide II band cannot be observed for the GO-GA-HRP product.

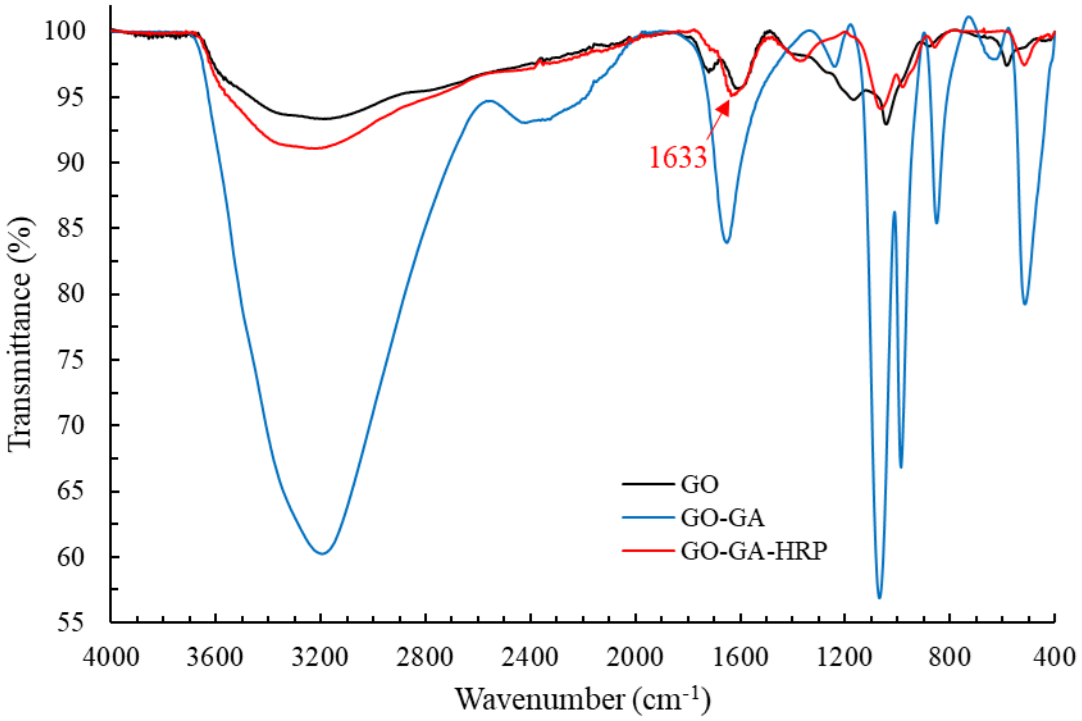

Figure 44. FTIR spectra from each step of HRP immobilization *via* GA.

Vibrations of the amide bonds of HRP are not as evident in the spectrum of GO-APTES-GA-HRP (Figure 45) compared to GO-GA-HRP. In addition, the spectra of GO-APTES-GA and GO-APTES-GA-HRP are almost identical. The peak at 1629 cm^{-1} of GO-APTES-GA-HRP could be of the amide I band or originate from imine bonds between APTES and GA or GA and HRP. Another peak at 1581 cm^{-1} indicating vibration of amide II could also originate from the presence of HRP. Nonetheless, a similar band in the spectrum of GO-APTES-GA at 1575 cm^{-1} suggests that in the case of successful protein immobilization, a vibration in GO-APTES-GA overlaps with the amide II vibration.

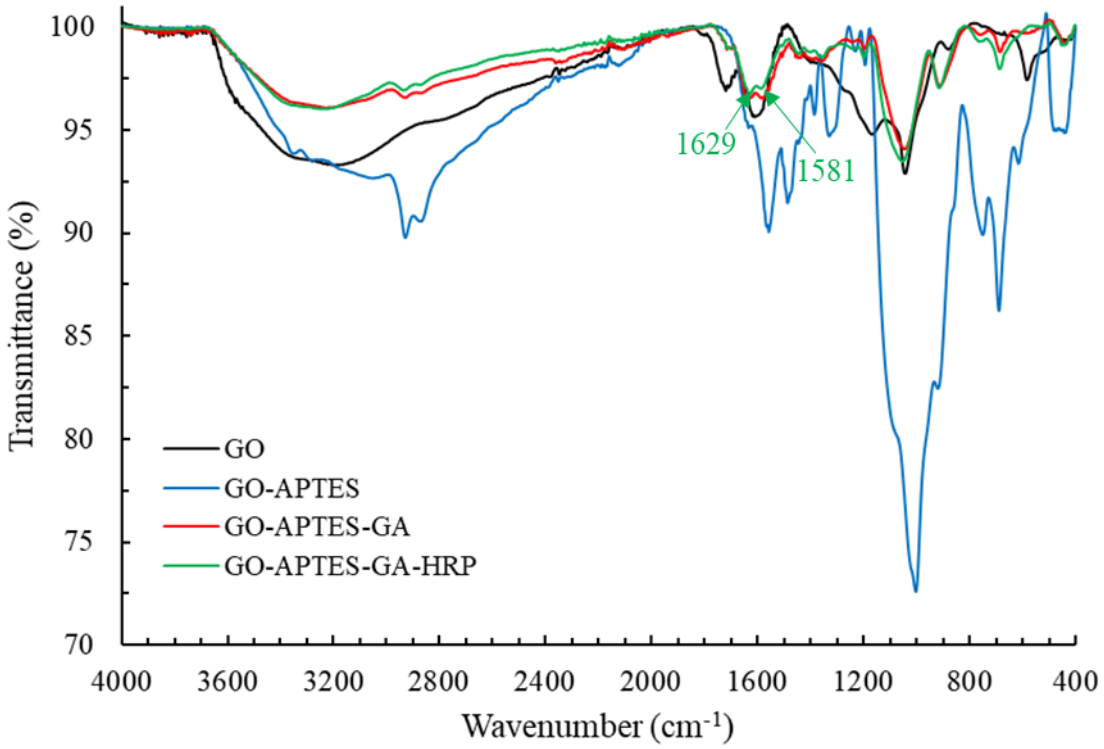

Figure 45. FTIR spectra from different stages of HRP immobilization *via* APTES and GA crosslinkers.

The peaks at 1699 cm^{-1} and 1633 cm^{-1} of GO-APTES-GA were assigned to imine bonds earlier in this thesis. Based on that, both bands at 1629 cm^{-1} (GO-APTES-GA-HRP) and 1633 cm^{-1} could result from imine bonds. This does not exclude amide I vibration of HRP at 1629 cm^{-1} because there was a similar peak (1633 cm^{-1}) in the spectrum of GO-GA-HRP assigned to originate probably from HRP (Table 5).

Table 5. Absorption bands of both HRP immobilized final products

Wavenumber (cm^{-1})	**Functional group**	**Vibrational mode**
GO-GA-HRP		
3334	NH	N-H stretching
1633	Amide I or imine	C=O and C-N or C=N stretching
GO-APTES-GA-HRP		
3342	NH of HRP (can also be NH of unreacted APTES)	N-H stretching
1629	amide I of HRP or imine	amide I: C=O and C-N stretching or C=N
1581	amide II of HRP	amide II: N-H bending (C-N, C-C stretching)

In Figure 46, the spectra of both final products, GO-GA-HRP and GO-APTES-GA-HRP, are presented for comparison. As can be seen, peaks originating from groups of HRP or imine bonds between the crosslinkers and HRP correspond quite well to each other regardless of the method. Differences in the spectra could be result from the use of different crosslinkers. The bands at 1211 cm^{-1}, 1195 cm^{-1}, 752 cm^{-1} and 686 cm^{-1} occur only in the spectrum of GO-APTES-GA-HRP indicating that the bands originate from APTES.

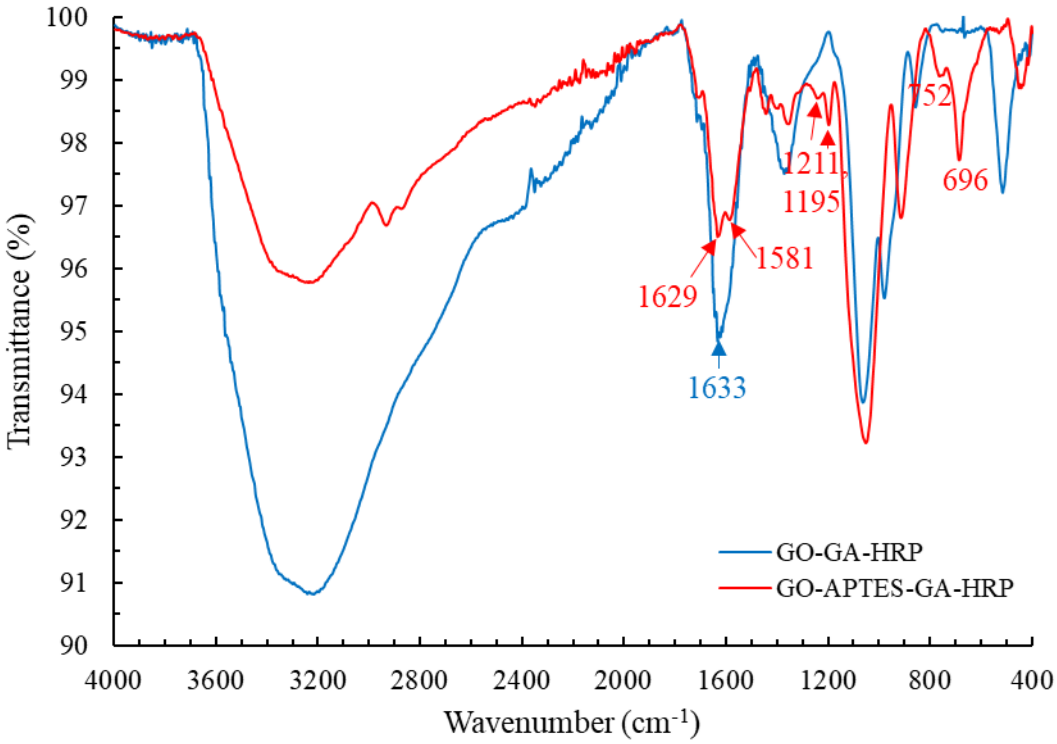

Figure 46. Comparison of the FTIR spectra of the final products.

In conclusion, both methods seem to work for covalent immobilization of HRP. The spectra of the final products resemble each other in the imine and amide bond regions indicating successful GA functionalization and/or covalent attachment of HRP to the GO-crosslinker systems. However, in this region, the bands from HRP amide groups and imine linkages between GA and HRP cannot be distinguished. The functional groups of APTES can be clearly observed from the spectrum of GO-APTES but the presence of GA could not be fully proved. At the end of the IR section, it is noteworthy that the intermediate and the final products were centrifuged before each FTIR measurement. This further confirms the presence of covalent interactions in the synthesized GO materials.

9.1.2 Raman

Three Raman spectra from each sample were recorded, and the spectra were normalized to the G band. The spectra of GO and GO-APTES-GA-HRP were recorded at a laser power of 10 mW and the spectra of GO-GA-HRP at a laser power of 0.5 mW. Average spectra of the samples are presented in Figure 47. The GO-APTES-GA-HRP spectrum differs from the other samples in the region of 2300 cm^{-1} - 3200 cm^{-1} and it cannot be evaluated reliably in that region. It could be that GO-APTES-GA-HRP has only a 2D band or both 2D and D + G bands in that region. Besides, there was a significant variation among three Raman spectra of GO-APTES-GA-HRP than among the spectra of GO-GA-HRP (Appendix 4). Hence, the average spectrum of GO-APTES-GA-HRP is not reliable. The variation could result from different flake sizes, stacking of flakes together, as well as random distribution and number of functional groups, crosslinkers and protein on the GO flake.[102] Also, a higher laser power during the Raman measurements of GO-APTES-GA-HRP can impact: The laser could induce additional damages in the graphene lattice of the functionalized GO flakes.

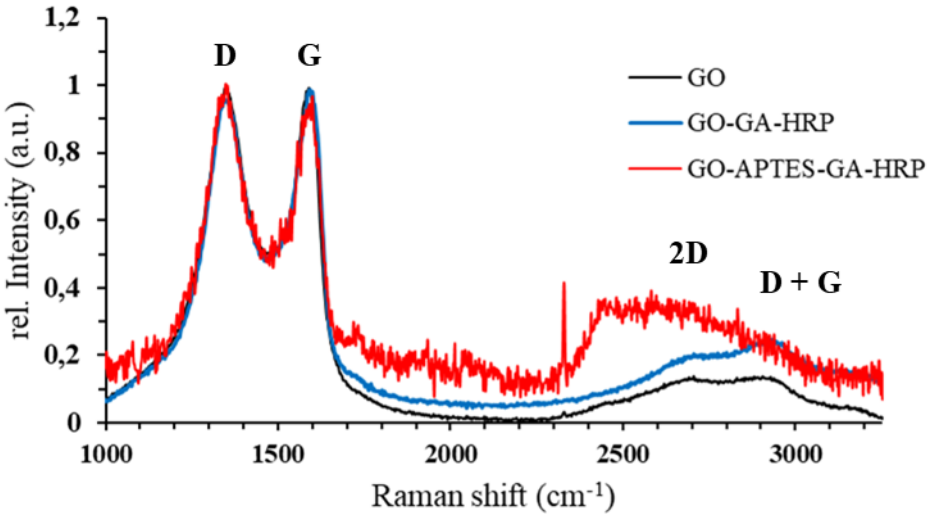

Figure 47. Average Raman spectra of flake samples GO, GO-GA-HRP and GO-APTES-GA-HRP.

The peak areas and shifts were defined by Origin peak fitting tool using the Lorentzian function. A_D/A_G ratios of the flake samples are 2.2 (GO) and 1.8 (GO-GA-HRP and GO-APTES-GA-HRP). Hence, there is a small difference between the functionalized samples and GO. Raman shifts of D, G and 2D bands are quite similar for all samples (Table 6), except for the 2D and D + G region of the GO-APTES-GA-HRP flakes, as described above. In conclusion, the lower

laser power for Raman measurements seemed to result in a better quality of the Raman spectra from the functionalized GO flakes, and the spectra from the same sample differed less from each other.

Table 6. Positions of D, G and 2D bands in the average Raman spectra of the flake samples

Sample	**D band (cm^{-1})**	**G band (cm^{-1})**	**2D band (D + G) (cm^{-1})**
GO	1351	1581	2722 (2924)
GO-GA-HRP	1351	1585	2720 (2926)
GO-APTES-GA-HRP	1348	1583	2641

9.1.3 Thermogravimetric analysis

Thermogravimetric (TG) and differential scanning calorimetric (DSC) curves were measured from the GO, GO-GA-HRP and GO-APTES-GA-HRP flake samples. By simultaneous TG/DSC measurement, information about the amount of heat transferred in material (heat flow) during each weight loss can be achieved. Earlier, TGA has been done from covalently immobilized bovine serum albumin (BSA)[29] and cytochrome-c (cyt-c)[103] on the GO. The TG curve of GO-BSA was a combination of the TG curves of pure GO, and BSA. Cyt-c was covalently attached to GO *via* C_6NH_2 crosslinker. Thermal degradation of the crosslinked cyt-c occurred at a higher temperature compared to the pure cyt-c. Previous studies motivated us to carry out TGA from our samples. The measurements aimed find out if the functionalized GO materials have different thermal behavior compared to pure GO. Besides, it was interesting to observe possible differences in the thermal behavior between the final products of the two immobilization methods.

TG (line) and DSC (dash line) curves of the samples are presented in Figure 48. In addition, the temperatures of the DSC peak maxima are shown for the two main thermal degradations of each sample. In the text, the temperature for thermal degradation is abbreviated as T_d.

Below 100 ºC, all samples start to lose weight, which is defined as evaporation of absorbed water from GO materials.[104] GO loses 15 % of its weight in the temperature range of 22 - 151 ºC. GO-GA-HRP and GO-APTES-GA-HRP have similar weight losses in the temperature ranges of 22 - 128 ºC (14 wt-%) and 22-137 ºC (9 wt-%).

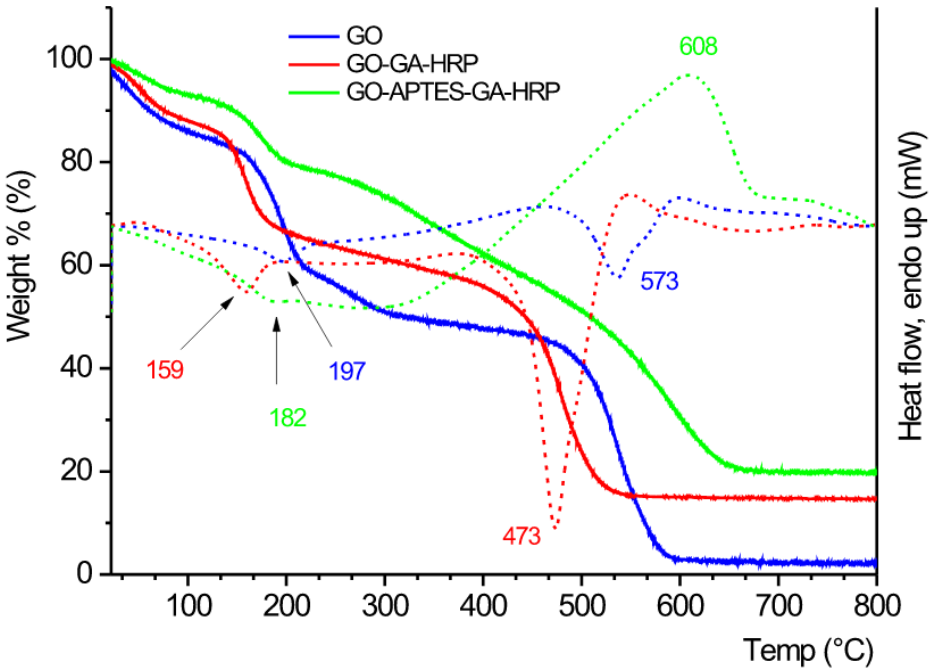

Figure 48. TG/DSC curves (line and dash line, respectively) of GO (blue), GO-GA-HRP (red) and GO-APTES-GA-HRP (green) with temperatures for the main thermal degradations.

GO has 24 % weight loss at 197 ºC (151 - 229 ºC) that signifies the removal of oxygen-containing functional groups and reduction of GO.[104] The main weight loss, 43 wt-%, occurs at 537 ºC (466 ºC - 634 ºC) indicating the removal of more stable functional groups leading to almost complete decomposition of GO. Oxygen-containing functional groups are evaporated from GO in the form of H_2O, CO_2 and CO molecules under air atmosphere.[103,104]

The GO and GO-GA-HRP samples have quite similar shaped TG curves whereas GO-APTES-GA-HRP has substantially deviating thermal behavior making it thermally the most stable. GO-GA-HRP has a 20 % weight loss at 159 ºC (128 - 201 ºC), and GO-APTES-GA-HRP has a 12 % weight loss at 182 ºC (137 - 214 ºC). These thermal degradations could partly result from the same reasons as in the case of GO. However, the lower T_d of the HRP immobilized GO samples indicate the presence of weaker bonds compared to pure GO.[104] Besides, the lower

weight loss of GO-APTES-GA-HRP around 200 ºC compared with GO can result from a lower amount of oxygen-containing functional groups in GO-APTES-GA-HRP which can decompose at this temperature range.[58] The epoxy groups of GO tend to decompose before hydroxyl groups.[105] Therefore, the thermal behavior of GO-APTES-GA-HRP indicates that the epoxy groups of GO have reacted with APTES. Serodre *et al.*[58] have observed a similar behavior between GO and GO-APTES materials from TGA measurements under inert nitrogen atmosphere (heating rate 5 ºC/min).

There is no uniformity in T_d of the main weight losses of the samples. GO-GA-HRP has a lower T_d of 473 ºC for 42 % weight loss (380 - 552 ºC), and GO-APTES-GA-HRP has a higher T_d of 608 ºC for 37 % weight loss (453 - 706 ºC) than GO (537 ºC). An explanation for the lower value of GO-GA-HRP could be the same as in the weight loss at 159 ºC: more weak interactions in the system. The higher T_d of GO-APTES-GA-HRP indicates stronger interactions[104] that could result from the incorporation of APTES. Unlike other samples, GO-APTES-GA-HRP has relatively high weight loss (22 %) in the range of 214 ºC - 453 ºC, possibly originating from the decomposition of oxygen and nitrogen-containing groups of APTES.[58] In addition, the main thermal degradation of GO-APTES-GA-HRP contains more endothermic than exothermic degradation (DSC curve, Figure 48).

It is also noteworthy that the functionalized GO materials have significantly greater residual weights than GO which has 2.7 wt-% above 634 ºC. The residual weight of GO-GA-HRP is 15 wt-% above 552 ºC and for GO-APTES-GA-HRP 20 wt-% above 706 ºC. These additional residues in the functionalized GO materials could be incombustible carbon material from the crosslinkers and HRP.

Scientific literature about the thermal degradation of pure HRP does not exist. HRP has a melting temperature of 76 ºC[90] (denaturation), but it is not useful in this context because melting does not cause weight loss to a TG curve. Although melting is always an endothermic process, it is hard to observe from the DSC curves of GO-GA-HRP and GO-APTES-GA-HRP. Hence, based on TGA, neither the degradation nor the presence of HRP can be concluded. Based on TG/DSC results, however, it can be concluded that APTES has reacted with GO *via* its epoxy groups. Also, the thermal behavior of both final products is different from pure GO and each other.

9.2 Immobilization of HRP on the graphene-based microchip

HRP immobilization on the laser-oxidized chip was accomplished by using GA as a crosslinker.[82] The chip consisted of a graphene monolayer on top of a silicon/silicon dioxide (300 nm) substrate. The graphene was oxidized *via* two-photon laser-oxidization[22], the pattern of which is shown in Figure 49. The chip was characterized by AFM imaging and Raman spectroscopy of the oxidized chip before and after HRP immobilization *via* GA crosslinker.

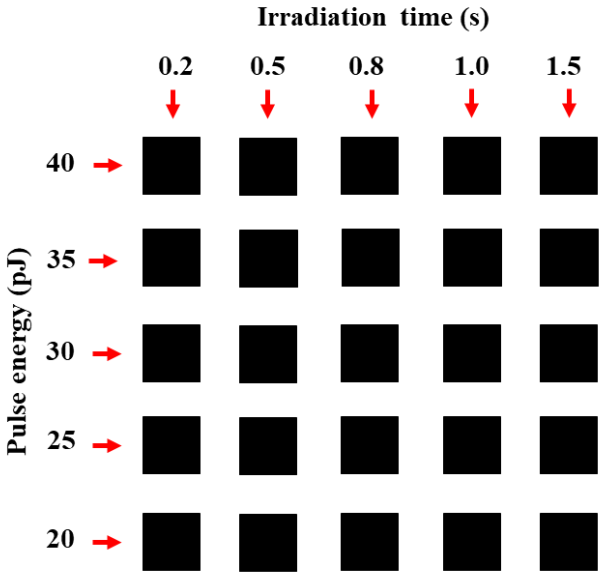

Figure 49. Schematic presentation of the laser oxidized chip showing laser pulse energies and irradiation times of two-photon laser-oxidation. Black squares illustrate oxidized areas.

The oxidized chip was incubated in PBS-GA solution for 4 h at RT (pH 7.3) protected from light to prevent light-induced GA polymerization. A low concentration of GA solution (8 % v/v) for the functionalization was used to minimize GA polymerization. The chip was washed with PBS to remove an excess of GA. The GA functionalized chip was incubated in PBS solution of HRP for 1h at the same conditions as in the first step. The concentration of HRP solution (0.625 U/mL) was the same used earlier in the non-covalent HRP immobilization on oxidized chip.[106]

It was hypothesized based on the preliminary studies with GO flakes that GA would react covalently with GO and further with HRP. Therefore, it was assumed that GA and HRP would prefer the oxidized areas of the chip compared to non-oxidized, pristine graphene.

9.2.1 AFM

The chip contained two oxidized areas, 1C and 8I. Based on AFM images of area 1C, the graphene layer was partly exfoliated during GA functionalization or HRP immobilization steps (Appendix 5). Raman measurements showed that the material below the peeled graphene was the silica layer (Appendix 5). Hence, further analysis was focused on the area 8I. As can be seen from the AFM images (Figure 50 a and b), dots and line-shaped structures occur after HRP immobilization, which could derive from HRP and GA polymer chains, respectively.

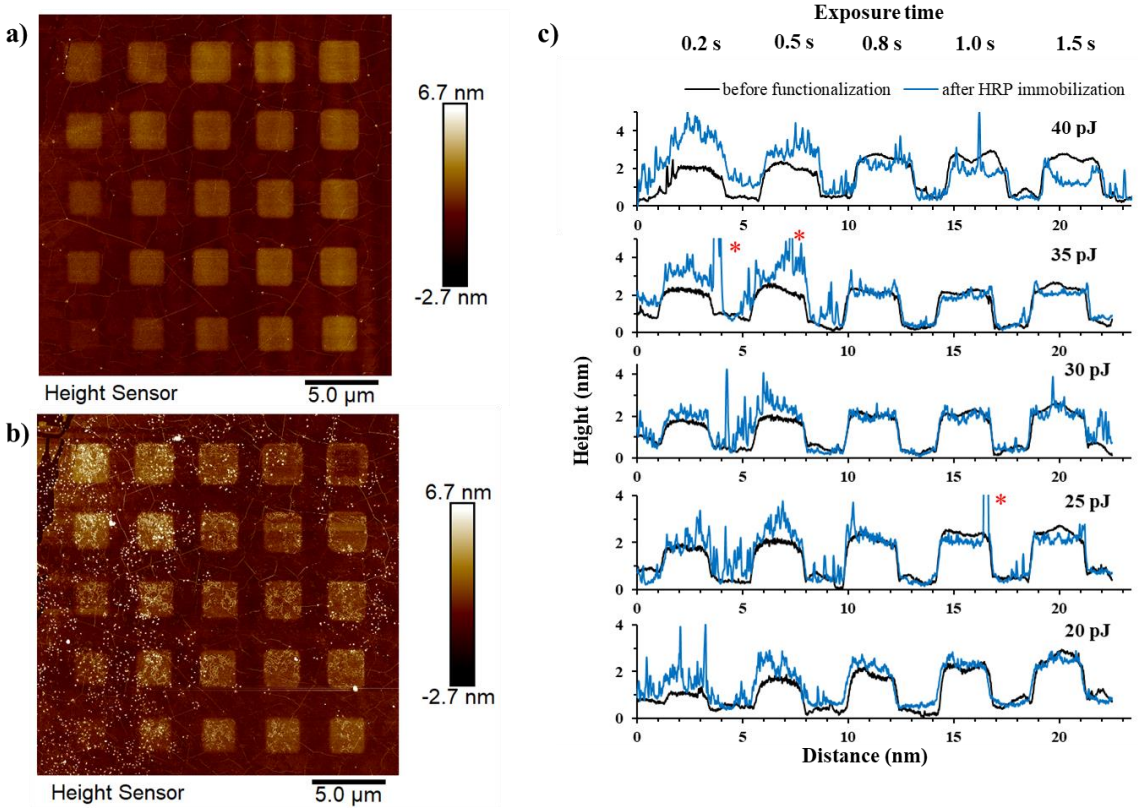

Figure 50. AFM height sensor images of the oxidized chip (8I area) a) before and b) after HRP immobilization. c) Height profiles of squares with different exposure times and laser pulse energies. (*: The heights are 12 nm (0.2 s, 35 pJ), 8 nm (0.5 s, 35 pJ) and 9 nm (1.0 s, 25 pJ))

Height profiles of the oxidized chip before and after functionalization with different laser pulse energies are presented in Figure 50 c. It is noteworthy that the following height measurements show the relative heights of the oxidized squares and particles regarding the graphene background. Hence, the measured heights are not absolute heights of the squares. The heights of the oxidized squares vary between different graphene oxidation stages due to different laser-oxidation conditions. After HRP immobilization, the heights of the oxidized areas are almost double with irradiation times of 0.2 s - 0.8 s and laser pulse energies of 40 pJ -35 pJ. With higher irradiation times (0.8 s -1.5 s), the heights of the oxidized areas are almost the same as before immobilization or even slightly lower. Based on these observations, it seems that HRP preferred oxidized graphene induced by 40 pJ and 35 pJ laser pulses with low irradiation times (0.2 s and 0.5 s) compared to the other oxidized areas.

The number of dots for the most favorable oxidized regions were calculated from Figure 51a. The amounts were 32 (40 pJ, 0.2 s), 31 (40 pJ, 0.5 s), 20 (35 pJ, 0.2 s) and 50 (35 pJ, 0.5 s), respectively. Crosslinkers (line-shaped structures) located more on the oxidized squares than on graphene (Figure 51b), and there were no significant differences between oxidized regions. The average cross-sections of the dots and line-shaped structures were measured by Nanoscope analysis software using section tool, and the whole chip was considered. The average cross-sections were 15.19 nm and 2.92 nm for the dots and lines, respectively. The presence of HRP and GA on the surface of the chip could be concluded based on the AFM results. HRP preferred the graphene oxidized by 40 pJ and 35 pJ laser pulses and 0.2 s and 0.5 s irradiation times, whereas GA crosslinkers preferred oxidized graphene over pristine graphene (Figure 51).

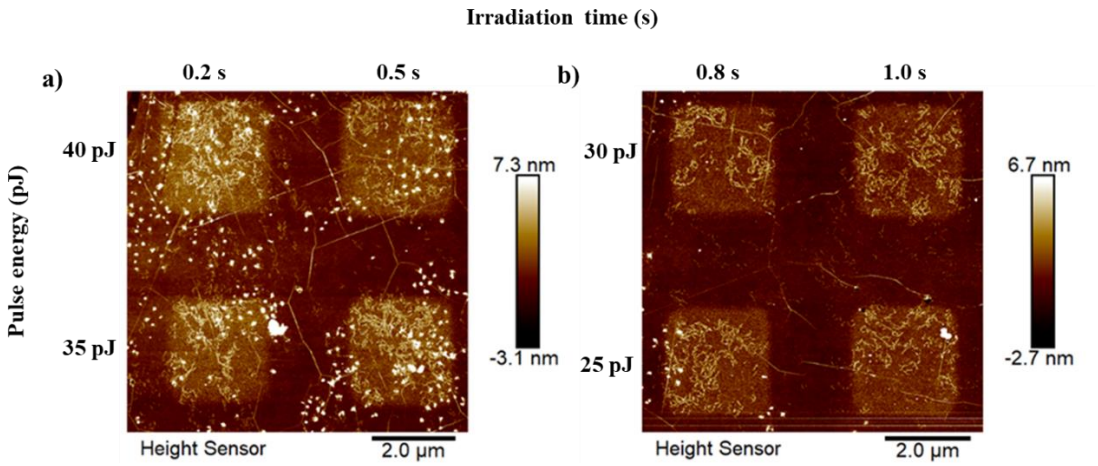

Figure 51. a) Distribution of the dots on the oxidized areas of 40 pJ and 35 pJ pulse energies and 0.2 s and 0.5 s irradiation times. b) Distribution of the line structures on the oxidized graphene induced by 30 pJ and 25 pJ laser pulse energies and 0.8 s and 1.0 s irradiation times.

9.2.2 Raman mapping

Raman mapping for the oxidized chip before and after GA and HRP treatments was done by a home-built Raman setup. Raman spectra were achieved from Raman maps by averaging three spectra from each oxidized square. As in the Raman spectra of the flake samples, D, G and 2D bands can be observed (Figure 52). In addition, there are weak G + D bands in the spectra of the squares, which were oxidized by laser pulse energy of 40 pJ (Figure 52 left). D, G and 2D bands shift to lower values after immobilization regardless of different oxidation conditions of the laser oxidation. The shift could be results from an increased electron density in the graphene lattice, originated by electron-donating interactions after functionalization.[107] Similar results have been observed in earlier studies of HRP immobilization on oxidized graphene-based chips *via* weak interactions.[106] However, especially the G band shifts are larger for covalent than non-covalent HRP immobilization.

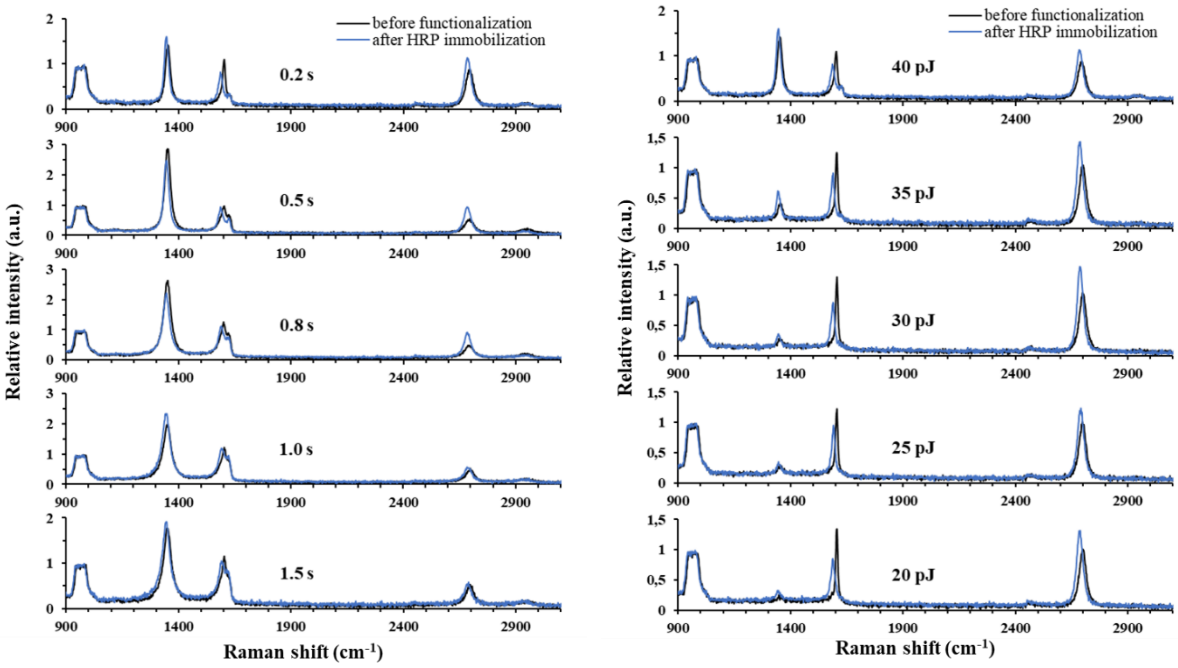

Figure 52. Raman spectra of the chip before and after HRP immobilization. Left: with different irradiation times at constant pulse energy of 40 pJ. Right: with different pulse energies at constant irradiation time of 0.2 s.

There is no apparent uniformity in the extents of the band shifts at a constant pulse energy of 40 pJ between different irradiation times and at a constant irradiation time of 0.2 s between different laser pulse energies (Table 7). At constant pulse energy of 40 pJ, the G band shifts decrease when irradiation time increases, except for the irradiation time of 1.5 s. Otherwise, D and 2D band shifts decrease up to an exposure time of 0.8 s and after it, the shifts increase. At constant irradiation time of 0.2 s, D and 2D band shifts increase while laser pulse energy decreases from 40 pJ to 35 pJ and after that the band shifts start to decrease until pulse energy of 25 pJ. 2D band shifts vary similarly, but the shift begins to decrease already at the pulse energy of 35 pJ.

Table 7. D, G and 2D band shifts after functionalization with GA and HRP for different laser-oxidation conditions

	D band shift (cm^1)	**G band shift (cm^1)**	**2D band shift (cm^1)**
Constant pulse energy of 40 pJ			
Irradiation time (s)			
0.2	-6.2	-14.8	-10.1
0.5	-5.6	-13.2	-9.9
0.8	-4.9	-8.6	-8.5
1.0	-5.5	-6.0	-11.0
1.5	-6.4	-6.1	-11.6
Constant irradiation time of 0.2 s			
Pulse energy (pJ)			
40	-6.2	-14.8	-10.1
35	-8.6	-17.6	-14.2
30	-8.0	-18.1	-13.4
25	-6.6	-14.6	-9.8
20	-9.7	-17.4	-14.6

The differences in the G and 2D band shifts were observed both from the flake samples and the chip. G band shifts of the GO flakes and the oxidized regions of the chip differed ~ 20 cm^{-1} from each other before HRP immobilization and ≤ 10 cm^{-1} after the immobilization (Appendix 6). In proportion, there was almost ~ 100 cm^{-1} difference between the GO flakes and the chip before and after HRP immobilization. On the other hand, D bands of the flakes and the chip before and after HRP immobilization had almost the same Raman shifts (difference ≤ 6 cm^{-1} between the flakes and the chip).

A_D/A_G ratios before and after HRP immobilization at a constant pulse energy of 40 pJ decrease slightly as irradiation time decreases, except for irradiation times of 0.2 s and 0.5 s (Table 8). Although A_D/A_G ratios after HRP immobilization are slightly lower than before, there are no significant differences. Besides, at a constant irradiation time of 0.2 s, the A_D/A_G ratio decrease as laser pulse energy decreases but the difference before and after HRP immobilization is small.

Table 8. A_D/A_G ratios before and after functionalization/HRP immobilization

	A_D/A_G before	**A_D/A_G after**
Constant pulse energy of 40 pJ		
Irradiation time (s)		
0.2	1.8	1.9
0.5	2.7	2.3
0.8	2.2	1.8
1.0	1.9	1.7
1.5	1.8	1.7
Constant irradiation time of 0.2 s		
Pulse energy (pJ)		
40	1.8	1.9
35	0.4	0.6
30	0.2	0.3
25	0.2	0.3
20	0.1	0.2

When A_D/A_G ratios of the chip experiments at a constant laser pulse energy of 40 pJ (Table 8) are compared with the flake results, there seem to be small differences. A_D/A_G ratio of GO flakes was 2.2 and for the GO-GA-HRP flakes was 1.8, which is exactly the same as in the chip results at irradiation time of 0.8 s (Table 8). In addition, the A_D/A_G ratios at constant irradiation time of 0.2 s are lower than A_D/A_G ratios of the flakes or oxidized areas of the chip at a constant pulse energy of 40 pJ (except for the highest pulse energy).

The D band areas for the chip before and after HRP immobilization are shown in the Raman maps below (Figures 53 a and b, respectively). The areas of the D bands increase after HRP immobilization. This could indicate a larger number of defects in the graphene lattice, resulting from the change in the hybridization of carbons (sp^2 to sp^3).[30]

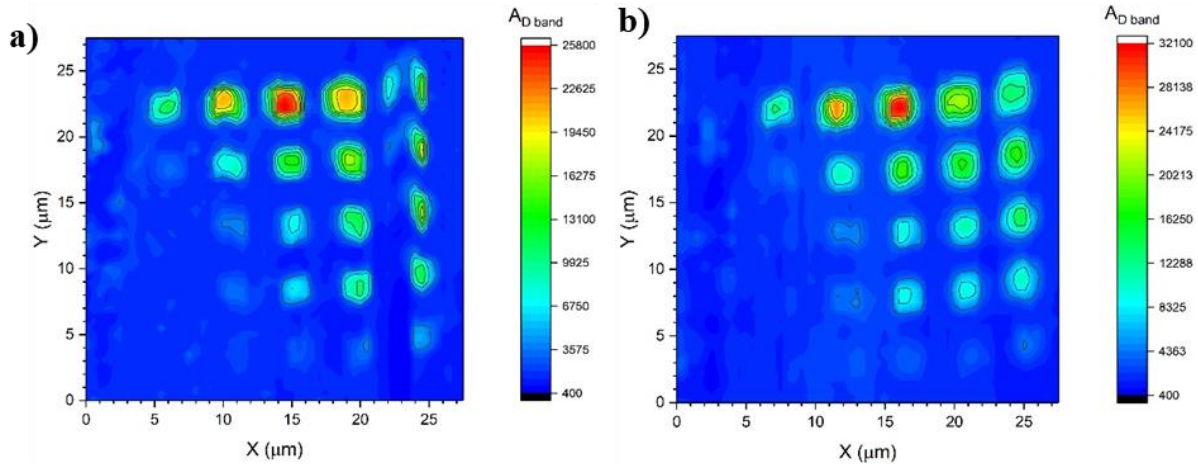

Figure 53. Raman maps of D band areas of the oxidized chip a) before and b) after HRP immobilization.

In conclusion, D, G, and 2D bands shifted to lower Raman shift values after HRP immobilization. In addition, the oxidation degree of the graphene layer seems to have no impact on the band shifts before and after HRP immobilization. The D band areas of the oxidized regions increased after HRP immobilization *via* GA crosslinker, indicating an increase in defects of the graphene lattice. Comparing the experiments with flakes and the chip shows a similar trend in the band shifts. Also, A_D/A_G ratios can be compared between the experiments at specific laser-oxidation conditions. Therefore, the flakes are a suitable model system for chip experiments.

10. Conclusions

The experimental part aimed at the covalent attachment of the HRP enzyme on the oxidized graphene surface using two crosslinker systems: GA and APTES-GA. Preliminary studies were performed with GO flakes, and based on them, HRP immobilization *via* GA crosslinker on a laser-oxidized graphene-based chip was performed.

The successful covalent immobilization of HRP on GO flakes with both crosslinker systems was proved by FTIR spectroscopy. No significant differences in the HRP immobilization outcome between the two crosslinker systems were observed. However, it could not be concluded if the peaks 1629 cm^{-1} and 1633 cm^{-1} originated from the amide group of HRP or imine bonds from the crosslinking reaction (samples GO-APTES-GA-HRP and GO-GA-HRP). The TGA results supported the success of covalent functionalization. Each final product and GO showed different thermal behavior. Especially notable is the thermal degradation of GO-APTES-GA-HRP: It strongly differs from GO and GO-GA-HRP, indicating the presence of more stable bonds due to the incorporation of APTES into the system.

In the AFM images of the graphene-based microchip, elevated dots and line-shaped structures could be observed after GA and HRP treatment, assigned to be HRP enzymes and GA crosslinkers, respectively. HRP seemed to have no preference towards the oxidized areas compared to pristine graphene, whereas GA crosslinkers were located more on the oxidized areas. The covalent HRP immobilization on the oxidized areas of the chip could not be proved by AFM. The Raman spectra of the oxidized areas showed shifting of the D, G and 2D bands towards lower Raman shifts after HRP immobilization. These results agree with the former results, indicating a successful immobilization of HRP. Also, the D band areas of the oxidized regions increased after HRP immobilization, which suggests an increased number of defects in the graphene lattice.

Based on the results from the experiments with the GO flakes and the chip, it could not be fully proved that HRP was covalently attached to GO *via* GA crosslinker. The IR results of the flakes indicated that covalent bonds formed in the GO-GA-HRP system. However, AFM and Raman data of the chip did not unambiguously support this. In the future, chip experiments with other

crosslinker systems, such as APTES-GA, should be done. AFM imaging should also be performed after every step of the protein immobilization to facilitate interpretation of AFM images. In the future experiments, the optimal oxidation conditions for the chip observed in the experiments (laser pulse energies of 40 pJ and 35 pJ and irradiation times of 0.2 s and 0.5 s) should be used.

The preparation process of the flakes must be developed further to achieve more reliable results from Raman and AFM measurements of pure and functionalized GO flakes. A lower concentration of GO in the suspension and sonication in every step could reduce the agglomeration of GO flakes. Also, better methods to detect HRP from the samples should be figured out. In biology, the detection of HRP has been done by the chemiluminescence detection method. The detection is based on the oxidation reaction where HRP oxidizes its chemiluminescent substrate, luminol, in the presence of peroxide. The oxidized form of luminol can emit light at 425 nm, which can be detected by a CCD camera (commonly used in biology).[108] This could also be possible for HRP detection from the graphene-based chip, but the method's applicability should be explored more carefully.

It is still unknown if the protein type affects the success of the covalent protein immobilization on GO. The type and number of amino acid side chains among different proteins vary, which could impact the reactivity of proteins with GO materials. Hence, the variation of both protein and crosslinker - or even the covalent immobilization without crosslinker - remains a topic of interest with many open questions to study.

References

1. Singh, D. P.; Herrera, C. E.; Singh, B.; Singh, S.; Singh, R. K. and Kumar, R., Graphene oxide: An efficient material and recent approach for biotechnological and biomedical applications, *Mater. Sci. Eng. C*, **2018**, *86*, 173–197.

2. Nanda, S. S.; Papaefthymiou, G. C. and Yi, D. K., Functionalization of Graphene Oxide and its Biomedical Applications, *Crit. Rev. Solid State Mater. Sci.*, **2015**, *40*, 291–315.

3. Raslan, A.; Saenz del Burgo, L.; Ciriza, J. and Pedraz, J. L., Graphene oxide and reduced graphene oxide-based scaffolds in regenerative medicine, *Int. J. Pharm.*, **2020**, *580*, 119226.

4. Kostarelos, K.; Vincent, M.; Hebert, C. and Garrido, J. A., Graphene in the Design and Engineering of Next-Generation Neural Interfaces, *Adv. Mater.*, **2017**, *29*, 1700909.

5. Reddy, S.; Xu, X.; Guo, T.; Zhu, R.; He, L. and Ramakrishana, S., Allotropic carbon (graphene oxide and reduced graphene oxide) based biomaterials for neural regeneration, *Curr. Opin. Biomed. Eng.*, **2018**, *6*, 120–129.

6. Dreyer, D. R.; Park, S.; Bielawski, C. W. and Ruoff, R. S., The chemistry of graphene oxide, *Chem. Soc. Rev.*, **2010**, *39*, 228–240.

7. Wang, Y.; Li, Z.; Wang, J.; Li, J. and Lin, Y., Graphene and graphene oxide: biofunctionalization and applications in biotechnology, *Trends Biotechnol.*, **2011**, *29*, 205–212.

8. Chen, Z.-L.; Kam, F.-Y.; Goh, R. G.-S.; Song, J.; Lim, G.-K. and Chua, L.-L., Influence of Graphite Source on Chemical Oxidative Reactivity, *Chem. Mater.*, **2013**, *25*, 2944–2949.

9. Chua, C. K.; Sofer, Z. and Pumera, M., Graphite Oxides: Effects of Permanganate and Chlorate Oxidants on the Oxygen Composition, *Chem. - A Eur. J.*, **2012**, *18*, 13453–13459.

10. He, H.; Klinowski, J.; Forster, M. and Lerf, A., A new structural model for graphite oxide, *Chem. Phys. Lett.*, **1998**, *287*, 53–56.

11. Lerf, A.; He, H.; Forster, M. and Klinowski, J., Structure of Graphite Oxide RevisitedII, *J. Phys. Chem. B*, **1998**, *102*, 4477–4482.

12. Aliyev, E.; Filiz, V.; Khan, M. M.; Lee, Y. J.; Abetz, C. and Abetz, V., Structural Characterization of Graphene Oxide: Surface Functional Groups and Fractionated Oxidative Debris, *Nanomaterials*, **2019**, *9*, 1180.

13. Hofmann, U. and Holst, R., Über die Säurenatur und die Methylierung von Graphitoxyd, *Berichte der Dtsch. Chem. Gesellschaft (A and B Series)*, **1939**, *72*, 754–771.

14. Ruess, G., Über das Graphitoxyhydroxyd (Graphitoxyd), *Monatshefte für Chemie*, **1947**, *76*, 381–417.

15. Scholz, W. and Boehm, H. P., Untersuchungen am Graphitoxid. VI. Betrachtungen zur Struktur des Graphitoxids, *Zeitschrift für Anorg. und Allg. Chemie*, **1969**, *369*, 327–340.

16. Szabó, T.; Berkesi, O.; Forgó, P.; Josepovits, K.; Sanakis, Y.; Petridis, D. and Dékány, I., Evolution of surface functional groups in a series of progressively oxidized graphite oxides, *Chem. Mater.*, **2006**, *18*, 2740–2749.

17. Erickson, K.; Erni, R.; Lee, Z.; Alem, N.; Gannett, W. and Zettl, A., Determination of the Local Chemical Structure of Graphene Oxide and Reduced Graphene Oxide, *Adv. Mater.*, **2010**, *22*, 4467–4472.

18. Hummers, W. S. and Offeman, R. E., Preparation of Graphitic Oxide, *J. Am. Chem. Soc.*, **1958**, *80*, 1339–1339.

19. Marcano, D. C.; Kosynkin, D. V.; Berlin, J. M.; Sinitskii, A.; Sun, Z.; Slesarev, A.; Alemany, L. B.; Lu, W. and Tour, J. M., Improved Synthesis of Graphene Oxide, *ACS Nano*, **2010**, *4*, 4806–4814.

20. Yu, H.; Zhang, B.; Bulin, C.; Li, R. and Xing, R., High-efficient Synthesis of Graphene Oxide Based on Improved Hummers Method, *Sci. Rep.*, **2016**, *6*, 36143.

21. Aumanen, J.; Johansson, A.; Koivistoinen, J.; Myllyperkiö, P. and Pettersson, M., Patterning and tuning of electrical and optical properties of graphene by laser induced two-photon oxidation, *Nanoscale*, **2015**, *7*, 2851–2855.

22. Koivistoinen, J.; Sládková, L.; Aumanen, J.; Koskinen, P.; Roberts, K.; Johansson, A.; Myllyperkiö, P. and Pettersson, M., From Seeds to Islands: Growth of Oxidized Graphene by Two-Photon Oxidation, *J. Phys. Chem. C*, **2016**, 22330–22341.

23. Johansson, A.; Tsai, H.-C.; Aumanen, J.; Koivistoinen, J.; Myllyperkiö, P.; Hung, Y.-Z.;

Chuang, M.-C.; Chen, C.-H.; Woon, W. Y. and Pettersson, M., Chemical composition of two-photon oxidized graphene, *Carbon N. Y.*, **2017**, *115*, 77–82.

24. Dreyer, D. R.; Todd, A. D. and Bielawski, C. W., Harnessing the chemistry of graphene oxide, *Chem. Soc. Rev.*, **2014**, *43*, 5288–5301.

25. Zhang, Y.; Wu, C.; Guo, S. and Zhang, J., Interactions of graphene and graphene oxide with proteins and peptides, *Nanotechnol. Rev.*, **2013**, *2*, 27–45.

26. Konkena, B. and Vasudevan, S., Understanding Aqueous Dispersibility of Graphene Oxide and Reduced Graphene Oxide through pK_a Measurements, *J. Phys. Chem. Lett.*, **2012**, *3*, 867–872.

27. Tiwari, A.; Syväjärvi, M. and Rvi, M., *Graphene Materials : Fundamentals and Emerging Applications*, 1st ed., John Wiley & Sons, Incorporated, 2015, pp. 108-109.

28. Liu, L.; Zhang, R.; Liu, Y.; Tan, W. and Zhu, G., Insight into hydrogen bonds and characterization of interlayer spacing of hydrated graphene oxide, *J. Mol. Model.*, **2018**, *24*, 137.

29. Shen, J.; Shi, M.; Yan, B.; Ma, H.; Li, N.; Hu, Y. and Ye, M., Covalent attaching protein to graphene oxide via diimide-activated amidation, *Colloids Surfaces B Biointerfaces*, **2010**, *81*, 434–438.

30. Childres, I.; Jaureguib, L. A.; Park, W.; Cao, H.; Chen, Y. P. Jang, J. I., *New Developments in Photon and Materials Research*, *Chapter 19: Raman spectroscopy of graphene and related materials,* Nova Science Publishers, USA, 2013.

31. Georgakilas, V.; Otyepka, M.; Bourlinos, A. B.; Chandra, V.; Kim, N.; Kemp, K. C.; Hobza, P.; Zboril, R. and Kim, K. S., Functionalization of Graphene: Covalent and Non-Covalent Approaches, Derivatives and Applications, *Chem. Rev.*, **2012**, *112*, 6156–6214.

32. Hernández-Cancel, G.; Suazo-Dávila, D.; Ojeda-Cruzado, A. J.; García-Torres, D.; Cabrera, C. R. and Griebenow, K., Graphene oxide as a protein matrix: influence on protein biophysical properties, *J. Nanobiotechnology*, **2015**, *13*, 70.

33. Nelson, D. L. and Cox, M. M., *Lehninger Principles of Biochemistry*, 6th ed., W. H. Freeman and Company, New York, 2013, a) pp. 76-89, b) pp. 115-142.

34. Rabe, M.; Verdes, D. and Seeger, S., Understanding protein adsorption phenomena at

solid surfaces, *Adv. Colloid Interface Sci.*, **2011**, *162*, 87–106.

35. Georgakilas, V.; Tiwari, J. N.; Kemp, K. C.; Perman, J. A.; Bourlinos, A. B.; Kim, K. S. and Zboril, R., Noncovalent Functionalization of Graphene and Graphene Oxide for Energy Materials, Biosensing, Catalytic, and Biomedical Applications, *Chem. Rev.*, **2016**, *116*, 5464–5519.

36. Zhang, M.; Yin, B.-C.; Wang, X.-F. and Ye, B.-C., Interaction of peptides with graphene oxide and its application for real-time monitoring of protease activity, *Chem. Commun.*, **2011**, *47*, 2399–2401.

37. Zhang, J.; Zhang, F.; Yang, H.; Huang, X.; Liu, H.; Zhang, J. and Guo, S., Graphene Oxide as a Matrix for Enzyme Immobilization, *Langmuir*, **2010**, *26*, 6083–6085.

38. Kuchlyan, J.; Kundu, N.; Banik, D.; Roy, A. and Sarkar, N., Spectroscopy and Fluorescence Lifetime Imaging Microscopy To Probe the Interaction of Bovine Serum Albumin with Graphene Oxide, *Langmuir*, **2015**, *31*, 13793–13801.

39. Zhang, Y.; Zhang, J.; Huang, X.; Zhou, X.; Wu, H. and Guo, S., Assembly of Graphene Oxide-Enzyme Conjugates through Hydrophobic Interaction, *Small*, **2012**, *8*, 154–159.

40. Sun, C.; Walker, K. L.; Wakefield, D. L. and Dichtel, W. R., Retaining the Activity of Enzymes and Fluorophores Attached to Graphene Oxide, *Chem. Mater.*, **2015**, *27*, 4499–4504.

41. Rosen, C. B. and Francis, M. B., Targeting the N terminus for site-selective protein modification, *Nat. Chem. Biol.*, **2017**, *13*, 697–705.

42. Hoyt, E. A.; Cal, P. M. S. D.; Oliveira, B. L. and Bernardes, G. J. L., Contemporary approaches to site-selective protein modification, *Nat. Rev. Chem.*, **2019**, *3*, 147–171.

43. Li, D.; Zhang, W.; Yu, X.; Wang, Z.; Su, Z. and Wei, G., When biomolecules meet graphene: from molecular level interactions to material design and applications, *Nanoscale*, **2016**, *8*, 19491–19509.

44. Camarero, J. A., Recent developments in the site-specific immobilization of proteins onto solid supports, *Biopolymers*, **2008**, *90*, 450–458.

45. Jiang, K.; Schadler, L. S.; Siegel, R. W.; Zhang, X.; Zhang, H. and Terrones, M., Protein immobilization on carbon nanotubes via a two-step process of diimide-activated

amidation, *J. Mater. Chem.*, **2004**, *14*, 37.

46. Vacchi, I. A.; Spinato, C.; Raya, J.; Bianco, A. and Ménard-Moyon, C., Chemical reactivity of graphene oxide towards amines elucidated by solid-state NMR, *Nanoscale*, **2016**, *8*, 13714–13721.

47. Imani, R.; Emami, S. H. and Faghihi, S., Nano-graphene oxide carboxylation for efficient bioconjugation applications: a quantitative optimization approach, *J. Nanoparticle Res.*, **2015**, *17*, 88.

48. Guo, S.; Raya, J.; Ji, D.; Nishina, Y.; Ménard-Moyon, C. and Bianco, A., Is carboxylation an efficient method for graphene oxide functionalization?, *Nanoscale Adv.*, **2020**, *2*, 4085–4092.

49. Salvio, R.; Krabbenborg, S.; Naber, W. J. M.; Velders, A. H.; Reinhoudt, D. N. and van der Wiel, W. G., The Formation of Large-Area Conducting Graphene-Like Platelets, *Chem. - A Eur. J.*, **2009**, *15*, 8235–8240.

50. Migneault, I.; Dartiguenave, C.; Bertrand, M. J. and Waldron, K. C., Glutaraldehyde: behavior in aqueous solution, reaction with proteins, and application to enzyme crosslinking, *Biotechniques*, **2018**, *37*, 790–802.

51. Tan, Y.; Song, Y. and Zheng, Q., Facile regulation of glutaraldehyde-modified graphene oxide for preparing free-standing papers and nanocomposite films, *Chinese J. Polym. Sci.*, **2013**, *31*, 399–406.

52. Hu, N.; Meng, L.; Gao, R.; Wang, Y.; Chai, J.; Yang, Z.; Kong, E. S.-W. and Zhang, Y., A Facile Route for the Large Scale Fabrication of Graphene Oxide Papers and Their Mechanical Enhancement by Cross-linking with Glutaraldehyde, *Nano-Micro Lett.*, **2011**, *3*, 215–222.

53. Clayden, Jonathan; Greeves, Nick; Warren, S., *Organic chemistry*, 2nd ed., Oxford University press, New York, 2012, pp. 136-137 and 302-327.

54. Hua, D.; Rai, R. K.; Zhang, Y. and Chung, T.-S., Aldehyde functionalized graphene oxide frameworks as robust membrane materials for pervaporative alcohol dehydration, *Chem. Eng. Sci.*, **2017**, *161*, 341–349.

55. Shariat, S. Z. A. S.; Borzouee, F.; Mofid, M. R. and Varshosaz, J., Immobilization of

lactoperoxidase on graphene oxide nanosheets with improved activity and stability, *Biotechnol. Lett.*, **2018**, *40*, 1343–1353.

56. Habeeb, A. F. S. A. and Hiramoto, R., Reaction of proteins with glutaraldehyde, *Arch. Biochem. Biophys.*, **1968**, *126*, 16–26.

57. Hermanson, G. T., *Bioconjugate techniques*, 3rd ed., Academic Press, London, 2013, a) pp. 292-294, b) pp. 535-537, c) pp. 769-774, d) pp. 6-15.

58. Serodre, T.; Oliveira, N.; Miquita, D.; Ferreira, M.; Santos, A.; Resende, V. and Furtado, C., Surface Silanization of Graphene Oxide Under Mild Reaction Conditions, *J. Braz. Chem. Soc.*, **2019**.

59. Kashefi, S.; Borghei, S. M. and Mahmoodi, N. M., Covalently immobilized laccase onto graphene oxide nanosheets: Preparation, characterization, and biodegradation of azo dyes in colored wastewater, *J. Mol. Liq.*, **2019**, *276*, 153–162.

60. Kolb, H. C.; Finn, M. G. and Sharpless, K. B., Click Chemistry: Diverse Chemical Function from a Few Good Reactions, *Angew. Chemie Int. Ed.*, **2001**, *40*, 2004–2021.

61. Chen, Y.; Xianyu, Y.; Wu, J.; Yin, B. and Jiang, X., Click Chemistry-Mediated Nanosensors for Biochemical Assays, *Theranostics*, **2016**, *6*, 969–985.

62. Kou, L.; He, H. and Gao, C., Click chemistry approach to functionalize two-dimensional macromolecules of graphene oxide nanosheets, *Nano-Micro Lett.*, **2010**, *2*, 177–183.

63. Shi, L.; Wang, L.; Chen, J.; Chen, J.; Ren, L.; Shi, X. and Wang, Y., Modifying graphene oxide with short peptide via click chemistry for biomedical applications, *Appl. Mater. Today*, **2016**, *5*, 111–117.

64. Hersel, U.; Dahmen, C. and Kessler, H., RGD modified polymers: biomaterials for stimulated cell adhesion and beyond, *Biomaterials*, **2003**, *24*, 4385–4415.

65. Mei, K.-C.; Rubio, N.; Costa, P. M.; Kafa, H.; Abbate, V.; Festy, F.; Bansal, S. S.; Hider, R. C. and Al-Jamal, K. T., Synthesis of double-clickable functionalised graphene oxide for biological applications, *Chem. Commun.*, **2015**, *51*, 14981–14984.

66. Stankovich, S.; Piner, R. D.; Nguyen, S. T. and Ruoff, R. S., Synthesis and exfoliation of isocyanate-treated graphene oxide nanoplatelets, *Carbon N. Y.*, **2006**, *44*, 3342–3347.

67. Wang, Z.; Ge, Z.; Zheng, X.; Chen, N.; Peng, C.; Fan, C. and Huang, Q., Polyvalent DNA–graphenenanosheets “click” conjugates, *Nanoscale*, **2012**, *4*, 394–399.

68. Vacchi, I. A.; Guo, S.; Raya, J.; Bianco, A. and Ménard-Moyon, C., Strategies for the Controlled Covalent Double Functionalization of Graphene Oxide, *Chem. – A Eur. J.*, **2020**, *26*, 6591–6598.

69. Guo, S.; Nishina, Y.; Bianco, A. and Ménard-Moyon, C., A Flexible Method for Covalent Double Functionalization of Graphene Oxide, *Angew. Chem. Int. Ed.*, **2020**, *59*, 1542–1547.

70. Bednarek, C.; Wehl, I.; Jung, N.; Schepers, U. and Bräse, S., The Staudinger Ligation, *Chem. Rev.*, **2020**, *120*, 4301–4354.

71. Soellner, M. B.; Dickson, K. A.; Nilsson, B. L. and Raines, R. T., Site-Specific Protein Immobilization by Staudinger Ligation, *J. Am. Chem. Soc.*, **2003**, *125*, 11790–11791.

72. van Dongen, S. F. M.; Teeuwen, R. L. M.; Nallani, M.; van Berkel, S. S.; Cornelissen, J. J. L. M.; Nolte, R. J. M. and van Hest, J. C. M., Single-Step Azide Introduction in Proteins via an Aqueous Diazo Transfer, *Bioconjug. Chem.*, **2009**, *20*, 20–23.

73. Inoue, N.; Onoda, A. and Hayashi, T., Site-Specific Modification of Proteins through N-Terminal Azide Labeling and a Chelation-Assisted CuAAC Reaction, *Bioconjug. Chem.*, **2019**, *30*, 2427–2434.

74. Muralidharan, V. and Muir, T. W., Protein ligation: an enabling technology for the biophysical analysis of proteins, *Nat. Methods*, **2006**, *3*, 429–438.

75. Luong, N. D.; Sinh, L. H.; Johansson, L.; Campell, J. and Seppälä, J., Functional Graphene by Thiol-ene Click Chemistry, *Chem. – A Eur. J.*, **2015**, *21*, 3183–3186.

76. Singh, K.; Srivastava, G.; Talat, M.; Srivastava, O. N. and Kayastha, A. M., α-Amylase immobilization onto functionalized graphene nanosheets as scaffolds: Its characterization, kinetics and potential applications in starch based industries, *Biochem. Biophys. Reports*, **2015**, *3*, 18–25.

77. Adamiak, K. and Sionkowska, A., Current methods of collagen cross-linking: Review, *Int. J. Biol. Macromol.*, **2020**, *161*, 550–560.

78. Liu, S.; Zhou, C.; Mou, S.; Li, J.; Zhou, M.; Zeng, Y.; Luo, C.; Sun, J.; Wang, Z. and

Xu, W., Biocompatible graphene oxide–collagen composite aerogel for enhanced stiffness and in situ bone regeneration, *Mater. Sci. Eng. C*, **2019**, *105*, 110137.

79. Kang, S.; Park, J. B.; Lee, T.-J.; Ryu, S.; Bhang, S. H.; La, W.-G.; Noh, M.-K.; Hong, B. H. and Kim, B.-S., Covalent conjugation of mechanically stiff graphene oxide flakes to three-dimensional collagen scaffolds for osteogenic differentiation of human mesenchymal stem cells, *Carbon*, **2015**, *83*, 162–172.

80. Luo, X.; Weaver, C. L.; Tan, S. and Cui, X. T., Pure graphene oxide doped conducting polymer nanocomposite for bio-interfacing, *J. Mater. Chem. B*, **2013**, *1*, 1340.

81. Stauffer, W. R. and Cui, X. T., Polypyrrole doped with 2 peptide sequences from laminin, *Biomaterials*, **2006**, *27*, 2405–2413.

82. Su, R.; Shi, P.; Zhu, M.; Hong, F. and Li, D., Studies on the properties of graphene oxide – alkaline protease bio-composites, *Bioresour. Technol.*, **2012**, *115*, 136–140.

83. Yu, Q.; Zhang, B.; Li, J. and Li, M., The design of peptide-grafted graphene oxide targeting the actin cytoskeleton for efficient cancer therapy, *Chem. Commun.*, **2017**, *53*, 11433–11436.

84. Xu, G.; Chen, X.; Hu, J.; Yang, P.; Yang, D. and Wei, L., Immobilization of trypsin on graphene oxide for microwave-assisted on-plate proteolysis combined with MALDI-MS analysis, *Analyst*, **2012**, *137*, 2757.

85. Veitch, N. C., Horseradish peroxidase: a modern view of a classic enzyme, *Phytochemistry*, **2004**, *65*, 249–259.

86. Hamid, M. and Khalil-ur-Rehman, Potential applications of peroxidases, *Food Chem.*, **2009**, *115*, 1177–1186.

87. Krainer, F. W. and Glieder, A., An updated view on horseradish peroxidases: recombinant production and biotechnological applications, *Appl. Microbiol. Biotechnol.*, **2015**, *99*, 1611–1625.

88. Li, Y.; Feng, L.; Shi, X.; Wang, X.; Yang, Y.; Yang, K.; Liu, T.; Yang, G. and Liu, Z., Surface Coating-Dependent Cytotoxicity and Degradation of Graphene Derivatives: Towards the Design of Non-Toxic, Degradable Nano-Graphene, *Small*, **2014**, *10*, 1544–1554.

89. Kotchey, G. P.; Allen, B. L.; Vedala, H.; Yanamala, N.; Kapralov, A. A.; Tyurina, Y. Y.; Klein-Seetharaman, J.; Kagan, V. E. and Star, A., The Enzymatic Oxidation of Graphene Oxide, *ACS Nano*, **2011**, *5*, 2098–2108.

90. Hassani, L.; Ranjbar, B.; Khajeh, K.; Naderi-Manesh, H.; Naderi-Manesh, M. and Sadeghi, M., Horseradish peroxidase thermostabilization: The combinatorial effects of the surface modification and the polyols, *Enzyme Microb. Technol.*, **2006**, *38*, 118–125.

91. Welinder, K. G.; Smillie, L. B. and Schonbaum, G. R., Amino acid sequence studies of horseradish peroxidase. I. Tryptic peptides., *Can. J. Biochem.*, **1972**, *50*, 44–62.

92. Sitsanidis, E. D.; Schirmer, J.; Lampinen, A.; Mentel, K. K.; Hiltunen, V.-M.; Ruokolainen, V.; Johansson, A.; Myllyperkiö, P.; Nissinen, M. and Pettersson, M., Tuning protein adsorption on graphene surfaces via laser-induced oxidation, *Nanoscale Adv.*, **2021**, *3*, 2065–2074.

93. Ranjbari, N.; Razzaghi, M.; Fernandez-Lafuente, R.; Shojaei, F.; Satari, M. and Homaei, A., Improved features of a highly stable protease from Penaeus vannamei by immobilization on glutaraldehyde activated graphene oxide nanosheets, *Int. J. Biol. Macromol.*, **2019**, *130*, 564–572.

94. Besharati Vineh, M.; Saboury, A. A.; Poostchi, A. A.; Rashidi, A. M. and Parivar, K., Stability and activity improvement of horseradish peroxidase by covalent immobilization on functionalized reduced graphene oxide and biodegradation of high phenol concentration, *Int. J. Biol. Macromol.*, **2018**, *106*, 1314–1322.

95. Özçakır, E. and Eskizeybek, V., A Facile and Effective Method for Size Sorting of Large Flake Graphene Oxide, *Conf. Proc. RAN'16, Proceedings of the World Congress on Recent Advances in Nanotechnology*, 2016.

96. Konios, D.; Stylianakis, M. M.; Stratakis, E. and Kymakis, E., Dispersion behaviour of graphene oxide and reduced graphene oxide, *J. Colloid Interface Sci.*, **2014**, *430*, 108–112.

97. Haeri, S. Z.; Ramezanzadeh, B. and Asghari, M., A novel fabrication of a high performance SiO_2-graphene oxide (GO) nanohybrids: Characterization of thermal properties of epoxy nanocomposites filled with SiO_2-GO nanohybrids, *J. Colloid Interface Sci.*, **2017**, *493*, 111–122.

98. Villa, S.; Riani, P.; Locardi, F. and Canepa, F., Functionalization of Fe_3O_4 NPs by Silanization: Use of Amine (APTES) and Thiol (MPTMS) Silanes and Their Physical Characterization, *Materials (Basel).*, **2016**, *9*, 826.

99. Majoul, N.; Aouida, S. and Bessaïs, B., Progress of porous silicon APTES-functionalization by FTIR investigations, *Appl. Surf. Sci.*, **2015**, *331*, 388–391.

100. IR spectrum table & chart: https://www.sigmaaldrich.com/technical-documents/articles/biology/ir-spectrum-table.html, Sigma Aldrich (10.11.2020).

101. Jabs, A., Jena library of biological macromolecules: Determination of Secondary Structure in Proteins by Fourier Transform Infrared Spectroscopy (FTIR): http://jenalib.leibniz-fli.de/ImgLibDoc/ftir/IMAGE_FTIR.html (15.11.2020).

102. Feicht, P. and Eigler, S., Defects in Graphene Oxide as Structural Motifs, *ChemNanoMat*, **2018**, *4*, 244–252.

103. Patila, M.; Pavlidis, I. V.; Kouloumpis, A.; Dimos, K.; Spyrou, K.; Katapodis, P.; Gournis, D. and Stamatis, H., Graphene oxide derivatives with variable alkyl chain length and terminal functional groups as supports for stabilization of cytochrome c, *Int. J. Biol. Macromol.*, **2016**, *84*, 227–235.

104. Sengupta, I.; Chakraborty, S.; Talukdar, M.; Pal, S. K. and Chakraborty, S., Thermal reduction of graphene oxide: How temperature influences purity, *J. Mater. Res.*, **2018**, *33*, 4113–4122.

105. Ganguly, A.; Sharma, S.; Papakonstantinou, P. and Hamilton, J., Probing the thermal deoxygenation of graphene oxide using high-resolution in situ X-ray-based spectroscopies, *J. Phys. Chem. C*, **2011**, *115*, 17009–17019.

106. Schirmer, J., *Functionalization of Graphene-Based Microchips for Neuroprosthetic Applications*, University of Jyväskylä and Universität Kassel, Department of Chemistry, 2019.

107. Das, A.; Pisana, S.; Chakraborty, B.; Piscanec, S.; Saha, S. K.; Waghmare, U. V.; Novoselov, K. S.; Krishnamurthy, H. R.; Geim, A. K.; Ferrari, A. C. and Sood, A. K., Monitoring dopants by Raman scattering in an electrochemically top-gated graphene transistor, *Nat. Nanotechnol.*, **2008**, *3*, 210–215.

108. Introduction to the Methods Used to Detect Proteins and Nucleic Acids Bound to Membranes: https://www.sigmaaldrich.com/technical-documents/articles/biology/detection-methods.html, Sigma Aldrich (2.12.2020).

Appendices

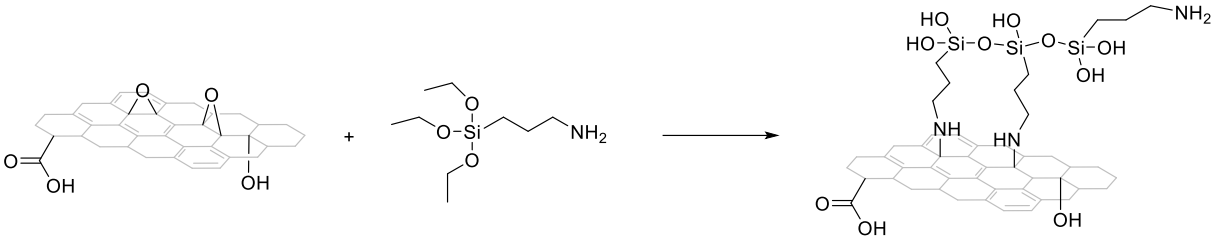

Figure A1. Other possible reaction between a GO flake and APTES.

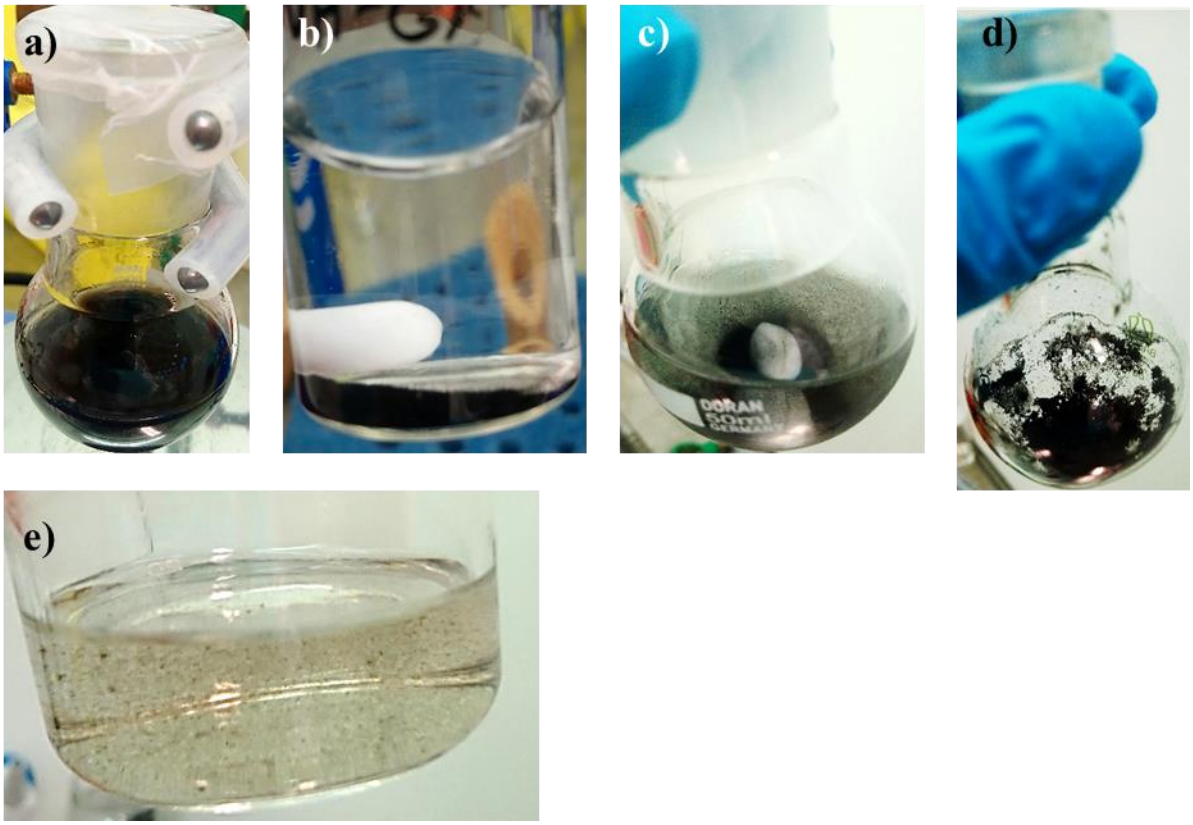

Figure A2. a) GO suspension in a solvent (PBS, ethanol). b) GO-APTES-GA-HRP product after mixing at 4ºC for 20 h (1st experiment). c) GO-APTES-GA-HRP product after mixing at 4ºC for 20 h (2nd experiment). d) Vacuum dried intermediate product. e) Supernatant containing flakes of GO material after centrifugation.

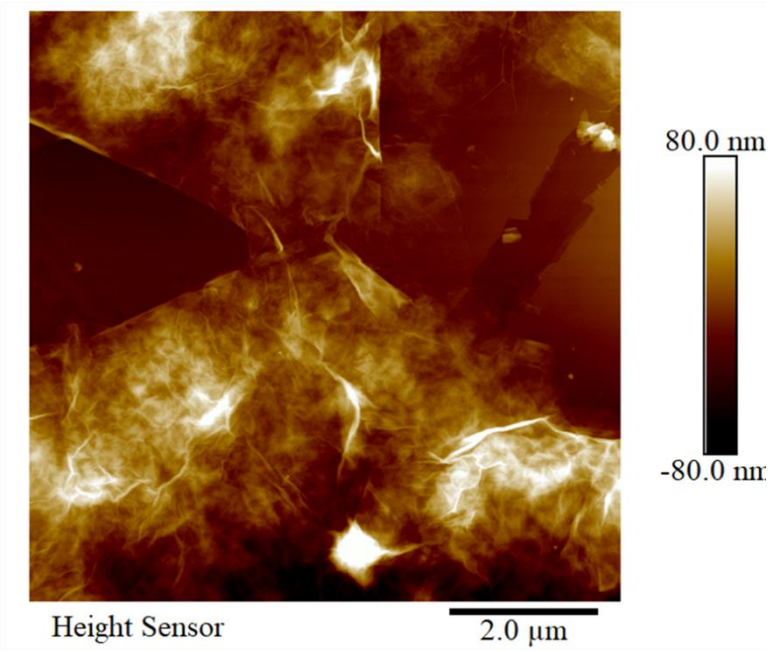

Figure A3. AFM height sensor image of the dried GO flake on mica disc.

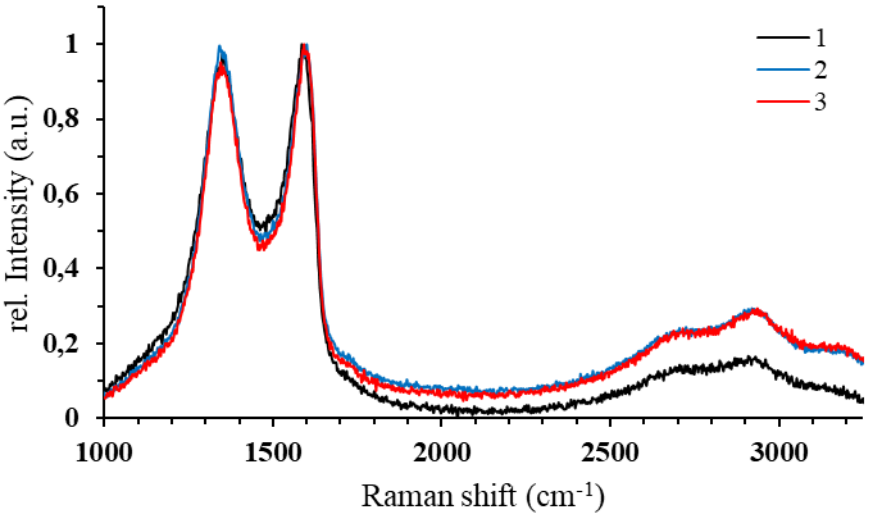

Figure A4a. Raman spectra of GO-GA-HRP from three trials.

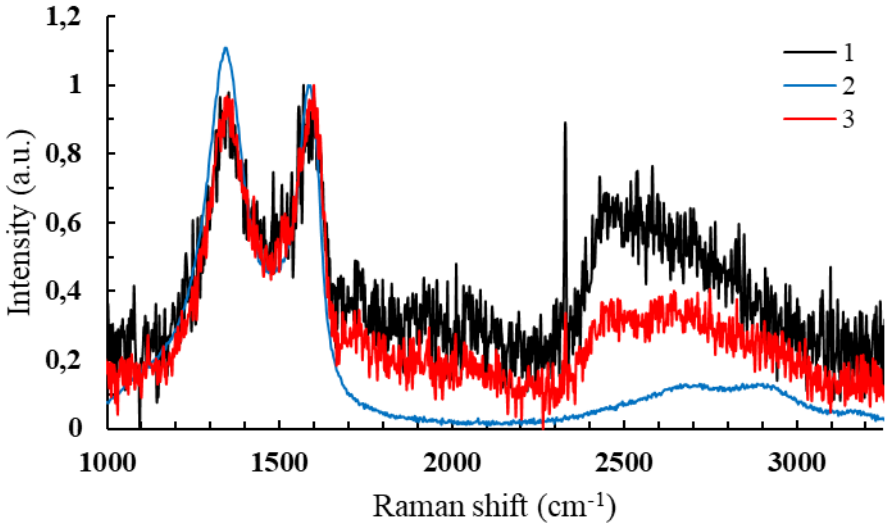

Figure A4b. Raman spectra of GO-APTES-GA-HRP from three trials.

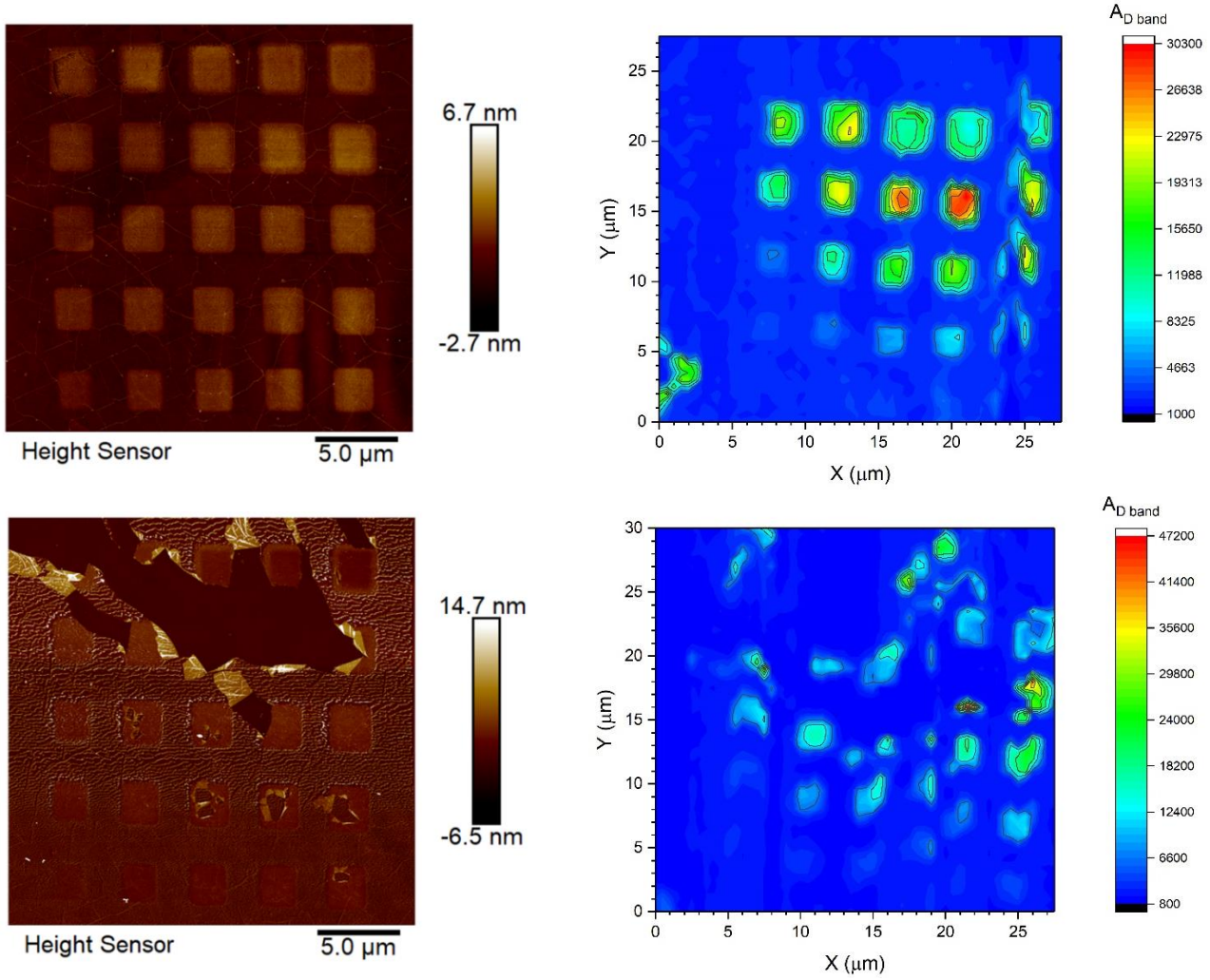

Figure A5a. AFM images and Raman maps of the area 1C before GA functionalization (upper row) and after HRP immobilization (lower row).

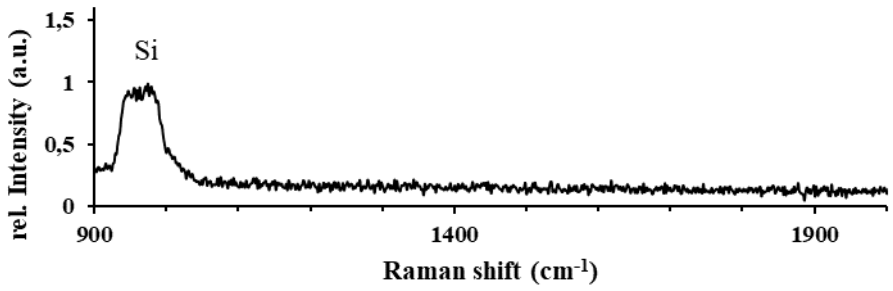

Figure A5b. Raman spectrum of the peeled off area of the chip after HRP immobilization.

Table A1. Raman band positions of the chip (area 8I) before and after HRP immobilization

	D band (cm^1) before/after	**G band (cm^1) before/after**	**2D band (cm^1) before/after**
Constant pulse energy of 40 pJ			
Irradiation time (s)			
0.2	1352/1346	1603/1589	2696/2686
0.5	1351/1346	1603/1590	2694/2684
0.8	1350/1345	1603/1594	2693/2685
1.0	1350/1344	1604/1598	2697/2686
1.5	1350/1343	1604/1598	2698/2686
Constant irradiation time of 0.2 s			
Pulse energy (pJ)			
40	1352/1346	1603/1589	2696/2686
35	1354/1346	1605/1588	2701/2686
30	1354/1347	1606/1588	2701/2687
25	1354/1347	1605/1591	2700/2690
20	1354/1345	1606/1588	2701/2686